SYNTHESIS OF POLYURETHANE INCORPORATED BY CALCIUM OXIDE AND MAGNESIUM OXIDE FOR HEAVY METAL REMOVAL FROM WATER

MOHSEN VAFAEI FARD

FACULTY OF ENGINEERING
UNIVERSITY OF MALAYA
KUALA LUMPUR

2020

SYNTHESIS OF POLYURETHANE INCORPORATED BY CALCIUM OXIDE AND MAGNESIUM OXIDE FOR HEAVY METAL REMOVAL FROM WATER

MOHSEN VAFAEI FARD

THESIS SUBMITTED IN FULFILMENT OF THE
REQUIREMENTS FOR THE DEGREE OF DOCTOR OF
PHILOSOPHY

FACULTY OF ENGINEERING
UNIVERSITY OF MALAYA
KUALA LUMPUR

2020

UNIVERSITY OF MALAYA

ORIGINAL LITERARY WORK DECLARATION

Name of Candidate: **MOHSEN VAFAEI FARD**

Matric No: **KHA140054**

Name of Degree: **DOCTOR OF PHILOSOPHY**

Title of Thesis: **SYNTHESIS OF POLYURETHANE INCORPORATED BY CALCIUM OXIDE AND MAGNESIUM OXIDE FOR HEAVY METAL REMOVAL FROM WATER**

Field of Study: **ENVIRONMENTAL ENGINEERING**

I do solemnly and sincerely declare that:

(1) I am the sole author/writer of this Work;
(2) This Work is original;
(3) Any use of any work in which copyright exists was done by way of fair dealing and for permitted purposes and any excerpt or extract from, or reference to or reproduction of any copyright work has been disclosed expressly and sufficiently and the title of the Work and its authorship have been acknowledged in this Work;
(4) I do not have any actual knowledge nor do I ought reasonably to know that the making of this work constitutes an infringement of any copyright work;
(5) I hereby assign all and every rights in the copyright to this Work to the University of Malaya ("UM"), who henceforth shall be owner of the copyright in this Work and that any reproduction or use in any form or by any means whatsoever is prohibited without the written consent of UM having been first had and obtained;
(6) I am fully aware that if in the course of making this Work I have infringed any copyright whether intentionally or otherwise, I may be subject to legal action or any other action as may be determined by UM.

Candidate's Signature Date:

Subscribed and solemnly declared before,

Witness's Signature Date:

Name:

Designation:

SYNTHESIS OF POLYURETHANE INCORPORATED BY CALCIUM OXIDE AND MAGNESIUM OXIDE FOR HEAVY METAL REMOVAL FORM WATER

ABSTRACT

Water contaminated by heavy metals such as copper, lead, nickel, and cadmium has significant adverse impacts on receiving water. In recent years, various methods, such as adsorption, chemical precipitation, and ion exchange, have been extensively studied for the elimination of heavy metals. Adsorption is one of the numerously and diversely reported mechanisms of removing heavy metals due to its simplicity and cost-effectiveness. In this study, highly permeable rigid polyurethanes (PU) incorporating calcium oxide (CaO) (PU/CaO) composite materials were prepared via a facile and economic one-pot synthesis method and characterized for remediation of heavy metal from water. To investigate the effect of CaO on heavy metal adsorption, the amount of CaO was varied from 0 to 25 of total weight (wt.%) of polyol and Methylene diphenyl diisocyanate (MDI). Among the media tested, 25% CaO-incorporated PU (PU/CaO-25) had the highest adsorption capacity ($Q_{max} = 35.6$ mg.g^{-1}) of Cu(II). The PU/CaO-25 is capable of removing Cu(II), Pb(II), Zn(II), and Ni(II) ions by both adsorption and ion exchange mechanisms. However, precipitation was the dominant mechanism for removal of metal ions due to the increase of pH in the solutions. Moreover, column tests were conducted to investigate various parameters, and data were interpreted using the Bed Depth Service Time (BDST) model to predict service time. Specific structural features of PU/CaO-25 and the remediation mechanism were also determined using FESEM/EDS, XRD, N_2 gas isotherm, and chemical equilibrium modeling. Moreover, column tests using simulated urban storm-water runoff (USR) showed that PU/CaO-25 removed all heavy metals such as Cu(II), Zn(II), Ni(II), and Pb(II) to below their regulation levels at ~1,100-bed volumes (BVs). In the second stage of this research to enhance the removal efficiency of heavy metals by using PU, commercial MgO was used, and a simple hydrothermal method was applied to the mixture of commercial MgO and granular PU (gPU). Three-dimensional (3D) flowerlike $Mg(OH)_2$ structures (FMH) were built on the surface of gPU (gPU-FMH). Hydrothermal process and gPU was the key factors for the assembly of the FMH. The synthesized hexagonal nanosheet petals of gPU-FMH provided a high surface area. The gPU-FMH showed the superb adsorption capacity ($Q_{max} = 472$, 1050, and 1293 $mg.g^{-1}$ for Cu(II), Cd(II), and Pb(II), respectively). The proposed hypothesis for the synthesis of gPU-FMH and the removal mechanism of the heavy metals has been proved through various spectroscopic analyses. It was found that $Mg(OH)_2$ dissociation in the metal solution produces two OH^- ions that subsequently react with the metal ions. Based on the stoichiometry, this reaction can render the production of insoluble precipitates through coupling with the anionic species that exist in the solution. Further, the precipitates will become trapped in the gaps of the FMH particles, and the precipitation might be the dominant removal mechanism at the higher metal-ion concentrations. In the results of the continuous-flow column study, gPU-FMH showed a much higher removal capacity (184 $mg.g^{-1}$) of Cu(II) than the other referenced media.

Keywords: Polyurethane (PU), Calcium oxide (CaO), Magnesium Oxide (MgO), Adsorption, Heavy metal removal.

SINTESIS POLIURETANA YANG DIPERBADANKAN OLEH KALSIUM OKSIDA DAN MAGESIUM OKSIDA UNTUK PENGELUARAN LOGAM BERAT DARI AIR

ABSTRAK

Air yang tercemar oleh logam berat seperti tembaga, plumbum, nikel dan kadmium mempunyai kesan negatif terhadap penerimaan air. Dalam kebelakangan ini, pelbagai kaedah seperti penjerapan, pemendakan kimia, pertukaran ion telah dikaji secara meluas untuk penghapusan logam berat. Penjerapan adalah salah satu mekanisme yang dilaporkan mengeluarkan logam berat disebabkan oleh kesederhanaan dan keberkesanan kosnya. Memandangkan kapasiti penjerapan kecil penyerap konvensional, mengenal pasti penyerap dengan keupayaan penyingkiran yang tinggi merupakan keperluan mendesak. Oleh itu, sintesis bahan kejuruteraan dengan laluan ekonomi dan dipraktikkan dalam permohonan sebenar merupakan permintaan yang tinggi. Walau bagaimanapun, penyerap-penyerap perlu dipisahkan selepas proses penjerapan dari air. Proses ini menunjukkan dominasi ke atas penyerap ini disebabkan kekurangan pengumpulan sorben koleksi daripada air selepas proses rawatan. Penapisan dengan pelbagai jenis penyerap menunjukkan janji hebat dalam penyingkiran logam berat dengan operasi mudah dan penjimatan ruang. Dalam kajian ini, poliuretan (PU) yang telap menggabungkan kalsium oksida (CaO) (PU/CaO) melalui kaedah sintesis mudah, ekonomi dan dicirikan untuk pemulihan logam berat daripada air. Komposit PU/CaO disediakan dengan menambahkan jumlah CaO yang telah ditetapkan (0 hingga 25%) kepada PU. Antara media yang diuji, 25% CaO yang diperbadankan dengan PU (PU/CaO-25) mempunyai kapasiti penjerapan yang tertinggi (Qmax = 35.6 $\mathrm{mg.g^{-1}}$) Cu (II). Selain itu, PU/CaO-25 mempunyai ketegaran 2.5 kali lebih tinggi (0.38 MPa) daripada polimer tegar 'tipikal' (0.15 MPa). Ujian kekonduksian hidraulik (HC) menunjukkan PU/CaO-25 mempunyai kebolehtelapan (0.108 cm s^{-1}) setara atau lebih tinggi daripada rujukan pasir. Ujian kolum telah dijalankan untuk menyiasat pelbagai parameter. Data telah ditafsirkan dengan menggunakan model Time Depth Bed Service (BDST) untuk meramalkan masa perkhidmatan. Ciri-ciri struktur khas PU/CaO-25 dan mekanisme pemulihan juga telah ditentukan dengan menggunakan pemodelan gas FESEM/EDX, XRD, N_2 gas dan pemodelan keseimbangan kimia. Ujian lajur yang menggunakan larian air hujan ribut simulasi (USR) menunjukkan bahawa semua logam berat telah dikeluarkan oleh PU/ CaO-25 ke bawah paras peraturan ia itu pada volum ~1,100-katil (BVs). Untuk meningkatkan kecekapan penyingkiran logam berat dengan menggunakan PU, dalam peringkat kedua kajian ini, MgO komersial telah digunakan dan kaedah hidrotermal mudah telah digunakan pada campuran MgO komersil dan PU granular (gPU). Struktur Mg $(OH)_2$ yang berbentuk tiga dimensi (3D) bunga (FMH) telah dibina di permukaan gPU (gPU-FMH). Proses hidrotermal dan gPU merupakan faktor utama untuk pemasangan FMH. Kelopak heksagon nanosheet gPU-FMH yang telah disintesis memberikan kawasan permukaan yang tinggi. Oleh itu, gPU-FMH menunjukkan keupayaan penjerapan yang luar biasa (Qmax=472, 1050 dan 1293 mg.g^{-1} Cu(II), Cd(II), dan Pb(II), masing-masing). Hipotesis cadangan sintesis gPU-FMH dan mekanisma penyingkiran logam berat telah dibuktikan melalui pelbagai analisis spektroskopik. Hasil daripada kajian kolum berterusan, gPU-FMH menunjukkan keupayaan penyingkiran yang lebih tinggi (184 mg.g^{-1}) daripada Cu(II) berbanding dengan pihak media lain.

Kata kunci: Poliuretana (PU), Kalsium oksida (CaO), Magnesium oksida (mandatori), Penjerapan, Pemuliahn logam berat

ACKNOWLEDGEMENTS

First of all, I would like to express my sincere gratitude to my supervisor, professor Shaliza Ibrahim, who has offered me kind guidance in my research work. Through her profound and conscientious discussions offered to me, I have mastered a great deal of knowledge and greatly broadened my views on research. From her valuable and meticulous guidance, I have immensely developed my effective brainstorming, planning, and scheduling skills. Her logic thinking, research enthusiasm, and deep insight has inspired me and will be of great benefits to my life-long study. Her willing to offer his academic help has greatly impressed me.

My next gratitude goes to professor Min Jang for offering me a great chance of carrying out my research work in his laboratory. His kind and continuous support has encouraged me to pursue my research curiosity, and his deep insight in the research area has greatly kept me on the right track of my research work.

I would also like to show my thanks to professor Ali Zinatizadeh, who has helped me in my research work. I would also appreciate the assistance from all the lab and professional officers in the Department of Civil Engineering and also the Faculty of Engineering staff.

Finally, I would like to give my dearest thanks to my family for their endless love, support, and encouragement.

Last but foremost, my deepest respect is going to my dearest late grandfather, grandmother, and my lovely late aunt, for their endless love and supports! I love you all, and will love you forever and ever, especially my loveliest aunt, “dear Mansoureh.”

TABLE OF CONTENTS

LIST OF FIGURES

LIST OF TABLES

LIST OF SYMBOLS AND ABBREVIATIONS

C_0	:	Initial concentration of metal ions in the liquid phase
C_e	:	Equilibrium concentrations of the metal ions in the liquid phase
Å	:	Angstrom
F	:	The linear flow velocity of the liquid phase
h	:	The head level across the specimen
K_L	:	The equilibrium constant
k_2	:	The rate constant of the second-order equation
K	:	Kelvin
K_C	:	Hydraulic conductivity
keV	:	Kilo electron volt
M	:	Molarity
N_0	:	The adsorption capacity
N	:	Normality
p	:	Working pressure during BET analysis
p°	:	Atmospheric pressure
Q	:	Flow rate
q_{eq}	:	Adsorption capacity
q_m	:	The maximum adsorption capacity
q_t	:	The amount of adsorption at a specific time
q_e	:	The amount of adsorption at equilibrium
wt. %	:	Weight percentage
w/w%	:	Weight per weight percentage
Z	:	The length of the column bed
3D	:	Three dimensional

AMD	:	Acid mining drainage
ASTM	:	American society for testing and materials
BDST	:	Bed depth service time
BET	:	Brunauer–Emmett–Teller
BJH	:	Barrett−Joyner− Halenda
BT	:	Breakthrough
BTP	:	Breakthrough point
BV	:	Bed volume
CLT	:	Column lifetime
CS-1	:	Control sample 1
CS-2	:	Control sample 2
DI	:	Distilled water
EDX	:	Energy-dispersive X-ray
EPA	:	Environmental potential agency
FESEM	:	Field-emission scanning electron microscope
FMH	:	Flowerlike magnesium hydroxide
FMO	:	Flowerlike magnesium oxide
FTIR	:	Fourier transform infrared spectroscopy
gPU	:	Granular PU
gPU-FMH$_{120}$	:	Synthesized granular polyurethane- flowerlike magnesium hydroxide at 120°C
gPU-FMH$_{80}$	:	Synthesized granular polyurethane- flowerlike magnesium hydroxide at 80°C
gPU-FMH$_{50}$	:	Synthesized granular polyurethane- flowerlike magnesium hydroxide at 50°C
HC	:	Hydraulic conductivity

HPU	:	Hydroxyapatite-PU foams
ICDD	:	International centre for diffraction data
ICP-OES	:	Inductively coupled plasma optical emission spectrometry
JCPDS	:	Joint committee on powder diffraction standards
MDI	:	Methylene diphenyl diisocyanate
NCO	:	Isocyanate group
NU	:	Nucleation
PE	:	Polyethylene
PEG	:	Polyethylene glycol
pH	:	Negative logarithm of hydrogen ions concentration
PP	:	Polypropylene
PU	:	Polyurethane
PU/CaO	:	polyurethane incorporating calcium oxide
PU/CaO-5	:	Prepared PU/CaO sample with 5% (w/w) of CaO
PU/CaO-10	:	Prepared PU/CaO sample with 10% (w/w) of CaO
PU/CaO-20	:	Prepared PU/CaO sample with 20% (w/w) of CaO
PU/CaO-25	:	Prepared PU/CaO sample with 25% (w/w) of CaO
PU/MgO	:	Polyurethane and magnesium oxide mixture
PU-FMH	:	3D-flowerlike $Mg(OH)_2$ incorporated polyurethane
PVDF	:	Polyvinylidene fluoride
PVP	:	Polyvinylpyrrolidone
SD	:	Spinodal decomposition
USR	:	Urban storm-water runoff
WHO	:	World health organization
XRD	:	X-ray powder diffraction

LIST OF APPENDICES

APPENDIX A: Adsorption efficiency, adsorption isotherm and kinetic model for Cu(II), Pb(II), and Cd(II) by PU-FMH$_{80}$

APPENDIX B: The first page of publications and papers presented

CHAPTER 1: INTRODUCTION

1.1 Background of study

Discharging heavy metals into the environment has a hazardous impact on the health and well-being of the humankind, animals, and plants. Hence, remediation actions centered on the efficient removal of heavy metals from industrial effluents and discharges are of great importance. Different industry wastewater, such as electroplating, mining, electric device manufacturing, and metal finishing, etc. are considered as the primary source of heavy metals ions. The features of heavy metal ions can be noted to toxicity, non-biodegradable, and highly carcinogenic, which are harmful to the environment and nature. Hence, some measurements should be done for efficient removal from wastewater before discharge into the environment. This concern has been an important scientific and engineering subject recently.

Moreover, these metals are considered as useful raw material in the industry from the economic point of view as can be separated and removed from the wastewater and reused in different industries. Also, not only heavy metal pollution by the source of industrials activities, but also urban storm-water runoff (USR) contaminated by heavy metals such as copper, lead, nickel, cadmium, and zinc, has significant adverse impacts on receiving water. Urban storm-water runoff can be contaminated with heavy metal ions from atmospheric fallout, corrosion, tires, automobile exhausts, Emission of gasoline-powered vehicles, gasoline additives, pavement wear, road salt, exterior paint, and terrestrial sources include zinc (Boxall & Maltby, 1995). Besides that, flooding is a 'traditional' problem due to typically heavy rainfall in tropical countries, which has especially become an issue with urbanization. Protection of agricultural land, urban rivers, and streams from flooding in inhabited urban areas, especially with polluted water, are essential for urban stormwater runoff management and treatment.

Heavy metal concentrations in residential and commercial catchments runoff is lower than industrial catchments (Joshi & Balasubramanian, 2010; Sanger et al., 1999). However, appropriately treated stormwater runoff can be used as a valuable source for drinking, cleaning, and farming water in urban areas (Razzaghmanesh et al., 2014). Thus, effectual separation and removal technology of heavy metals from wastewater and stormwater runoff are considered as important research and practical concern. According to the various concentration of heavy metals in stormwater runoff from residential and commercial area, the range of metal concentration were found from ppb to ppm for zinc, lead, and copper, which can be summarized as follows: zinc (0.007-1.127 $mg.L^{-1}$), lead (0.00057-0.26 $mg.L^{-1}$), and copper (0.00006-1.41 $mg.L^{-1}$) (Joshi & Balasubramanian, 2010). Therefore, several techniques have been used in this regard, which can be pointed out to chemical precipitation (Chen et al., 2009), Filtration (J. Huang et al., 2010), solvent extraction (Yun et al., 1993), flotation (Yuan et al., 2008), ion exchange (Hassan & Carr, 2018), coagulation and flocculation (Duan et al., 2010; Tokuyama et al., 2010), electrochemical treatment (Nanseu-Njiki et al., 2009), and adsorption (Hua & Odelius, 2016; Musico et al., 2013), for the water treatment. However, in comparison with available technologies, adsorption process has gained much more attention in separation and removal of heavy metal ions (Hua & Odelius, 2016; Musico et al., 2013). Adsorption indicates the advantages of effective heavy metal ions removal in high and quite low concentrations, with no additional environmental pollution or other chemical consumption, and capability to attain high selectivity to distinct types of heavy metal ions.

In this process, adsorbents play a significant role as an adsorption media. Given the low adsorption capacities of conventional adsorbents, such as low-cost adsorbent and waste materials (Ghaedi & Mosallanejad, 2018), particularly nano-oxides (Wan et al., 2015), there is a dire need for identifying adsorbents with a high removal capacity. Adsorption through filtration is one of the treatment procedures to eliminate heavy metals in low concentration in stormwater runoff. Thus, it requires that the filter media have high removal capacities for heavy metals and high hydraulic conductivity. Furthermore, as a great advantage of adsorption, a filtration system can be designed readily and established at any location with flooding for the case of USR treatment.

Recently, polymers have been investigated extensively in removing heavy metals and have been explored in terms of treatment efficiency and removal mechanisms of heavy metals (Choi et al., 2014). Especially from the engineering aspect, polymers can be easily tailored in terms of strength, pore structure, and functionalization. Several kinds of polymers are being considered due to improvement in efficiency and selectivity in heavy metal ion separation. The flexibility in selection of the polymer structures and properties leads the polymeric adsorbents flexible for many various adsorption applications. The considerable industrial production also provides polymer adsorbents proper for batch and packed column mode operation in small land large scales operation simultaneously.

1.2 Problem Statement

The largest sources of heavy metal pollution are industrial activities and vehicles. However, nowadays, not only industrial activities, but also urban storm-water runoff contaminated by heavy metals such as copper, lead, and nickel has significant negative impacts on receiving water (Huber et al., 2016; Hwang et al., 2016). Especially, urbanized countries with limited land and water resources must treat USRs and reuse them as an alternative water resource. Flooding is also a ‘traditional’ problem due to typically heavy rainfall in tropical countries, which has especially become an issue with urbanization. Appropriately treated USRs can be used as a valuable source of drinking water, irrigation for urban landscapes, and green-roof purposes during the dry season. Thus, urbanized countries with limited land and water resources must treat USRs and reuse them as an alternative water resource. Through various strategies, storm-water management practice such as filtration, and wetland have been conducted to reduce, control, and prevent stormwater runoff (De Gois et al., 2015; Feng et al., 2012; Sample et al., 2012). However, USRs treatment through filtration has attracted much attention due to its simplicity, cost-effectiveness, and space-saving (Park et al., 2016). According to low sorption capacity and slow hydraulic conductivity of the conventional adsorbents (Cao et al., 2012), the volume of filter needs to be designed to achieve an acceptable filter lifetime.

To address this issue, adsorption through filtration is a promising and suitable technique due to its simplicity, convenience, flexibility in design and ease of operation, low maintenance costs, and high efficiency (Fu & Wang, 2011). However, it requires that the filter media have high adsorption capacity and permeability. Furthermore, the filtration system can be designed readily and established at any location with flooding. Thus, it requires that the filter media have high removal capacities for heavy metals and high hydraulic conductivity, which is the main challenge of the filtration process. Polymers have been investigated extensively in removing heavy metals and have been explored regarding treatment efficiency and removal mechanisms of heavy metals (Choi et al., 2014).

Especially from the engineering aspect, polymers can be easily tailored in terms of strength, pore structure, and functionalization. Thus, synthesis of a functionalized polymer with a high porosity that can support high hydraulic conductivity with high sorption capacity is an efficient way to treat the stormwater runoff. In association with a water-treatment demand, much attention has been paid to the evolution of metal oxides with three-dimensional (3D) flowerlike nanostructured materials that use nanosized building blocks to remove heavy metals (Zhang et al., 2012). It is believed that compared with the traditional adsorbents, the specific surface areas of the 3D flowerlike nanomaterials are much larger, which could improve its heavy-metal adsorption capacities (Nasiri et al., 2018). Among all of the metal oxides, calcium oxide (CaO), magnesium oxide (MgO), and magnesium hydroxide ($Mg[OH]_2$) have been considered since they are not only cheap, innocuous, and environmentally friendly, but their adsorption properties for heavy-metal removal are also excellent (Cao et al., 2012). However, the synthesis of the 3D flowerlike metal oxide using a simple and economic route is still a huge research demand. Ethylene–glycol-mediated process, for example, was developed for the synthesis of 3D flowerlike nanostructured materials in an earlier research study (Zhong et al., 2006), but this process is costly and complicated because various expensive chemicals such as polyvinylpyrrolidone (PVP), polyethylene glycol (PEG), urea, and numerous preparation methods are needed (Ma et al., 2014). Chang and Jin (Cao et al., 2012) developed a microwave-assisted solvothermal process to obtain flowerlike-MgO (FMO) nanostructures with an excellent adsorption capacity for the removal of heavy metals. The FMO was prepared using magnesium nitrate [$Mg(NO_3)_2$], urea, and ethanol, and the synthesized product was irradiated using a microwave at 150^{o}C, followed by calcination at 400^{o}C. Flowerlike $Mg(OH)_2$ (FMH) have also been synthesized using various chemicals such as ammonia (NH_3), urea, and $Mg(NO_3)_2$ via a continuous procedure that includes heating, centrifuging, and calcination (Liu et al., 2015). As fine-sized powders, synthesized FMO and FMH seem to be impractical not only because it is complicated to separate them from the liquid phase once they are saturated, but also they cannot be applied in a column system since they significantly reduce the hydraulic conductivity.

1.3 Research Aim and Objectives

This study aims to develop a rigid functionalized polyurethane foam by using metal oxide for the removal of heavy metal ions from water. The specific objectives of this study include the following:

(1) To synthesize functionalized polyurethane foam with CaO (PU/CaO) for heavy metal removal as well as to explore the hydraulic conductivity, compressive strength, and the specific structural features of the PU/CaO.

(2) To investigate the maximum heavy metals removal capability of PU/CaO using a fixed-bed column. Furthermore, the adsorption capability of PU/CaO for the treatment of simulated urban stormwater runoff (USR) will be determined in column mode.

(3) To synthesize and characterize three dimensional (3D) flowerlike magnesium hydroxide (FMH) on the surface of ground polyurethane (gPU) as gPU-FMH for efficient removal of heavy metals from water.

(4) To determine the potential of gPU-FMH for the adsorption of heavy metals in batch and column mode. The specific structural features of gPU-FMH will be investigated by using FESEM/EDX, Elemental mapping, FTIR, XRD, and N_2 gas isotherm after adsorption of heavy metals.

1.4 Research Novelty and Significance of this Study

In the first stage of this study, a rigid polyurethane incorporating calcium oxide (PU/CaO) was synthesized via a facile, rapid, and economical synthesis route, and assessed its feasibility for removing heavy metals in urban stormwater runoff. As a widely practiced remediation method, alkaline chemicals have been applied to remove heavy metals via hydrolysis. Among alkaline materials, calcium oxide is economically feasible because of its rapid reaction. However, when CaO is applied to remove heavy metals, its surface is susceptible to becoming covered by hydrolyzed colloids of heavy metals, so that the CaO present is not used fully. Hypothetically, when CaO is incorporated into PU, the armoring possibility could be reduced because CaO is located mainly in the framework of the PU and hydrolyzed heavy metal colloids are deposited on pores in the PU. From this, PU should be strong enough to hold the CaO within the framework even in the case of high-flow-rate operations. Although PU rigidity can be varied by the ratio of methylene diphenyl diisocyanate (MDI) and polyol, which are the main precursors of PU, the addition of CaO can also affect the physical strength as filler. Accordingly, a systematic approach is needed to address both goals of flood control and heavy metal treatment. Thus, highly-permeable rigid functional polyurethane (PU/CaO) was synthesized in a simple, rapid, and economical manner, and tested for remediation of heavy metals contaminated urban stormwater runoff.

In the second stage of this study, for the first time, a novel self-assembled 3D-flowerlike $Mg(OH)_2$ incorporated polyurethane (PU-FMH) was developed for superb adsorption of metal ions from water. PU-FMH can be prepared via a single-step, simple, rapid, and economical process using ground polyurethane, commercial MgO, and distilled water and under simple hydrothermal method at 50-120°C. Synthesis of PU-FMH without using expensive chemicals, solvents, and calcination process, which is common for the synthesis of flowerlike materials, make PU-FMH as a potential candidate with other reported studies and can be applied as an adsorbent for the real water treatment applications.

1.5 Research Contribution

The first phase of the present work dealt with the synthesis of functionalized polyurethane foam with CaO (PU/CaO) for heavy metals removal using a fixed-bed column as well as the treatment of simulated urban stormwater runoff (USR). The immediate outcome and contribution of this research to the world of knowledge comprises research articles published in scientific journals.

The second phase of the project concentrated on the synthesis of three dimensional (3D) flowerlike magnesium hydroxide (FMH) on the surface of ground polyurethane (gPU-FMH) to enhance the removal efficiency of heavy metals. The outcome of this part of the research has also been published in research publications.

1.6 Research Scope

The present research aims to integrate environmental engineering and materials science to develop water treatment applications with desirable heavy metal removal from water through the filtration process. This rigid polyurethane media showed a higher compressive strength in comparison with typical polyurethane foam as well as high hydraulic conductivity characteristics. The synthesized adsorbent also needed to be characterized in terms of morphological and chemical behaviors. The morphological properties of the developed adsorbent were investigated using field emission scanning electron microscopy (FESEM). The X-ray diffractometry (XRD), energy dispersive spectroscopy (EDS), and Brunauer–Emmett–Teller (BET) was employed for sample characterization. However, the regeneration and reusability, and capability evaluation of the adsorbents in a larger column scale fall beyond the scope of this project and may be performed in further research.

1.7 Thesis Outline

Chapter 1 outlines the importance of heavy metal removals before discharging to the environment, the negative health effects of metal ions in water resources, and the significance and novelty of this study with the research objectives. Chapter 2 outlines the effect of heavy metals in drinking water, heavy metal removal technologies, and adsorption of heavy metals from water. Chapter 3 presents the experimental works and also the chemical reagents and materials, which was involved in the synthesis of polyurethane incorporated by Calcium oxide (PU/CaO). Next, the synthesis of self-assembled 3D flower-like magnesium hydroxide coated granular polyurethane (gPU-FMH) and the effect of parameters on the synthesis of flowerlike $Mg(OH)_2$ was studied. Chapter 4 presents the performance of heavy metal removals by PU/CaO and PU-FMH in batch and column mode, and also, the structure of both adsorbents was observed by several characterization methods and techniques before and after heavy metal adsorption. Then, the results have discussed the effect of CaO on the PU, heavy metal removal efficiency by PU-CaO and PU-FMH, and the synthesised mechanism of 3D-FMH was obtained. Chapter 5 summarizes the finding of this research and recommending commands for future research.

CHAPTER 2: LITERATURE REVIEW

2.1 Review of heavy metals

Heavy metals, which include Copper (Cu), Lead (Pb), Nickel (Ni) and Zinc (Zn), etc. are often referred to as the metallic elements with high density which are toxic at low concentrations. The density and permissible level of Cu(II), Pb(II), Ni(II), and Zn(II) according to standard A (Malaysia) are reported in Table 2.1 (MDC Sdn Bhd, 1974). The extensive use of these metals in the industry and agriculture resulted in the economic development and improvement of the nation. Though, heavy metal ions are non-biodegradable and often hazardous due to bio-accumulation in the human body. Therefore, the application of heavy metals that contributes towards environmental and health problems requires being efficiently evaluated. In the following section, the common heavy metals, with their industrial applications, the source of pollution and their toxicity to human health, are provided. The above-mentioned heavy metals can accumulate at any time and gather faster than their excretion; in addition to this, they are highly toxic to humans and the environment. Even at a low concentration of heavy metals, the effects are highly adverse to aquatic environments, and natural degradation does not occur. This is since it reduces the activity of microorganisms, which is already present in the waste streams. Henceforth, nowadays, researchers are highly focussed on the heavy metal removal from the waste effluent.

Table 2.1: Heavy metals properties

Heavy metals	Density (g.cm^{-3})	Standard A (µg. L^{-1})
Copper	8.96	200
Lead	11.40	100
Nickel	8.90	200
Zinc	7.14	2000
Manganese	7.43	200
Cadmium	8.70	10

2.1.1 Copper

Copper is one of the heavy metals which is widely used in industries such as wiring, plumbing, pesticide manufacturing, and domestic metal. Hence, this pollution is mostly produced by industries such as printed circuit board industry, electroplating, pipe corrosion, and mining (Qing et al., 2015). In the areas where mining industry is done, the copper concentration in wastewater has been reported by up to 200 mg.L^{-1} (Davis & Ashenberg, 1989). Despite its contamination, this heavy metal is essential for human beings at the trace level. It is combined with a kind of protein in human blood, which plays an important role as an antioxidant. However, it can be highly toxic if a high dose (more than 1.2 Mg.L^{-1}) is consumed. World health organization (WHO) estimated that the maximum of copper requirements for adults is about 2.5 µg.kg^{-1} of body weight/day and about 50 µg.kg^{-1} of body weight/day for children (Sarvestani & Aghasi, 2019). Copper accumulation in the human body causes Wilson's disease that damages the liver, moreover, the kidney and central nervous system is also affected. Nausea, vomiting, and diarrhoea are common symptoms caused by copper poisoning (Nasiri et al., 2018).

2.1.2 Lead

Lead contamination has become a worldwide concern and poses extravagant damage to the environment and human beings. Various industry and agriculture sections, including battery manufacturing, medical production, use of pesticides and fertilizers, and food production are the main sources of this pollution. Other sources may include leaded gasoline burning, lead leaching from pipes, and solid household wastes. Lead can be very perilous to human beings, and absorption, breathing, or skin contact of lead poses a threat to people's health. Furthermore, the accumulation of lead in plants and animals also creates the main hazard to people as used in the food chain. The toxicity of this heavy metal causes harm to the human kidney and liver affect the central nervous system to a large extent and also anaemia, muscular atrophy or even cancer may occur (Nasiri et al., 2018; Sarvestani & Aghasi, 2019).

2.1.3 Cadmium

Cadmium is extensively used in the industries of electroplating, battery manufacturing, and plastic (pigment) production. Cadmium compounds are used in stabilizer, fertilizer, and alloy manufacturing. It is also considered as one of the common contaminants to water. The main source of cadmium contamination often includes Acid Mine Drainage (AMD), waste sludge, and industrial waste effluents. Furthermore, cadmium is easily absorbed by crops, and it poses a risk to the health of people through the food chain. The cadmium toxicity may include hypertension, lung, and liver diseases as well as bone degradation (Nasiri et al., 2018).

2.1.4 Nickel

Nickel is often applied as a surface-finishing metal for decoration and protection purposes in electroplating industries. After the electroplating, the washing process brings a large number of nickel ions into waste effluent. A higher concentration of this heavy metal creates a major threat to natural waters. The water which is produced by the battery industry, silver refinery, and forging are contaminated by nickel. Serious effects due to additional uptake of nickel include harm to lungs, malfunction of kidneys, incoordination of neural system, and cancer problems (Nasiri et al., 2018). Therefore, nickel ions removal is essential for the reduction of its damage to people.

2.1.5 Zinc

Zinc is widely used in the galvanization process for iron protection. Iron keeps zinc from rusting due to excellent resistance towards corrosion and the preparation of precious metals such as gold and silver. Furthermore, a wide range of industries producing catalysts, fertilizers, and preservatives utilize zinc salts. Therefore, drinking water contains more than 5 mg.L^{-1} of zinc compounds brings potential health problems to human beings. In contrast, a lack of zinc in human body would typically cause growth delay. However, an excess amount of zinc may lead to dizziness, stomachache, vomiting, dehydration, and lack of muscular coordination (Nasiri et al., 2018).

2.2 Treatment technologies

The polluted aquatic environment with metals has a prospective risk and health impact, hence there is an essential need to remove or decrease the pollution level. Some methods have been used in this regard, such as chemical precipitation, ion exchange, membrane filtration, adsorption, electrochemical process, coagulation, and flocculation, etc. Among those approaches, chemical precipitation, ion exchange, and adsorption are the most conventional methods in the applied application (Bolisetty et al., 2019).

2.2.1 Chemical precipitation

Chemical precipitation is a simple method in equipment, easy operation, and appropriate capacity in metal removal, which is generally used in industrial wastewater treatment. Dissolved ions through the chemical reaction with precipitants are changed to the insoluble solid phases, which typically are alkali, sulfide or chelate compound (Azimi et al., 2017). The precipitates, through the process of sedimentation or filtration, can be separated. Chemical precipitants such as CaO, MgO, 1,3-benzenediamidoethanethiolate, and 1,3,5-hecahydrotriazinedithiocarbamate have been studied in Zn(II), Cu(II), Cr(II), and Pb(II) removal. The results showed a removal efficiency higher than 90% (Chen et al., 2009). Despite the advantages of this process, chemical precipitation is accompanied by some limitations such as the generation of the large volumes with low-density sludge, difficulty in treating mixed metals water due to the varying ideal pH for different metals, inhibition by complexing agents coexist in the water, and problems with harmful treatment sludge disposition (Fu & Wang, 2011). Moreover, chemical precipitation is a fast-conventional method in the heavy metal ions removal but inefficient in relatively low concentrations of heavy metal ions. Furthermore, this approach generates solid waste during the process, which includes environmental disposal problems. Lack of sufficient selectivity and consumes surplus chemicals, and high cost makes this approach less practical within the industry (Crini & Lichtfouse, 2019).

2.2.2 Ion exchange

For the recovery and removal of metal ions in the liquid phase, a technique has been used for many years, which is referred to as the non-consumption technique. In this method, the ions of metal are firstly concentrated on the exchange resin, then followed by release from the resin and through regeneration process are dissolved. This whole process has several advantages, namely, high removal efficiency, easy resin's regeneration, high selectivity, and fast kinetics (Bashir et al., 2019).

Concerning the most common cation exchangers can be pointed out to two different types of resin. First is the weakly acid resin, which is -COOH groups (carboxylic acid), and the second is $-SO_3H$ acid groups, which are strongly acidic resins with sulfonic acid groups. Some other factors that can affect ion exchange resins, such as initial metal concentration, pH, temperature, and contact time (Zewail & Yousef, 2015). The cationic exchanger is the most favourable, and it comprises of weak basic resins and strong acidic resins. Basic resins involve carboxylic acid groups, and sulfonic acid groups are available in acidic resins (Fu & Wang, 2011). Hydrogen ions can deliver the transmutable ions with the metal cations. Cationic exchange resins were used in previous studies for the removal of Fe(III) and Pb(II) that was stimulated by the ionic charge present in the resins (Abo-Farha et al., 2009). For natural organic matter removal, magnetic ion exchange resin, which was the first ion exchange resin, was used in 1995 (Ambashta & Sillanpaa, 2010). Ion exchange systems are of two types, anion exchange resins and cation exchange resins.

For less contaminated wastewaters, anionic exchange resins are considered most appropriate. For example, previously, Mn(II) and Cr(VI) were removed through anion and cation exchangers by Kononova et al. (Kononova et al., 2015). The main drawback of ion exchange is the ion exchange resin regeneration through chemical reagents as they cause secondary pollutants. In addition to this, operation cost is high, and the method cannot be applicable in a real application or on a large scale of treatment due to the price (Bilal et al., 2013).

2.2.3 Membrane filtration

Membrane filtration is one of the separation techniques which can be used for heavy metal removal from water. Hence, besides removing metal ions, disinfection also can take place as well in the membrane filtration process (Lyu et al., 2016). The particle separation performance can be changed by several factors, such as applied pressure, pH, solution concentration, and size of the particle in the solution (Ibrahim et al., 2019). There are two types of membrane material; polymer and ceramic. In general, due to the resistance of ceramic to chemicals, it is used for industrial wastewater treatment rather than polymer (Mutamim et al., 2012). The hydrophobic capacity is also present in ceramic material. The high cost of construction is the main disadvantage of ceramic materials. However, according to the chemical resistance properties of some polymers such as Polyethylene (PE), Polypropylene (PP), and Polyvinylidene fluoride (PVDF), they are commercially used in the market. Due to their hydrophobic nature, it can foul easily (Mutamim et al., 2012). There is a high intercommunication between heavy metal and polymeric membranes. It is possible to obtain membrane permeability by membrane material’s pore size (Fu & Wang, 2011). The cleaned solution and the solute can be separated on two different sides of the membrane. Due to its simple operation, less space requirement, and high efficiency of heavy metal removal, membrane filtration is a hopeful technology for heavy metal removal (Ibrahim et al., 2019; Saeedi et al., 2020).

Moreover, organic compounds and suspended solids can also be efficiently removed through this technology. However, due to the high cost, periodic replacement of membrane, and complex process, membrane filtration is only limited to the removal of heavy metal (Fu & Wang, 2011). Hence, pre-treatment is required for the removal of dissolved organic matter and organic matter from water. Thus, by removing organic matters from water, the performance of the membrane can be increased (Tran et al., 2015). To find the non-polluting separating technique, pressure-driven membrane filtration process like microfiltration, ultrafiltration, nanofiltration, and reverse osmosis has been used for the isolation of heavy metal from wastewater depending upon the size of metals. These processes can handle a large volume of aqueous solutions for heavy metal removal.

2.2.4 Coagulation and flocculation

This is the substitute procedure that is available for the precipitation of metal ions to make low soluble compounds, e.g., hydroxides, carbonates, and sulfides (Visa, 2016). A colloid is a suspension atom/molecule with the density equal to the density of water. These particles are not able to settle down due to its low density (Ghernaout et al., 2015). Several treatment strategies are being used to increase the density of the particles. Several factors can affect the coagulation process such as; types of coagulant, pH, temperature, mixing rate and conditions, alkalinity, and the dosage of coagulant. In the process of flocculation and coagulation, several reagents or inorganic flocculants such as $FeCl_3$, $Fe_2(SO_4)_3$, and $Al_2(SO4)_3$ and their derivatives like poly aluminium chloride and poly ferric chloride happen to be used as flocculants in the treatment of wastewater to make bigger particles with the help of stirring and mixing. These large particles can easily be separated from the wastewater. Chang et al. have been reported a new type of macromolecule flocculants such as mercaptoacety by reacting chitosan with mercaptoacetic acid, which resulted in the removal of Cu(II) along with water turbidity

(Chang et al., 2009). In another study, poly aluminium-zinc silicate chloride used in oil wastewater treatment and an approximate removal of turbidity and COD was reported up to 98.9% and 71.8%, respectively (Yu et al., 2017).

With the help of coagulation process, the removal of arsenic was studied by Yan et al. The removal of arsenic ions was with the assistance of ferric salts and aluminium, as they are considered quite effective for this purpose. The results showed an excellent removal efficiency of arsenic ions, which was achieved by using less dosage of ferric coagulant (Yan et al., 2010). With the help of neutralizing process, the colloidal process is destabilized by the coagulants. Then, the sludge formation occurs due to the large utilization of chemicals in this separation process. This is considered as one of the main drawbacks of this process. However, sometimes water-soluble polymeric flocculants such as carboxylic acid polymers and sulfonic acid can be used in the process of separation instead of using inorganic chemical reagents (Yan et al., 2010).

Polymers are environment-friendly, easily accessible, have low sludge formation, and are easy to use (Huang et al., 2016). Certain scientists previously tried to use ferric chloride and poly-aluminium chloride for the removal of metal ions. The results showed that great coagulant could be achieved in the solution around the optimum concentrations of these two popular chemicals (ferric chloride and poly-aluminium chloride) (El-Samrani et al., 2008). Researchers also tried to remove bounded heavy metals by using the coagulation/flocculation process. For example, metal ions complex removal was carried out by using polyelectrolyte flocculation method and then followed by centrifugation and filtration (Fu & Wang, 2011).

Some metal ions such as Pb(II) and Zn(II) bound with the humic acid material, and that gets coagulated with the cationic polyelectrolyte polydiallyldimethylammonium chloride, which is a polyelectrolyte flocculation technique used to remove the heavy metal ions from the solution. However, this method was not able to remove the heavy metal ions from wastewater completely. Thus, some other techniques needed to be used to complete the treatment process, such as precipitation. For example, a combined technology of spontaneous reduction-coagulation process was used by Bojic et al. for the removal of Cu(II) and Zn(II) from wastewater. In different concentrations, the Zn(II) and Cu(II) ions can be efficiently removed through this process (Bojic et al., 2009). Smoluchowski coagulation theory showed that nanoparticles could precipitate the colloids immediately present in the surface water (Tao et al., 2016). In regards to the usage of nano coagulant in the process of coagulation and flocculation, it was found that the organic matter also can be removed in the wastewater as well as heavy metal ions by using silver nanoparticles (Tao et al., 2016).

In overall, in the process of coagulation, sludge contains heavy metals is formed due to the massive quantity of sediment congregation, which is due to the usage of coagulants. Hence, different solutions, such as reuse, recycling, and recovery of the sludge, are proposed for sludge management (Ahmad et al., 2016). Coagulation and flocculation can consider as an efficient heavy metal removal method from wastewater. However, the process can create secondary pollutants such as flocks. Also, required chemical solvents for the coagulation process are not reusable and can be harmful to both the human and environment.

2.2.5 Adsorption

One of the efficient and selective methods to remove heavy metal ions from water and wastewaters is adsorption. Adsorption is easy in operation and monitoring, and also can be an economical process for metal removal. Heavy metal ions are often significantly toxic and are non-biodegradable. Therefore, this process, as a primary physical or physicochemical process, plays an essential role in the heavy metal ions removal for the prevention of their harmful health influence on human beings. The process compared to chemical precipitation or ion exchange technologies proposes flexibility in design and operation and has the potential to many of the confines (Hu & Shipley, 2013). In the twentieth century, adsorption has gained great importance, as it played a significant role in many industrial separations and purification applications. The definition of the term “adsorption” was changed marginally over the time, but it has now been commonly considered as the concentration or accumulation of a certain component from a mixture onto the surface of the substrate exposed to the combination. As early as in the 18th century, to remove the toxic gases and discoloration of dye solutions, adsorption was efficiently applied (Hayes, 1970). As science and technology are being developed, more phenomena have been discovered due to the application of adsorption process. Several adsorbents have been advanced and used in many industries.

Moreover, different theories of this process have been advanced according to the distinctly observed adsorption phenomena. In recent years, adsorption has become progressively vital in numerous industrial applications, particularly for separation and purification (Chang et al., 2019; Chitsiga et al., 2018; Czikkely et al., 2018; Ibrahim & Fakhre, 2019; Ni et al., 2019; Sahmoune & Mohamed Nasser, 2019; Siyal et al., 2018). Adsorption can occur in some reactions, such as catalytic reactions that are essential in the chemical or petroleum industry. This process is also applied to the separation of gases and purification of liquids, which have varied applications in the disengagement and storage of gases, discoloration of dyes, refining of oils, concentration of bio-products, and removal of heavy metal ions (Chitsiga et al., 2018; Czikkely et al., 2018). To remove the organic compounds (likely volatile components) that cause odor and taste, adsorption is used accordingly (Lalezary et al., 1986).

2.3 Heavy metal removal by adsorption

2.3.1 General

Adsorption is one of the most efficient techniques for removing toxic heavy metals from water due to its significant advantages. Activated carbon, bio sorbents, carbon nanotubes, and some low-cost sorbents such as agricultural wastes, industrial products and wastes, and natural substances are used as common adsorbents for metal removal (Xu et al., 2018). Hence, it is observed that highly porous adsorbents can supply sufficient surface area for adsorption and showed a higher adsorption capacity. Nevertheless, parameters such as intraparticle diffusion may cause a decrease in the rate and adsorption capacity, particularly for macromolecules. For practical engineering applications, an optimum adsorbent involves small diffusion resistance and large surface area.

2.3.2 Characteristics of adsorbents

Adsorbents are the indispensable part, which assumes an important role in the adsorption process. The adsorption performances are related to the physical or chemical properties of the adsorbents, such as surface area, morphology, and surface functional groups. Therefore, it is needed that adsorbents with specified properties be advanced for the different industrial separation and purification applications. As a suitable adsorbent, the material should have excellent mechanical properties and be chemically stable, implying that it should be resistant to the acidic or basic environment.

Moreover, an excellent adsorbent must have a high surface area to weight ratio to attain a high capacity in adsorption of heavy metal ions. Furthermore, rapid adsorption kinetics is estimated for the adsorbents, so that the adsorption process can be significantly shortened. Other benefits can be regarded as the ease of reuse, recycling, and low cost, etc.

2.3.3 Type of adsorbents

2.3.3.1 Activated carbon

Activated carbon is considered as one of the traditional adsorbents which are widely used in various industrial applications for the heavy metal ions removal from wastewater. However, activated carbon is commonly recognized to have slow adsorption rate and low adsorption capacity and also shows poor selectivity towards a targeted type in the separation of heavy metal ions (Yang et al., 2019). The most common and significant adsorbent employed for hundreds of years is activated carbon. This adsorbent is produced through a heating treatment of carbon materials, which is done by steam or chemical treatment, due to providing higher specific surface area and porosity. Based on the range of pores, a different application can be optimized in this process. Activated carbon with micropores can provide a specific surface area as high as 1000 $m^2.g^{-1}$ (Ruthven, 1984). The application of this adsorbent dates back to the 18th century, which was used to remove odor from water. Even today, it is still widely used in the deodorization, and organic pollutants removal, such as dyes (Al-Ghouti & Sweleh, 2019) and benzene (Khan et al., 2019; Kutluay et al., 2019).

2.3.3.2 Chitin and chitosan

One of the poly-saccharides that exist abundantly in the skeleton of the Crustacea animals, particularly in the skeleton of crabs is chitin, which contains the $–NHCOCH_3$ groups. Moreover, chitin is also ample natural polymers in nature. Chitosan is the deacetylated form of chitin and is used in many applications. Chitin and chitosan are considered important adsorbents mainly for wastewater treatment. Chitosan has the chelation properties of heavy metal ions, which have been investigated as a separation mechanism for heavy metal removal (Anastopoulos et al., 2017; Zia et al., 2019).

2.3.3.3 Zeolite

It has been proved by several researchers that zeolite has an excellent cation exchange capacity for the removal of heavy metals (Hong et al., 2019). The structure of zeolite is crystalline, comprise of aluminium and silicate atoms, which are connected through oxygen bridges. Hence, Na(I), K(I), Ca(I), and Mg(II) are alkaline charge balancing cations responsible for the ion exchange efficiency of zeolites, and these cations bound electrostatically with the aluminium atoms. The previous study shows that zeolites have a great potential for the removal of chromium ions in indirect methodology as the zeolites are formerly altered to avoid the repulsion from the negative ions (Figueiredo & Quintelas, 2014). In other studies, zeolites were used as ion exchange for the removal of nickel, and the results showed an excellent removal efficiency of nickel. To remove Cd(II), Cu(II), Zn(II), and Pb(II) from wastewater, Jamil et al. were observed an approximately 98% of the metal removal through zeolites by using Egyptian Kaolin (Jamil et al., 2010). Three years later, Pepe et al. investigated the removal efficiency of Barium from wastewater by using Campanian ignimbrite, which is a natural zeolite tuff. As an exchange phase in the structure, Campanian ignimbrite comprises of chabazite and phillipsite, and the study was observed interesting results. (Pepe et al., 2013).

2.3.3.4 Calcium oxide/hydroxide

Natural deposits of limestone, whose main component is calcium carbonate ($CaCO_3$), are abundant, composing nearly three percent of the earth's crust. With abundant supply, low cost, extensive history for removing sulfur, and high removal capacity, the calcium oxide/calcium carbonate has the potential for economically removing heavy metal ions from water (Iakovleva et al., 2015; Inyang et al., 2016).

2.3.3.5 Magnesium oxide and Magnesium hydroxide

(a) *Production of magnesium hydroxide ($Mg(OH)_2$)*

Magnesium hydroxide ($Mg(OH)_2$) is a mineral found naturally in the crystalline limestone or as a product of magnesium silicates by decomposition. It can also be recovered from seawater, and the magnesium-containing brines and bitterns by precipitation, or it can be produced by the reaction of magnesium-containing minerals (such as magnesite or dolomite) with an acid followed by precipitation (Aral et al., 2004). In the laboratory, magnesium hydroxide is prepared by the reaction of magnesium oxide (MgO) obtained from magnesium carbonate ($MgCO_3$) with a range of hydrating agents, where water is the most preferred hydrating agent.

(b) *Magnesium hydroxide ($Mg(OH)_2$) from magnesium oxide (MgO)*

Magnesium hydroxide ($Mg(OH)_2$) is the product of magnesium oxide (MgO) by the hydration process. It includes the reaction of a specific quantity of Mg(II) with the hydrating agent and procedure of hydration (Tang et al., 2015). In terms of chemical, hydration means when the reaction of water takes place with a solid chemical compound, which leads to the making of a hydrated compound. Throughout this process, a specific amount of Mg(II) can react with a limited amount of hydrated solution, for specific periods and on a certain temperature. Furthermore, precipitate made here is dried and filtered off as well. During this process, a few of the chemical and physical properties can be investigated such as hydration kinetics, MgO surface properties, and the obtained products, hydration mechanism, and product mass, etc. (Cao et al., 2012).

(c) *Applications and uses of magnesium hydroxide ($Mg(OH)_2$)*

Magnesium hydroxide has been applied in many applications, such as; neutralization of acid effluents, flue gas scrubbing, and heavy metal ions removal from industrial wastewaters. Magnesium hydroxide can be incorporated into the structure of the polymer as smoke and flame-retardant filler, and as the precursor for the production of other magnesium chemicals. Moreover, in flue-gas desulphurization plants, Magnesium hydroxide can be replaced with lime and gypsum, specifically in incineration and power generation plants. Hence, scrubbing with lime produces gypsum has to be landfilled, though scrubbing with sodium hydroxide is costly (Aral et al., 2004). Magnesium hydroxide has medication benefits, such as laxative for short-term treatment of constipation and it also can help as an antacid for short-term relief of stomach upset (usually called ‘milk of magnesia’).

(d) *Application of magnesium hydroxide ($Mg(OH)_2$) in wastewater treatment*

Magnesium hydroxide can be used for the treatment of industrial wastewater as 58-62% of weight solids slurry to raise the solutions with high acidity. In terms of safety, magnesium hydroxide is particularly safer especially if being compared with other neutralizing compounds, e.g., sodium hydroxide (caustic soda) and lime, which are usually used for acidic metal-bearing industrial (Aral et al., 2004). Magnesium hydroxide is non-toxic, does not cause chemical burns, with the advantage of having a smaller chance of drastic pH changes when compared to lime and sodium hydroxide. The pH of the treated wastewater by $Mg(OH)_2$ will not exceed more than pH= 9-10, even by adding more $Mg(OH)_2$ into the solution. However, an increase in the amount of hydrated lime or sodium hydroxide will result in the pH=12 and higher, which is above the environmentally accepted alkalinity levels to discharge to the environment.

2.3.3.6 Synthetic polymer adsorbents

Recently many research has been conducted to synthesize the new polymers for the adsorption of heavy metals. Hence, in comparison with the conventional adsorbents, polymeric adsorbents may have numerous benefits as follows;

Firstly, depending on the type of applications, polymer adsorbents can be synthesized in various desirable shapes, such as beads, membranes, and fibers. Secondly, several techniques have been advanced through such processes as polymer brush formation, ligand immobilization, and molecular imprinting, to amend the surface and synthesize a vast family of adsorbents with different functions to meet the specific separation need for targeted adsorbents. And finally, functionalization can be used to achieve selective adsorption through functionalizing the polymer substrate with the appropriate ligands that have selectivity. More recent development about the need for new adsorbents with good selectivity to simplify the separation process and enhance bioengineering has brought productivity towards the target compound. Therefore, the synthetic polymer adsorbents can be the candidate for evolving new adsorbents with good selectivity.

(a) *Polyurethane foams*

Polyurethanes are synthesized by the reaction of a polyol $(-OH)_n$ (an alcohol with more than two reactive hydroxyl groups per molecule) with a diisocyanate (-NCO) or a polymeric isocyanate in the presence of catalysts and additives. Therefore, a variety of diisocyanates and polyols can be used to produce polyurethanes with specific applications.

Polyurethane foams were primarily advanced in the 1930s and started to develop after the 1940s (Lee et al., 2006). The main feature of polyurethane foams turns in proficiency to provide a wide range of cell structures, densities, inflexibility, and foam morphologies. Polyurethane foams are exceptionally probable in performance and known for their strength, surface feel, and robustness. Polyurethane foams can be classified into rigid, flexible, and semi-rigid/flexible Foams. Rigid polyurethane foams have high insulation capability accompanied by its rigidity; hence, primarily applied in construction, recreation, automotive and appliance applications. Alternatively, flexible polyurethane foams show exceptional elastic and deformation-recovery features as are made with a shorter polyol and less functional groups. Flexible polyurethane foams are proper to be used for furniture, packaging, and flexible hoses. From an economic point of view, polyurethane foam market involves a strong division due to using polyurethane foam in a wide range of industrial processes. High performance, lightweight properties along with rising demand from automotive, electronic appliances for usage in interior trims, refrigeration insulation, and seat cushioning should fuel the polyurethanes market growth. Government support for infrastructure development has facilitated the overall construction industry. The global industry spending was over USD 8 trillion in 2015 and projected to cross USD 10 trillion by 2020. Hence, China, along with Brazil, India, and Mexico, will be the key contributing countries. The product is widely used as an insulator in construction (Global Market Insights, 2017). However, the industry does face some challenges, comprising concerns over improper installations.

Regarding residential construction, walls and foundations are proposed to be the fastest-growing application. In commercial construction, roofing is considered the primary use but external walls will be the fastest-growing application at 23% once a year (Abo-Farha et al., 2009). The global polyurethane market is categorized into flexible foam, rigid foam, coatings, adhesives, elastomers, and sealants. Flexible polyurethane foam is extensively applied in automotive seating, upholstery, and bedding. Increasing nonrefundable income and changing lifestyles in developing economies such as Brazil, China, and India has caused the development of furniture industry. Increasing infrastructure spending in China, Brazil, UAE, India, Saudi Arabia, and Qatar are projected to fuel the request for rigid polyurethane foam. Another factor concerning market growth is the growing demand for electronic appliances like refrigerators. Polyurethane varnishes, due to their abrasion resistance and durability, are used for hardwood floors. In the formation of polyurethane, three primary chemical reactions are involved.

(b) *Foaming mechanism of polyurethane*

The foamed polymers production contains three stages within the polymer: firstly, is the implementation of gas, secondly, expansion of gas, and finally, stabilization of the polymer (Woods, 1982). In the implementation stage, the solubility limit of the gas in the polymer is considered as a predominant factor which depends on the surrounding pressure, temperature, and interaction with the polymer. The amount of gas blended or produced during the reaction into the polymer is a manageable processing parameter that affects the melt solution homogenization, foaming dynamics, and stabilization. As the gas solubility limit takes place, the gas phase tends to isolate from the polymer phase. According to the stability of the separated phases, two mechanisms initiate the foaming process viz. nucleation (NU) and spinodal decomposition (SD). Nucleation causes the formation of gas bubbles in the polymeric phase during foaming time. A nucleated bubble formed is referred to critical bubble, which is unsteady and also grows further. The bubble growth generates a concentration gradient in the system, causing the gas diffusion from the polymeric solution, which feeds the growth process. As nucleation is an unsteady phenomenon, growth takes place, expansion, and gas diffusion arise concurrently. Bubble growth is an intricate process containing mass, momentum, and heat transfer. Alternatively, spinodal decomposition is considered as a mechanism, a solution of two or more components can be divided into distinct phases with definitely diverse chemical compositions and physical characteristics. This mechanism due to spinodal decomposition happens regularly throughout the material and not just at separate nucleation sites, and it varies from the classical nucleation as phase separation.

The cell size and number in foams depends on the nucleation process. This process is a step in which energy is controlled, and the stable nuclei obtain energy to balance the opposing forces to grow. Unlike spinodal decomposition, nucleation does not happen consistently through the polymeric which changes the paths available for heat and mass transfer over the foam (Bowen, 1970; Sundarram et al., 2014; Venerus & Yala, 1997).

The foaming mechanism in PU foams has been studied extensively to understand the foaming models because of the simplicity of processing at room temperature and the absence of visual barriers to perceive the foaming process. Sites for nucleation and the polymerization reaction are concurrently being formed by agitating the pre-polymer mixture; the blowing agent starts bubble formation as well. Suitable catalysts and surfactants can perform the rate of the gelling and blowing reactions, which can generate a stable foam. The final foam characteristic is dictated by the ratio of the polyol and isocyanates. To gain sheets, blocks and firm, flexible or integral skin, polyurethane foams are produced by casting and reaction injection molding, respectively (Lee & Flumerfelt, 1996).

(c) *Polyurethane in water treatment*

The basic structure of polyurethane is based on the size and degree of crosslinking, chemical nature, molar mass, and distribution of hard and soft segments. These structures determine the secondary structure, such as the configuration of the polymeric chain, crystallinity, and ultimately the morphology of the polyurethanes. The last features of the polyurethanes are dependent on the chemical structure (Lee et al., 2006). However, tailoring the synthesis is an effective solution to alter the chemical structure to get the characteristic for an individual application. The above-mentioned properties of PU and their ease of processing has retracted the researchers to devise novel applications to use it in water treatment applications. Likewise, PU foam with open-pore structures for the removal of pollutants from water was developed another unique use of PU foam in water treatment.

The foamed polymer has been considered in sorption processes which date back to the past five decades (the 1970's). Extensive studies have been conducted on PU foams for the treatment of polluted water. For example, in 1970, Bowen proposed a new method of separation for organic and inorganic components by flexible polyurethane foam form water (Bowen, 1970). In 1971, Gesser et al. projected the use of untreated PU foams by a batch technique for organic contaminants sorption from the water (Gesser et al., 1971). The first applications of polyurethane foams for chromatographic separation were published by Braun and Farag. Farag et al. indicated that open-pore PU microspheres show low cation exchange capacity (Braun & Farag, 1972). The foams prepared by chemical bonding of specific functional groups (-SH), which was used to absorb mercury ions from mercury (II) chloride and methylmercury (II) chloride in the range of 0.4 to 400 ppb in their research. These studies showed that the use of loaded and unloaded PU foams (polyester and polyether type) for the determination of organic and inorganic species using separation and pre-concentration techniques. The application of chemical reagents to change the physical and chemical structure of the polyurethane caused an improvement of unloaded and loaded polyurethane foams. Loaded polyurethane foams experienced some chemical treatment while unloaded polyurethane foams were not treated with any reagents. Following the complex formation, unloaded polyurethane foams can only adsorb the metal ions. Hence, organic and inorganic ligands can be employed in this operation. Therefore, many batch and on-line processes have been determined in the following manner. In a batch test, for instance, the ions of molybdenum (VI) were quantitatively removed with unloaded polyurethane foams after thiocyanate complexes formation (Lemos et al., 2007). An on-line system was projected to determine the zinc in biological environments, where zinc (II) ions reacted on-line with thiocyanate ions, and the formed complexes were adsorbed in a mini-column packed including unloaded polyurethane foams (D. W. Lee & Halmann, 1976). Loaded polyurethane foams suggest a vast field of applications as compared to the unloaded polyurethane foams. However, it is possible to determine the loaded ligand if the process of extraction is selective or non-selective, i.e., multi-element. Loaded polyurethane foams can also be employed in batch or online operations as well. Polyurethane foam loaded with dimethylglyoxime was suggested for the selective extraction of nickel (Ramesh et al., 2001). Another study was conducted by using polyurethane foams loaded with piperidine dithiocarbamate, and a multi-element process was projected for concurrent preconcentration and determination of cobalt, cadmium, manganese, copper, nickel, lead and zinc in water (Proc. Conf., 1996). Both techniques were performed based on a batch operation, which resulted in the improvement in functionalized polyurethane foams in the late 90s.

Other research showed that to adjust the surface energy and develop the hydrogen bonding in polymers, functional groups such as hydroxyl, ketone and carboxylic acids have been found quite useful (Moawed et al., 2006). This feature causes an effective elimination of heavy metal ions either by adsorption or pre-concentration mechanisms. Since that time, functionalizing polyurethane foams has raised a lot of interest among scientists for PU surface modification and or structural modification. Hence, functionalization of PU foams by surface modification has led to the system capacity for the removal of heavy metal ions from water (Fournier et al., 2009; Krupadam et al., 2010; Rao et al., 2009). Polyurethane foam surface modification was carried out by Azevedo at al. and was examined for the removal of cobalt (II) and nickel(II) (Azevedo Lemos et al., 2006). In another study, polyvinyl acetate/acetone as the binding agent was used to prepare the composite ion exchange polyurethane foam by coating copper-ferrocyanide and hydrous manganese oxide powders. The composite was examined for the treatment of low-level radioactive liquid wastes such as cesium and strontium (Rao et al., 2009). In comparison with the copper-ferrocyanide/PU foam for cesium, the manganese oxide/PU foam had a higher exchange capacity for strontium. According to the ion exchange capacities, higher amounts of copper-ferrocyanide/PU foams were included in the cartridge.

Grafting acrylonitrile and acrylic acid by gamma irradiation method were used to modify the PU foams for removal of Zn(II), Fe(II), Ca(II), Ni(II), Cu(II), and Pb(II) by Meligi (Meligi, 2007). The adsorption process of heavy metal ions was affected by pH, atomic weight, and initial concentration of contaminants. The results indicated that the adsorption capacity of the grafted polyurethane foam was highest for Pb(II) ions as compared to the other metal ions evaluated in the study. The degree of adsorption affinity observed was Pb(II)> Ni(II)> Co(II)> Zn(II)> Cu(II) > Fe(II). The results showed that the ionic radii, ionic charge, electronic structure, and some hydration capacity of adsorbents are the man parameters to explain the change in the degree of adsorption affinity for different metal ions. Another study reported the synthesize of hydroxyapatite-PU foams (HPU) for Pb(II) removal (Jang et al., 2008). HPU is a main inorganic component of teeth, bones, and a natural source of phosphate, which has a great capacity for the removal of metal ions. Natural and synthetic HPU has gained a lot of interest to immobilize the Pb(II) ions from soil and water to understand the mechanism involved in the pb(II) removal and its application for filtration. By applying various weight percent of hydroxyapatite, the hydroxyapatite-PU composites were synthesized into a commercial PU-prepolymer (Jang et al., 2008). The study shows that the dispersion of hydroxyapatite on PU composite was uniform at 20 wt.% in comparison with the amount of 50 wt.%. The obtained composite foam was proficient at having a maximum adsorption capacity of 150 $mg.g^{-1}$ for the composite with 50 wt.% hydroxyapatite-PU after 48 hours of contact time. The result also determined that higher hydroxyapatite-PU concentration showed higher Pb(II) ion adsorption capacity. As the hydroxyapatite dispersed in the less uniformity state in the foam, it will cause slower adsorption, which is dominant at higher pH levels. Sone et al., synthesized another type of polyurethane composite foam containing alginate, which had a structure like that of a weak cation exchanger (Sone et al., 2009). The main component of brown algae is alginate, which has carboxyl functional groups. To produce the foam, a commercial pre-polymer mixture can be mixed with aqueous sodium alginate. The SEM image of the bulk foam indicated that the capacity of the PU alginate foam to adsorb Pb(II) ions was 3.3 mg.L^{-1} equivalent to 16 µmol.g^{-1} over 2 hours contact time. It was realized that the adsorption capacity is highly sensitive to the pH of the sample solution. Moreover, it was found that competing ions such as Mg(II), Ca(II), and Cd(II) lead to reduced selectivity and adsorption capacity of Pb(II) ions. Similarly, researchers have advanced numerous adsorption and ion exchange media according to polyurethane foams by changing the surface chemistry or the chemical structure of the PU foams. In another study, polyurethane foam was used with a sulphonic functional group. And, N,N-bis(2-hydroxylethyl)-2-aminoethanesulfonic acid was selected as a functionalizing agent because of two hydroxyl groups and a sulfonic acid group in the chemical structure (Yeon et al., 2002). The hydroxyl groups in N,N-bis(2-hydroxylethyl)-2-aminoethanesulfonic acid reacts with the remaining isocyanate groups in the polyurethane pre-polymer, which will lead to an extended chain pre-polymer. The sulfonic acid group in N, N-bis(2-hydroxylethyl)-2-aminoethanesulfonic acid is therefore accessible for the reaction at a later time. This functional group for a continuous electro-deionization process was used to deionize water. The ion exchange capacity of the functionalized PU foam was measured as 2.5 meq.g^{-1}, and the PU foam synthesized using N,N-bis(2-hydroxylethyl)-2-aminoethanesulfonic acid determined as a cation exchange media.

Recently, Kalaivani et al. were studied the synthesis of polyurethane resin for the removal of metal ions (Kalaivani et al., 2016b). In this study Ni(II) and Pb(II) was removed from water and the effect of several parameters such as contact time, the dosage of the adsorbents, pH, and initial metal ion concentration was studied for the removal of heavy metal ions. The results showed a high adsorption capacity and reported at 217.5, and 236.5 mg.g^{-1} for Ni(II) and Pb(II) ions in the batch test, respectively.

Moreover, a porous polyurethane was synthesized, and keratin was incorporated onto the polyurethane to synthesize a hybrid membrane. Porous polyurethane–keratin hybrid membrane was examined for the removal of chromium. The result indicated that keratin supply active sites for the biosorption of chromium and polyurethane was played a significant role as the support to protein (Saucedo-Rivalcoba et al., 2011). Another study reported that synthesized polyurethane foams were functionalized by sulfonic acid groups, which was found as a strong cation exchanger. The synthesized polyurethane foam was used to exchange Pb(II) ions from aqueous solutions (Gunashekar & Abu-Zahra, 2015). The maximum Pb(II) ions exchanged per gram of the polyurethane foam was determined to be 50-54 µg from 100 µg of Pb(II) in the solution.

Polyurethane forms were used by some other researchers for the removal of metal ions from water such as batch as column test for the removal of Ni(II) by Mangaleshwaran et al. (Mangaleshwaran et al., 2015), removal of Pb(II) by Gunashekar et al. (Gunashekar & Abu-Zahra, 2014) and Zhuang et al. (Zhuang et al., 2016), polyurethane foam modified by nanoclay for the removal of oil contaminants from water by Nikkhah et al. (Nikkhah et al., 2015), Carboxymethlyated cellulose nanofibrils (CMCNFs) embedded in PU foam for the removal of Pb(II), Cu(II), and Cd(II) from water (Hong et al., 2018), PU resin was synthesised and examined for removal of Pb(II), and Ni(II) by Kalaivani (Kalaivani et al., 2016a), Synthesis of PU cellulose acetate blend membrane for the removal of Cr(VI) (Riaz et al., 2016), and PU composite sponges were used for the removal of Hg(II) from water (W. Li et al., 2018).

2.4 Summary

From the above comprehensive review, it can be seen that adsorption is one of the efficient and selective methods to remove heavy metal ions from water, which is an operational and economical process for metal removal. As a great advantage of adsorption, a filtration system can be designed readily and established at any location with flooding for the case of urban stormwater runoff treatment. Filtration is one of the treatment procedures to eliminate heavy metals in stormwater. However, the filter media (adsorbent) requires to have a have high removal capacities for heavy metals and high hydraulic conductivity. Polymers have been investigated extensively in removing heavy metals and have been explored in terms of treatment efficiency and removal mechanisms of heavy metals. In particular, from the engineering aspect, polymers can be easily tailored in terms of strength, pore structure, and functionalization. Several kinds of polymers are being considered due to improvement in efficiency and selectivity in heavy metal ion separation. The flexibility in selection of the polymer structures and properties leads the polymeric adsorbents flexible for various adsorption applications. The considerable industrial production also provides polymer adsorbents properly for batch and packed column mode operation in small land and large scales operation simultaneously. In regard to heavy metal adsorption by polymers, synthesis of polyurethane (PU) has been developed for heavy metal removal from water and the modify PU foams show great potential for removal of various types of metal ions.

CHAPTER 3: METHODOLOGY

3.1 Introduction

As presented in chapter 2, in the last decade, many studies have been carried out to synthesis potential adsorbents for wastewater treatment applications. However, synthesis an adsorbent with a facile and economic method, which can have a great removal efficiency of heavy metal ions from water is a challenge.

In this study, not only a simple method but also a cost-effective route for the preparation of PU incorporated by nano metal oxides with high permeability was investigated. Besides, the synthesize of a media with an excellent removal efficiency of metal ions with high permeability, are potential to be used in column mode was one of the main targets. Thus, the separation process for the adsorbents with high permeability from water could be designed in a simple filtration process. Adsorbents with the mentioned advantages can be practical in real water treatment applications and may have the potential to be commercialized. Therefore, in the third chapter, PU/CaO (in section 3.3), and PU-FMH (in section 3.4) was examined for the removal of heavy metal ions through column mode by adjusting a short bed contact time. Several heavy metal ions such as Cu(II), Cd(II), Ni(II), Pb(II), and Zn(II) was selected as the reprehensive metal ions in the water. The interactions of PU/CaO and PU-FMH with heavy metals was studied and characterized by several methods. Urban stormwater runoff was simulated and was treated by PU/CaO, and the lifetime of PU/CaO was studied in a column mode.

Furthermore, PU-FMH was synthesized to achieve better removal efficiency. PU-FMH was examined for the removal of Cu(II), Cd(II), and Pb(II) in column mode, and the results showed an excellent removal efficiency of the metal ions. The flowchart of methodology of this study shows in Figure 3-1.

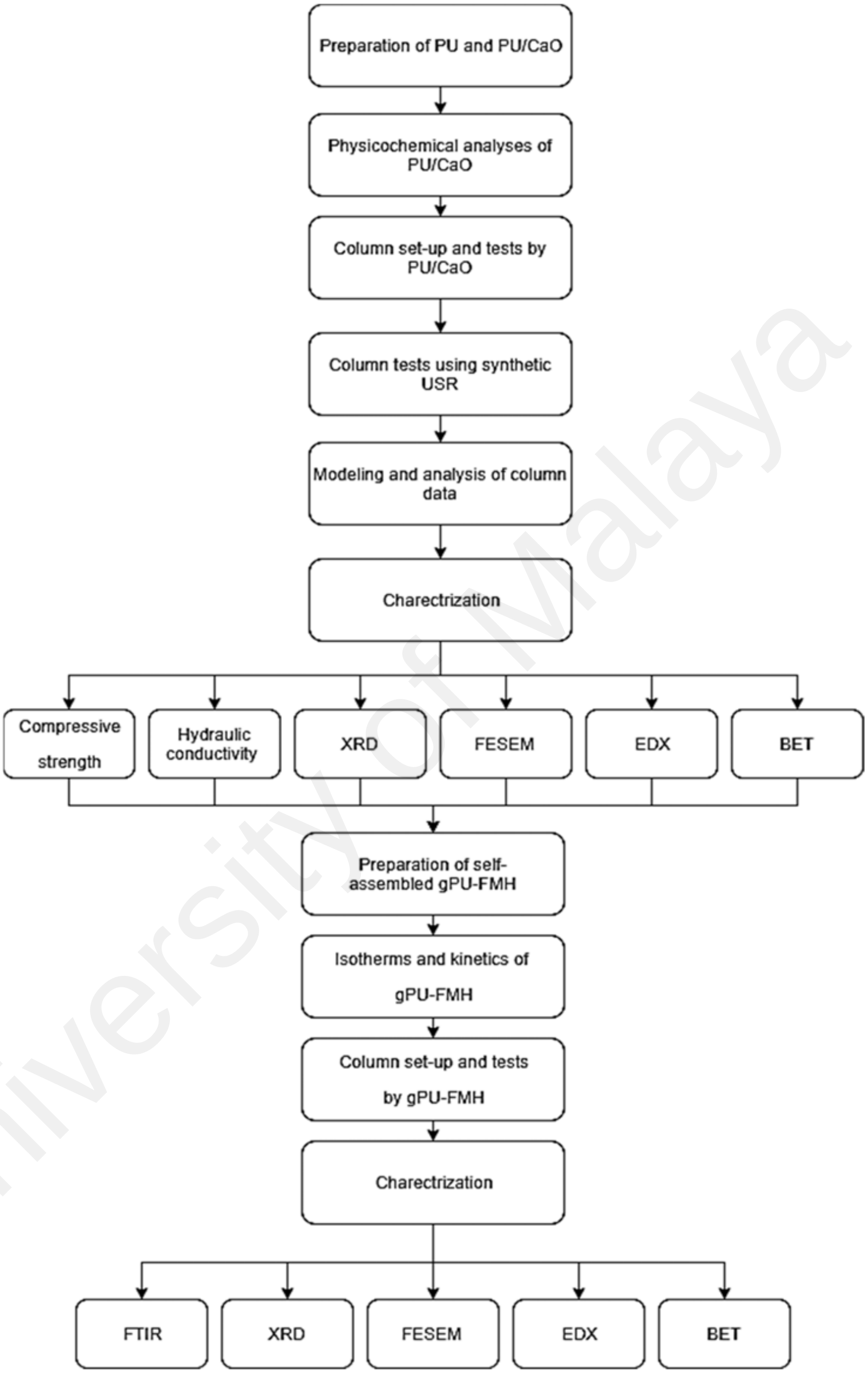

Figure 3-1: Flowchart of methodology

3.2 Chemical reagents

Polyol with chemical formula of $C_2H_6O_2$ and methylene diphenyl diisocyanate (MDI) with chemical formula of $C_{15}H_{10}N_2O_2$ were purchased from Portal Trading, Penang, Malaysia. Powdered Calcium oxide (CaO) with purity >99% was purchased from R&M Marketing, Essex, the United Kingdom. Commercial MgO powder with a purity of more than 99% was purchased from R&M Marketing, Essex from U.K. All aqueous solutions were prepared using deionized water with conductivity lower than 1 $\mu s.cm^{-1}$. NaCl was purchased from R&M Marketing, Essex, the UK with purity more than 99%. Stock solutions containing various heavy metals were prepared by dissolving the required amount of heavy metals salts namely: $Cu(NO_3)_2$, $Pb(NO_3)_2$, $Cd(NO_3)_2$, $Zn(SO_4)_2$, or $Ni(SO_4)_2$ with purity >99% purchased from Sigma-Aldrich, Malaysia in distilled water at room temperature and were used to prepare the feed solutions. Heavy metals in all prepared samples were analyzed by inductively coupled plasma atomic emission spectrometry (ICP-OES, Perkin Elmer, Optima 8300, U.S.A). The concentration of all prepared stock solutions was measured and checked before the experimental works.

3.3 Synthesis of polyurethanes (PU) incorporating calcium oxide (CaO)

3.3.1 Preparation of PU and PU/CaO

The PU materials were made by exothermic reactions between polyol, having reactive hydroxyl (-OH) groups, and MDI, containing the isocyanate group (-NCO). First, to determine the optimum combination of precursors for PU, 13 samples prepared with different ratios of polyol, MDI, and CaO were synthesized. Then, the compressive strength and density of the 13 PU/CaO samples were measured. PU/CaO composites were prepared by adding predetermined amounts of CaO to the mixture of polyol and MDI, which can be seen in Figure 3-2. To investigate the effect of CaO on heavy metal adsorption, the amount of CaO was varied from 0 to 25% of the total weight of polyol and MDI. The amounts of CaO were 0%, 5%, 10%, 20%, and 25% in PU, which corresponded to pure PU, PU/CaO-5, PU/CaO-10, PU/CaO-20, and PU/CaO-25, respectively. The chemical compositions of PU and CaO-loaded PU are shown in Table 3.1. First, 0, 2.5, 5.1, 10.2, or 12.8 g of CaO was hand-mixed with 17.0 g of polyol in paper cups for 60 seconds. Then, 34.0 g of MDI was added to the CaO and polyol mixture with stirring at 2,000 rpm for 20 s. The mixture was allowed to rise freely in the paper cup. Then, samples were kept at room temperature for 24 h after the cream time (the time from mixing to the initiation of foaming) and rise time (the time from mixing to full expansion of foaming) (Figure 3-3). All PU/CaO composites were cut (Figure 3-4A), and ground (Figure 3-4B). Then, they were sieved to collect 0.2–0.3-mm samples to be used for the column tests. Figure 3-5 (A-D) shows FESEM for all prepared PU/CaO samples with 5, 10, 20, and 25% of CaO, as (A) PU/CaO-5, (B) PU/CaO-10, (C) PU/CaO-20, and (D) PU/CaO-25, respectively.

Figure 3-2: Prepared PU/CaO samples

Table 3.1: Chemical composition and physical properties of different PU samples

No. Sample	Polyol (g)	MDI (g)	CaO (g)	Compressive strength (K.N/m^2)	Vol (mL)	Mass (g)	Density (g.cm^{-3})
1	17.0	17.0	7.65	175.56	900	35.30	0.04
2	34.0	17.0	7.65	23.04	1450	51.80	0.04
3	**17.0**	**34.0**	**7.65**	**261.70**	**900**	**53.00**	**0.06**
4	34.0	34.0	7.65	131.26	1750	64.00	0.04
5	17.0	25.5	5.10	191.96	940	43.00	0.05
6	34.0	25.5	5.10	89.03	1700	56.00	0.03
7	17.0	25.5	10.20	168.92	940	47.00	0.05
8	34.0	25.5	10.20	78.60	1650	35.00	0.02
9	25.5	17.0	5.10	85.56	1300	40.30	0.03
10	25.5	34.0	5.10	165.16	1300	58.00	0.04
11	25.5	17.0	10.20	79.84	1200	45.41	0.04
12	25.5	34.0	10.20	199.98	1300	61.50	0.05
13	25.5	25.5	7.65	118.78	1300	51.67	0.04

Table 3.2: Composition of PU/CaO and experimental design for column tests

No. Test	Polymer	PU/CaO (w/w) (%)	Preparation of PU/CaO (g)			Bed Height (mm)	Flowrate (mL.min^{-1})	Metal conc. (mmol.L^{-1})	Metal
			CaO	Polyol	MDI				
1	Pure PU	0.00	0.0	17.0	34.0	45.0	2.50	0.94	Cu(II)
2	PU/CaO-5	5.00	2.5	17.0	34.0	45.0	2.50	0.94	Cu(II)
3	PU/CaO-10	10.0	5.1	17.0	34.0	45.0	2.50	0.94	Cu(II)
4	PU/CaO-20	20.0	10.2	17.0	34.0	45.0	2.50	0.94	Cu(II)
5	PU/CaO-25	25.0	12.8	17.0	34.0	45.0	2.50	0.94	Cu(II)
6	PU/CaO-25	25.0	12.8	17.0	34.0	**45.0**	1.20	1.00	Cu(II)
7	PU/CaO-25	25.0	12.8	17.0	34.0	**35.0**	1.20	1.00	Cu(II)
8	PU/CaO-25	25.0	12.8	17.0	34.0	**25.0**	1.20	1.00	Cu(II)
9	PU/CaO-25	25.0	12.8	17.0	34.0	45.0	**1.20**	1.00	Cu(II)
10	PU/CaO-25	25.0	12.8	17.0	340	45.0	**0.50**	1.00	Cu(II)
11	PU/CaO-25	25.0	12.8	17.0	34.0	45.0	**2.50**	1.00	Cu(II)
12	PU/CaO-25	25.0	12.8	17.0	34.0	45.0	1.20	**1.00**	Cu(II)
13	PU/CaO-25	25.0	12.8	17.0	34.0	45.0	1.20	**0.54**	Cu(II)
14	PU/CaO-25	25.0	12.8	17.0	34.0	45.0	1.20	**0.31**	Cu(II)
15	PU/CaO-25	25.0	12.8	17.0	34.0	45.0	1.20	1.00	**Cu(II)**
16	PU/CaO-25	25.0	12.8	17.0	34.0	45.0	1.20	1.00	**Ni(II)**
17	PU/CaO-25	25.0	12.8	17.0	34.0	45.0	1.20	0.99	**Zn(II)**
18	PU/CaO-25	25.0	12.8	17.0	34.0	45.0	1.20	0.31	**Pb(II)**

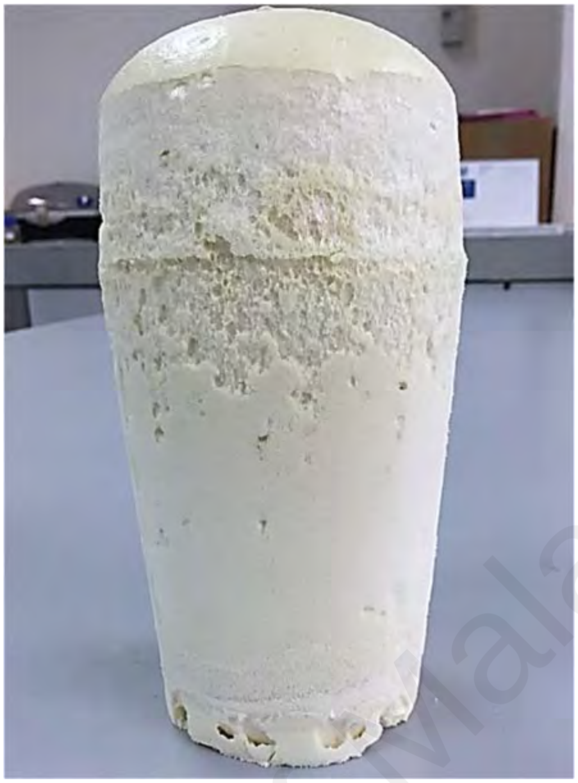

Figure 3-3: Synthesized PU/CaO-25

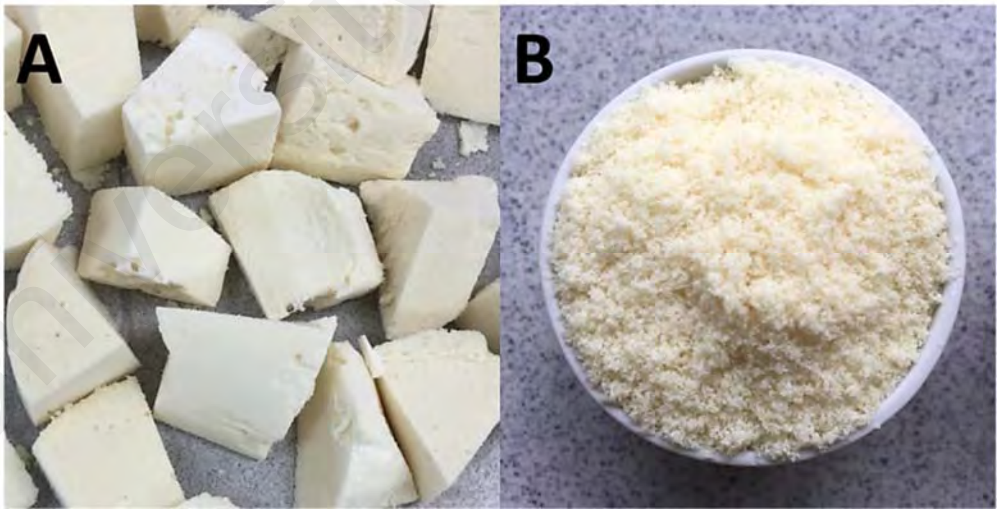

Figure 3-4: (A) cut into pieces and (B) ground PU/CaO-25

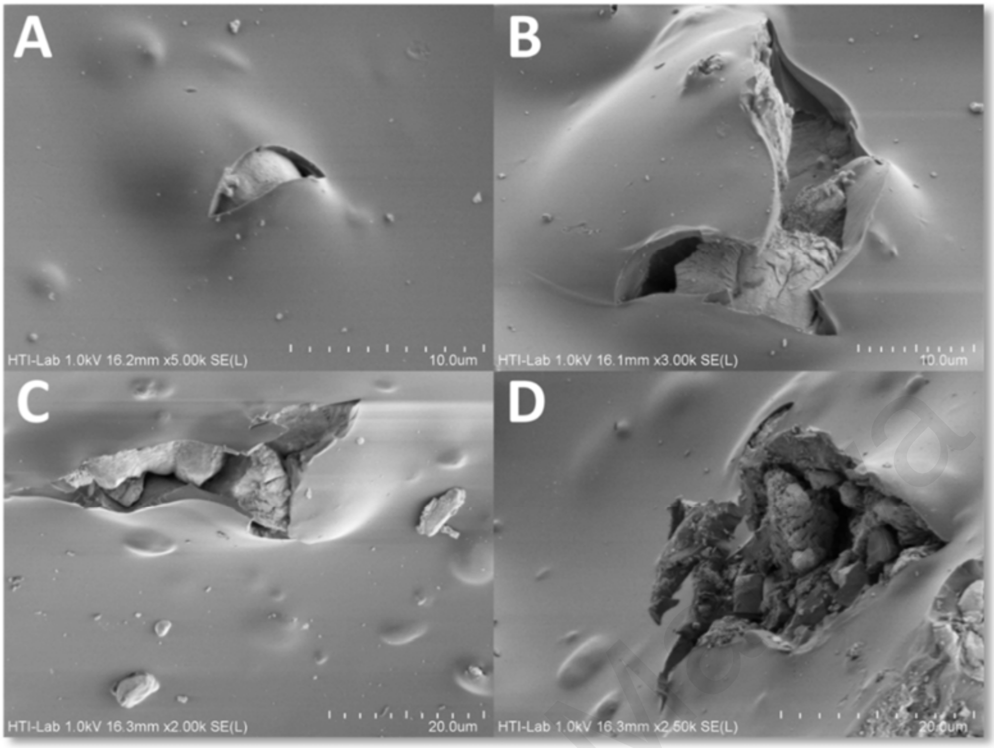

Figure 3-5: FESEM images of (A) PU/CaO-5, (B) PU/CaO-10, (C) PU-CaO-20, and (D) PU-CaO-25

3.3.2 Column set-up and tests by PU/CaO

The column tests were carried out with small-scale columns [16-mm inner diameter × 45-mm Length]. Glass wool was used at the bottom and top of the column (Figure 3-6). The prepared PU/CaO was added to the column, and distilled water was pumped into the column to remove loose particles of CaO. Then, a solution containing heavy metals was flowed into the column using a peristaltic pump at the designed flow rate, and samples at the outlet were obtained at various bed volumes (BVs). To avoid hydrolysis and precipitation of heavy metals due to high pH, the pH of the inlet water was adjusted to 4.0. Stock solutions of Cu(II), Ni(II), Zn(II), and Pb(II) at 0.31, 0.54 and 1 mmol.L^{-1} were prepared using DI water, at which the ionic strength was adjusted to 0.1 M using sodium chloride (NaCl). The column was run using an upflow mode to remove any channeling effect (Netpradit et al., 2004). The pH was measured at the column outlet. Continuous-flow column tests were conducted to assess the effects of important parameters such as CaO content, bed height, flow rate, concentration, and type of heavy metals, which can be seen in Table 3.2. However, the weight of CaO (g) used in PU/CaO (w/w) composite samples is based on the total mass of polyol and MDI, which was 17 and 34 g, respectively.

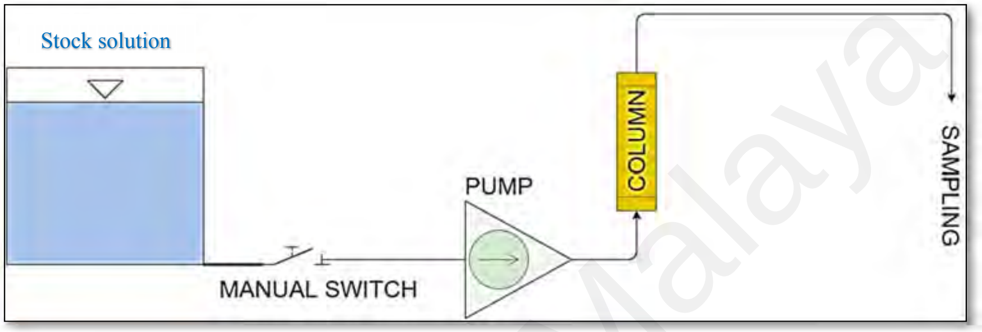

Figure 3-6: Schematic of column set-up

3.3.3 Column tests using synthetic USR

In this study, synthetic Urban Stormwater Runoff (USR) containing Cu(II), Zn(II), and Pb(II) was prepared by dissolving the required amount of heavy metals salts namely: $Cu(NO_3)_2$, $Pb(NO_3)_2$, and $Zn(SO_4)_2$ purchased from Sigma-Aldrich, Malaysia using tap water. The concentration of heavy metals in the synthetic USR was followed the actual USR data from Singapore which was published in June 2010 (Joshi & Balasubramanian, 2010) because its precipitation and urbanization are similar to Malaysia where few data are available. The results of the study in Singapore showed that the distribution of several heavy metals in water in urban runoff from residential and industrial sites was studied. 240 sequential urban runoff samples from 39 different locations were collected during the raining time. All the samples were analyzed for the measurement of several heavy metals such as Al(III), Cd(II), Cu(II), Fe(III), Pb(II), Ni(II), and Zn(II). All the samples were collected from January until November (in 2006) during the raining time by following two factors. The first factor was rainfall precipitation has to be more than 10 mm. The second factor was that the antecedent dry period between each sampling time was at least 24 hours. A total of 39 storm events were investigated with the total number of samples processed being 240. The reported concentration ranges for Cu(II), Zn(II), and Pb(II) were 44.8–241, 436.4–1127, and 52.3–90.3 $\mu g.L^{-1}$, respectively (Joshi & Balasubramanian, 2010). To start the experiments, firstly two columns were packed with 2.0 g of PU/CaO-25 with 45 mm of column bed height. Column tests were run at 0.5 and 1.2 $mL.min^{-1}$ flow rates to assess the effect of residence time in slow and fast conditions of USR for the removal of heavy metals. The column was run using an upflow mode to remove any channeling effect (Netpradit et al., 2004). Both columns were fed with synthetic USR with 320, 820, and 130 $\mu g.L^{-1}$ of Cu(II), Zn(II), and Pb(II), respectively. The operational pH was 6.9, while hardness and sulfate were 38 $mg.L^{-1}$ (as $CaCO_3$) and 10 $mg.L^{-1}$, respectively (Ong et al., 2007). In the tap water, other heavy metals, such as Al(III), Fe(III), and Ni(II), were also detected, at concentrations of 141, 298, and 30 $\mu g.L^{-1}$, respectively (Table 3.3).

Table 3.3: Water quality of simulated USR

Parameters	Values	Unit
pH	6.9	-
Copper	90.00	$\mu g.L^{-1}$
Zinc	259.00	$\mu g.L^{-1}$
Lead	95.00	$\mu g.L^{-1}$
Calcium	13,430.00	$\mu g.L^{-1}$
Magnesium	1073.00	$\mu g.L^{-1}$
Manganese	28.00	$\mu g.L^{-1}$
Iron	298.00	$\mu g.L^{-1}$
Cadmium	20.00	$\mu g.L^{-1}$
Sodium	12,250.00	$\mu g.L^{-1}$
Aluminum	141.00	$\mu g.L^{-1}$
Nickel	30.00	$\mu g.L^{-1}$
Hardness	38.00	mg $CaCO_3.L^{-1}$
Sulphate	10.00	$mg.L^{-1}$

3.3.4 Physicochemical analyses of PU/CaO

3.3.4.1 Compressive strength and hydraulic conductivity

The compressive strength of the PU/CaO-25 foam was measured with an Instron 600KN (Singapore). Samples were prepared at 95-mm diameter and 120-mm length. The tests were performed at a cross-head speed of 5 mm.min^{-1} according to ASTM D-1621 (Standard, 2010) at room temperature. Hydraulic conductivity (HC) tests were also conducted on PU/CaO-25 using a standard method (ASTM D 5856-95) (Standard, 2007). To prepare for the HC text, first, 105 g of PU/CaO-25 was filled inside the permeameter cell of 160-mm length and 74-mm inner diameter. Compaction was conducted to check for and avoid a preferential flow path between the inner wall and the medium. The inlet on the top of the permeameter was connected to the water tank. Manometers were connected to the top, middle, and bottom of the permeameter (Figure 3-7). Initially, a low flow rate was applied to the PU/CaO-25 to ensure uniform saturation. The HC was measured when the inlet and outlet flow rates were in steady state (Figure 3-8). To achieve steady state and validate the measurement of hydraulic conductivity, the water flow at the outlet was measured at various time points (30, 70, 150, and 300 s) for 7 days. The HC was determined according to the following equation (Eq 3.1):

$$K_C = \frac{QL}{Ath} \tag{3.1}$$

where K_C is HC (cm.s^{-1}), Q is the flow rate at the outlet (mL.s^{-1}), L is the length of the specimen along the path of flow (cm), *A* is the cross-sectional area of the specimen (cm^2), *t* is the time interval (s) over which the flow Q occurs, and *h* is the head level across the specimen (cm).

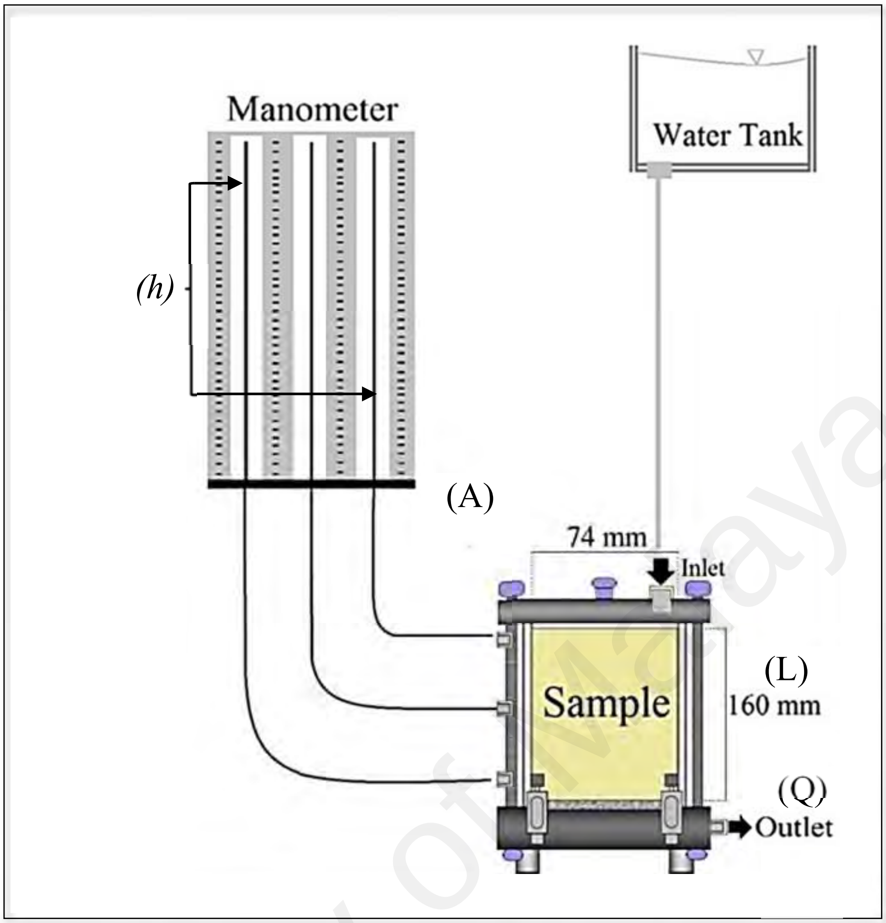

Figure 3-7: Hydraulic conductivity test schematic using permeameter

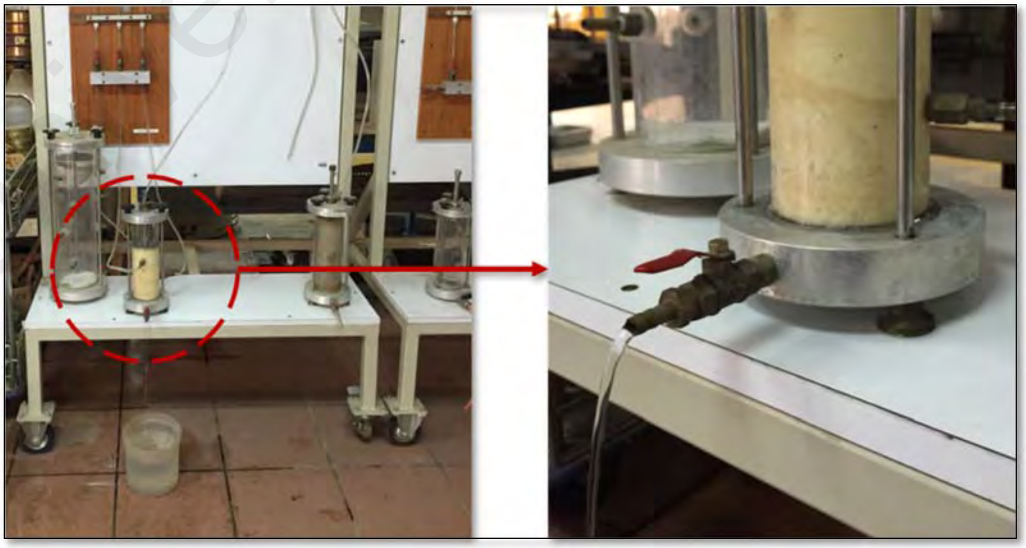

Figure 3-8: Hydraulic conductivity measurement of PU/CaO–25

3.3.4.2 XRD analysis

X-ray diffraction (XRD) analysis was performed on a Panalytical Empyrean X-ray diffractometer to determine the crystal structure of calcium carbonate, PU, and PU/CaO composites. Samples were placed in a small sample holder, and analysis 47 was conducted at angles from 5-70° 2θ with 2 seconds dwell time. The diffractometer was operated (with Cu Kα radiation, λ = 1.54443 Å) at 40 kV and 40 mA, at a step size of 0.02° 2θ.

3.3.4.3 FE-SEM and EDX analysis

SU 8000, FESEM (Hitachi, Japan) scanning electron microscope (SEM), fitted with secondary, gaseous secondary and backscattered electron detectors and a fully standardized EDX, X-ray analysis system (Bruker XFlash) were used to analyze a selection of samples. Samples were mounted on aluminium stubs by using adhesive graphite tape and sputter-coated with carbon using K450 sputter-coater prior to analysis to determine the most suitable imaging method for detection of precipitation pattern. Quantitative analysis of the chemical composition of samples was also conducted on the samples using an energy dispersive microanalysis of X-ray spectrometer (EDX) at an accelerating voltage of 20 keV. This was done to confirm that the crystals observed in the images were CaO crystals on the PU and to detect whether there was any precipitation of heavy metals on the surface of PU/CaO in the samples after adsorption process.

3.3.4.4 BET analysis

For BET analysis, a volumetric sorption analyzer (Micromeritics TriStar II 3020) was used to determine the specific surface area of the samples through nitrogen adsorption. Desorption branch of nitrogen isotherms [Barrett−Joyner− Halenda (BJH) method] was calculated. The specific surface areas were determined by the Brunauer-Emmett-Teller

(BET) method in the relative pressure range of 0.05-0.35 (in terms of p/pº, where p is the working pressure during BET analysis, and pº is the atmospheric pressure).

3.3.4.5 Heavy metal measurement

Heavy metals in all samples were analyzed by inductively coupled plasma atomic emission spectrometry (ICP-OES, Perkin Elmer, Optima 8300, U.S.A). The ICP was calibrated with five standard samples to get the calibration curve with the accuracy of correlation coefficient more than 0.99999 before starting the analysis of the samples. However, the four points that used to make the calibration curve was the blank 0 ppm (by using deionized water), 1 ppm, 3 ppm, 5 ppm, and 10 ppm to get correlation coefficient with accuracy more than 0.99999 before sample analysis.

3.3.5 Modeling and analysis of column data

3.3.5.1 Bed depth service time model

The bed depth service time (BDST) model is one of the most commonly used for the adsorption of heavy metals in column studies. The model was first proposed by Bohart and Adams and later modified by Hutchins (Hutchins, 1973). The analysis of BT curves was conducted using the BDST model. The BT point (BTP) was the time at which the metal concentration in the effluent peaked under conditions acceptable for the discharge of industrial effluent ("Standard A") in Malaysia (MDC Sdn Bhd, 1974). BDST is a model that describes the relationship between bed height (Z) and service time (t). It has been widely used for heavy metal liquid-solid systems, and the equation can be expressed as follows (Eq. 3.2):

$$t = \frac{N_0}{C_0 F} Z + \frac{1}{K_a C_0} \ln\left(\frac{C_0}{C} - 1\right) \tag{3.2}$$

where C_0 is the initial concentration of solute in the liquid phase (mg.L^{-1}), C is the effluent concentration of solute in the liquid phase (mg.L^{-1}), K_a is the sorption rate constant for the column (L.mg^{-1}.min^{-1}), N_0 is the adsorption capacity (mg.L^{-1}), F is the linear flow velocity of the liquid phase (m.min^{-1}), and Z is the length of the column bed (m). A linear relationship between service time and bed depth can be represented as (Eq. 3.3);

$$t = m_x - b \tag{3.3}$$

Where m_x is the slope of the BDST line, and the intercept of this equation (b) represents as (3.4). Thus, N_0 and K_a can be calculated from the slope (m_x) and the intercept (b) of the plot of t versus Z, respectively.

$$b = \frac{1}{K_a C_0} \ln\left(\frac{C_0}{C} - 1\right) \tag{3.4}$$

3.3.5.2 Chemical equilibrium diagram software Medusa

Medusa software is a database program to retrieve equilibrium constants for a desired chemical system. In this study, Medusa is used to find out the complicated equilibrium calculations and understanding the governing factors for chemical reactions. The application of chemical equilibria, including the precipitation equilibrium of metal ions and species distribution calculations, is demonstrated by Medusa software (Danna, 2015). Besides, Medusa allows the user to create different diagrams such as fraction and logarithmic concentration diagram, which can be seen in Figure 3-9.

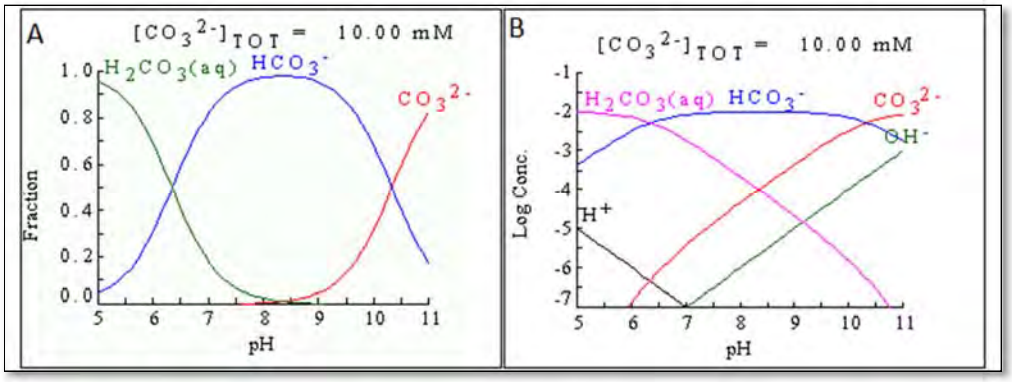

Figure 3-9: (A) Fraction, and (B) Logarithmic diagram of Medusa program

3.4 Synthesis of three-dimensional flowerlike magnesium hydroxide – incorporated granular polyurethane (gPU-FMH)

3.4.1 Preparation of self-assembled gPU-FMH

The PU material was synthesized using the exothermic reactions between the polyol with a reactive hydroxyl (–OH) groups and the MDI containing the isocyanate group (–NCO). The gPU was simply synthesized by the transferal of 17 (g) of the polyol into a paper cup, followed by the addition of 34 (g) of the MDI. The mixture was immediately stirred for a few seconds at room temperature using a mixer at the speed of 1,000 rpm. The prepared gPU was ground and sieved to the size range of 70–20 U.S. Mesh, which is equal to 210–841 µm of particle size.

Moreover, the water-absorption degree of the gPU was measured as 3 $mL.g^{-1}$. Then 18 g of the MgO were dissolved in 60 g of distilled H_2O. Once 20 g of the gPU was placed into a plastic bottle, the MgO suspension was gradually added and homogeneously mixed with the gPU. The description of all prepared samples was listed in Table 3.4 The gPU–MgO mixture was divided into three separated samples, and the different hydrothermal temperatures of 50°C, 80°C, and 120°C, corresponding to the gPU-FMH_{50}, gPU-FMH_{80}, and gPU-FMH_{120}, respectively, were applied for 24 h.

To investigate the roles of the gPU and the hydrothermal treatment for the synthesis of gPU-FMH$_{80}$, two control samples were prepared as follows: a control sample 1 (CS-1) was prepared using the same procedure as that of the gPU-FMH$_{80}$, but it was directly dried at 80°C for 24 h without an autoclave heating. For the control sample 2 (CS-2), the same gPU-FMH$_{80}$-synthesis procedure was applied to the MgO without incorporation of the gPU to investigate the effect of the gPU in the growth and formation of the 3D flowerlike structure, which can be seen in Table 3.4.

Table 3.4: The description for the preparation of growth, and control samples

Samples		gPU (g)	MgO (g)	Hydrothermal treatment	
				Temperature (°C)	Time (h)
Growth samples	gPU-FMH$_{50}$	20	18	50	24
	gPU-FMH$_{80}$	20	18	80	24
	gPU-FMH$_{120}$	20	18	120	24
Control samples	CS-1	20	18	-	-
	CS-2	0	18	80	24

3.4.2 Characterization of self-assembled gPU-FMH

The PANalytical Empyrean X-ray diffractometer (XRD) device (PANalytical Empyrean, The Netherlands) was used to obtain copper (Cu)-Kα-radiation (λ = 1.54443 Å at 40 kV and 40 mA) patterns for an assessment of the retention capacity of the gPU-FMH$_{80}$ regarding the Cu(II), Cd(II), and Pb(II) that correspond to the Cu(II)/gPU-FMH$_{80}$, Cd(II)/gPU-FMH$_{80}$, and Pb(II)/gPU-FMH$_{80}$, respectively.

A morphological study of the commercial MgO, gPU, gPU-FMH$_{50}$, gPU-FMH$_{80}$, gPU-FMH$_{120}$,Cu(II)/gPU-FMH$_{80}$, Cd(II)/gPU-FMH$_{80}$, and Pb(II)/gPU-FMH$_{80}$ was also conducted, for which the SU 8000 field-emission scanning electron microscopy (FE-

SEM) device (Hitachi, Japan) was used with the XFlash 6|30 energy-dispersive X-ray spectroscopy (EDX) device (Bruker, Germany) and the Octane Super EDX device (EDAX, U.S.A.).

The surface area was measured using the Brunauer–Emmett–Teller (BET) theory, while the pore-size distributions (PSDs) of the gPU, commercial MgO, and gPU-FMH$_{80}$ were calculated using the TriStar II 3020 surface-area and porosity analyzer (Micromeritics, U.S.A.) according to the desorption branch of the nitrogen (N) isotherms and the Barrett−Joyner−Halenda (BJH) method.

An infrared (IR) spectrum of gPU and gPU-FMH$_{80}$ was identified using the Tensor 27 Fourier transform infrared spectrophotometer (FTIR) device (Bruker, Germany) over the frequency range of 4000–400 cm^{-1} at a resolution of 4 cm^{-1}.

3.4.3 Isotherms and kinetics of gPU-FMH

The effect of the gPU-FMH$_{80}$ on the removal of the heavy metals, sorption isotherm, and kinetic tests were studied. For the isotherm studies, Cu(II), Cd(II), or Pb(II) containing H_2O were prepared with various concentrations ranging from 50–1400 mg.L^{-1} under a 0.1 M ionic strength (0.1 M NaCl). The pH value of the prepared solution was adjusted to 4±0.1 to avoid the possibility of the heavy-metal hydrolysis. For the isotherm study, 0.1 g of the gPU-MFH$_{80}$ was added to 100 mL of a heavy-metal solution, and it was then shaken for 24 h at room temperature (25±1°C) at 150 rpm. A mass of the heavy-metal ions that were absorbed at equilibrium, q_{eq} (mg.g^{-1}), was calculated using the following equation (Eq. 3.5):

$$q_{eq} = (C_0 - C_{eq})V/w \tag{3.5}$$

Where C_0 and C_e are the initial and equilibrium concentrations of the metal ions (mg.L^{-1}), respectively, and V and w are the solution volume and the adsorbent mass (g), respectively. The adsorption data were fitted with the Langmuir model, as follows:

$$q_{eq} = \frac{q_m K_L C_{eq}}{\left(1 + K_L C_{eq}\right)} \tag{3.6}$$

Where q_m is the maximum adsorption capacity and K_L is the equilibrium constant that is related to the adsorption energy.

For the kinetic studies, a 500-mL solution containing 500 mg.L^{-1} of the initial concentration of the Cu(II), Cd(II), or Pb(II) (0.1 M ionic strength) was poured into a conical flask, and 0.5 (g) of the gPU-FMH$_{80}$ was added to each solution. The pH of the solution was adjusted at the pH of 4±0.1, and the conical flask was shaken at 150 rpm for 24 h at room temperature (25±1°C). At specific time intervals, 5.0-mL samples were collected and filtered using a 0.45-µm-pore filter. The filtrates were analyzed using ICP-OES. The experimental data were fitted using a pseudo-second-order model, as follows:

$$\frac{1}{q_t} = \frac{1}{k_2 q_e^2} + \left(\frac{1}{q_e}\right) t \tag{3.7}$$

where k_2 is the rate constant of the second-order equation (g.mg^{-1}.min^{-1}), q_t is the amount of adsorption at a specific time (mg.g^{-1}), and q_e is the amount of adsorption at equilibrium (mg.g^{-1}). The parameters k_2 and q_e can be determined from the intercept and the gradient of the linear graph that is obtained from the plotting ($1/q_t$) versus t.

3.4.4 Column set-up and tests by gPU-FMH

Small-scale column tests were carried out in a column with a 16-mm internal diameter (ID) × a 50-mm length (L). Glass wool was used at the bottom and top of each column. Three columns were filled with 2.0 (g) of the gPU, 0.44 g of the commercial MgO, and 1.80 g of the gPU-FMH$_{80}$ and named column 1, column 2, and column 3, respectively.

The column was run using an upflow mode to remove any channeling effect (Netpradit et al., 2004). All the materials were washed by passing 100 mL of distilled H_2O through the columns before the treatment process. Then, the Cu(II) solution (65 mg.L^{-1} concentration of Cu(II) solution and, 0.1 M ionic strength) was flowed at a flow rate of 1.2 mL.min^{-1} [empty bed contact time (EBCT) of 7.5 min] into the columns using a peristaltic pump, and the samples at the outlet were obtained at various bed volumes. The initial pH of the Cu(II) solution was adjusted to 4.0±0.1 to avoid the hydrolysis and precipitation of the heavy metals. The breakthrough point, according to the Environmental Protection Agency (EPA) guideline (0.2 mg.L^{-1}) is the maximum acceptable discharge Cu(II) concentration regarding the environment. The ionic strength was also adjusted to 0.1 M using sodium chloride (NaCl).

CHAPTER 4: RESULTS AND DISCUSSION

4.1 Polyurethane incorporated calcium oxide (PU/CaO)

4.1.1 Effect of CaO on the PU matrix

PU media incorporating various amounts of CaO (0%, 5%, 10%, 20%, and 25%) were prepared and used to fill columns to a 4.5-cm height. Column tests were performed to investigate the effect of CaO amount incorporated into PU for removing Cu(II) from water. The Cu(II) solution with the initial concentration of 65 mg.L^{-1} or 1 mmol.L^{-1} was passed through the columns with a flow rate of 2.5 mL.min^{-1}.

Figure 4-1A shows the outlet concentrations of Cu(II) for all PU/CaO media for 800 BVs. It is clear that Cu(II) removal increased as the CaO amount increased, from 0% to 25%. PU/CaO-20, -15, -5, and pure PU removed dissolved Cu(II) up to 5, 4, 2, and 1 BVs, respectively. The Cu(II) concentration in the outlet increased sharply and 50% BT occurred at 9, 7, 4, and 2 BVs. However, PU/CaO-25 showed a higher removal capacity than the other media. For example, Cu(II) was completely removed by PU/CaO-25 until 8 BVs and increased slowly; 50% BT occurred after passing 116 BVs.

The pH profiles were also measured at the outlet during the column tests for all media and are presented in Figure 4-1B. The pure PU increased the pH from 4.0 to 7.0 for 5–6 BVs, followed by a dramatic decrease to 4.5. However, PU/CaO-5, -10, -20, and -25 showed pH increases to 8.7, 10.5, 10.8, and 11.1, and then the pH decreased gradually to 5, 6.1, 6.2, and 6.5 at 200 BVs, respectively. Thus, the CaO incorporated in the PU had a major effect in raising the pH.

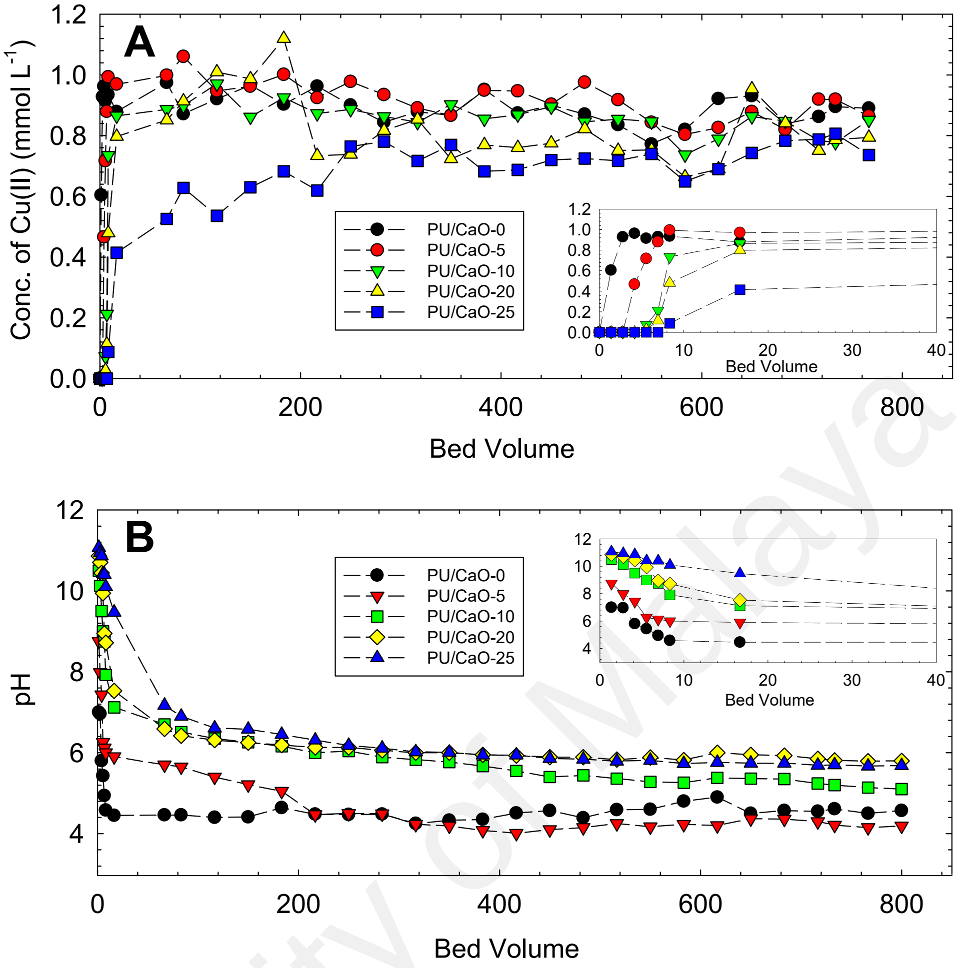

Figure 4-1: (A) Cu(II) concentration, and (B) pH changes at the outlet

Figure 4-2 shows the accumulated removal capacities (ARCs) of Cu(II) for all (PU/CaO) media, which were calculated by using the BT curve. The ARC was calculated using the following equation (Eq. 4.1):

$$ARC = QA = Q\int_{t=0}^{t=t_e} C_{Ad}\, dt \tag{4.1}$$

Where ARC (mg.g^{-1}) can be calculated by multiplying flow rate (Q, mL.min^{-1}) and area (A) under the BT curve that can be obtained by integrating the adsorbed Cu(II) concentration (C_{Ad}, mg.L^{-1}) at each time t (min). C_{Ad} can be calculated by subtracting the outlet concentration of Cu(II) from the inlet Cu(II) concentration (C_0).

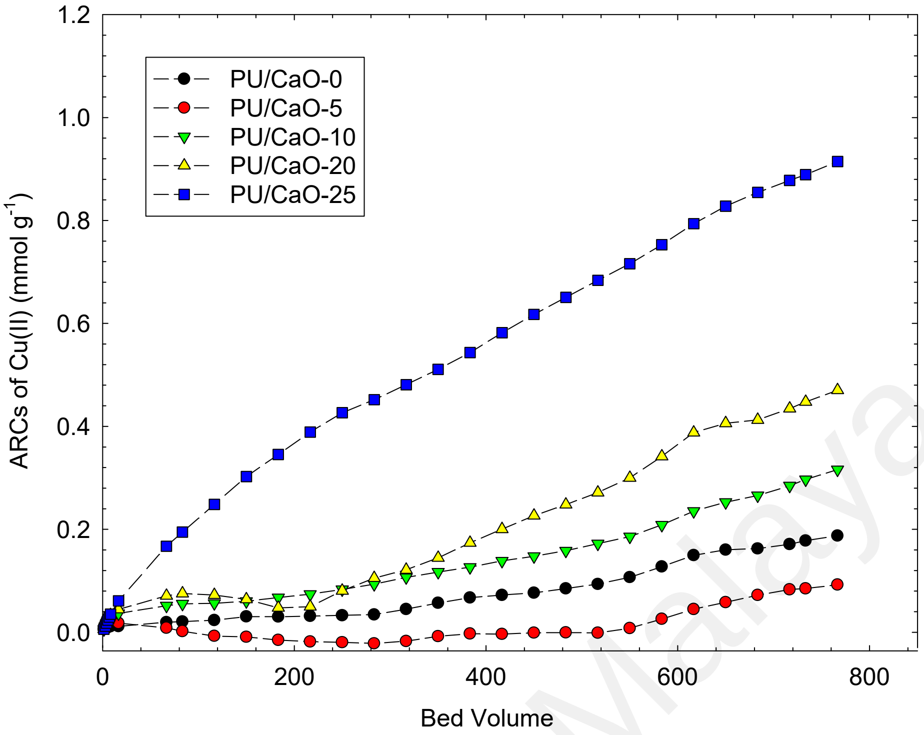

Figure 4-2: Accumulated removal capacities of Cu(II)

Figure 4-3 shows the Accumulated removal capacities (ARCs) according to the contents of CaO. Cu(II) uptake did not increase linearly with the increase in CaO, and PU/CaO-25 had a considerably higher ARC (0.94 mmol.g^{-1}) than PU/CaO-20 (0.47 mmol.g^{-1}) at 800 BV. Given these results, we suggest that the occupation site of CaO in the PU matrix for PU/CaO-20 and PU/CaO-25 may differ. In the case of 25% CaO incorporation, the higher amount of CaO may be more exposed at the surface and contact the solution, while at lower percentages CaO may exist predominantly within the frameworks of PU. This exposure of CaO could be a channel of hydroxide (OH^{-}) ions. Because PU/CaO-25 showed the highest removal efficiency, it was used in subsequent experiments.

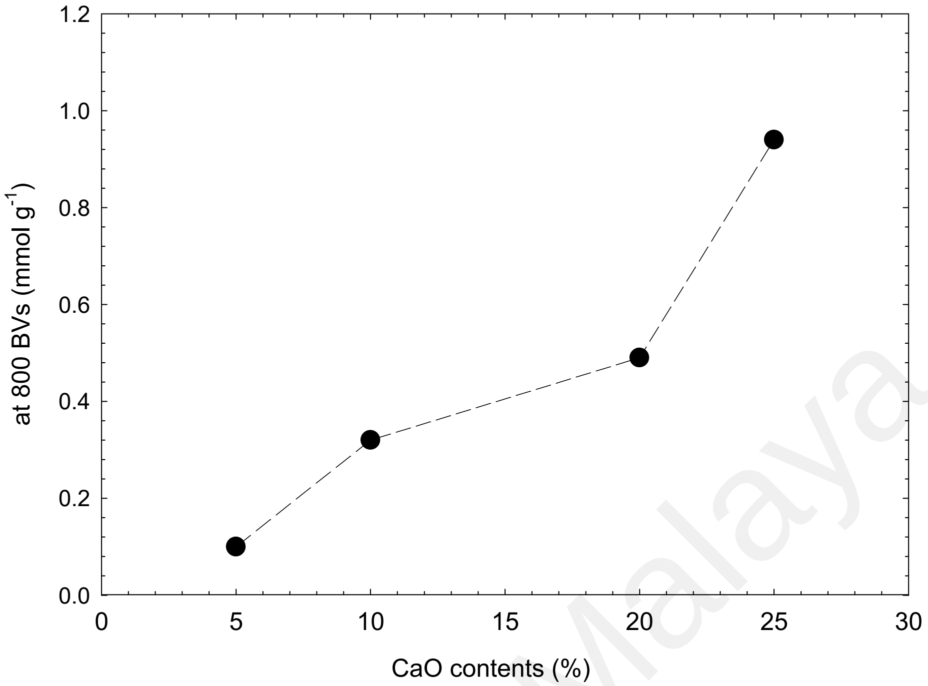

Figure 4-3: Accumulated removal capacities at 800 BVs with CaO contents

4.1.2 Effect of flow rate

The effect of flow rate was studied by varying it from 0.5 to 2.5 mL.min^{-1}. The initial concentrations of Cu(II) and the bed height were maintained at 1 mmol.L^{-1} and 4.5 cm, respectively. The BT profiles are presented in Figure 4-4A. The BTP decreased slightly, from 102 to 97 BVs, as the flow rate increased from 0.5 to 1.2 mL.min^{-1}. However, when the flow rate increased to 2.5 mL.min^{-1}, Cu(II) increased immediately at the outlet, and BTP was shortened significantly, to 9 BVs. Because the solute in the solution should have a sufficient time to penetrate and react with OH^{-}, a longer BTP could be obtained with a lower flow rate (Charumathi & Das, 2012; Vijayaraghavan et al., 2005b). Table 4.1 shows the ARCs of Cu(II) by PU/CaO-25 were 0.61 and 0.28 mmol.g^{-1} for 0.5 and 2.5 mL.min^{-1}, respectively, at 300 BVs. In more detail, when the flow rate decreased, N_0 and K_a increased, from 4,091 to 8,640 mg.L^{-1} and 0.27 to 0.31 L.mg^{-1}.h^{-1}, respectively.

Subsequent experiments were conducted at 1.2 mL.min^{-1}, which was selected as the optimum flow rate.

4.1.3 Effect of heavy metal concentrations

The effects of the influent concentration of metals (0.31, 0.54, or 1 mmol.L^{-1}) on the removal of Cu(II) by PU/CaO-25 were assessed under conditions of 4.5-cm bed height, and a 1.2 mL.min^{-1} flow rate (Figure 4-4B); the modeling parameters are presented in Table 4.1. Lower concentrations of Cu(II) in the inlet showed longer BTPs. PU/CaO-25 became saturated early at higher concentrations versus lower concentrations, and BTPs of Cu(II) removal were observed at 97, 100, and 110 BVs for 0.31, 0.54, and 1 mmol.L^{-1}, respectively. A lower concentration gradient caused the slower transport of metal ions due to a decrease in mass transfer diffusion (Aksu & Gonen, 2004; Uddin et al., 2009). With a higher concentration, the availability of metals for the adsorption sites is higher, leading to a higher uptake despite the BTP being shorter than that with a lower concentration. Better column performance at higher inlet metal concentrations might also be related to the higher driving force due to the greater differences in concentration between solid and solution phases. These results are consistent with the reports by Zulfadhly et al., Vijayaraghavan et al., and Porter et al. (Ko et al., 2000; Vijayaraghavan et al., 2005a; Vijayaraghavan & Prabu, 2006; Zulfadhly et al., 2001b). The highest ARC (0.60 mmol.g^{-1}) of Cu(II) with PU/CaO-25 was obtained at 1 mmol.L^{-1} Cu(II), which reported in Table 4.1.

4.1.4 Effect of column bed height

Column tests of Cu(II) removal by PU/CaO-25 was conducted to assess the effect of bed height. To generate different bed heights, 1.3, 1.7, and 2.0 g of PU/CaO-25 were added to the column to prepare bed heights of 2.5, 3.5, and 4.5 cm, respectively. Column tests were conducted at a 1.2 mL.min^{-1} constant flow rate and 1 mmol.L^{-1} initial Cu(II) concentration. Figure 4-4C shows that Cu(II) removal capacity was dependent on the amount of PU/CaO-25. When the bed height increased from 2.5 to 4.5 cm, BTPs (0.003 mmol.L^{-1} or 0.2 mg.L^{-1}) increased from 25 to 97 BVs. The increase in adsorption with greater bed depth was simply due to the increase in adsorbent mass, which provides more adsorption sites for metal ions (Zulfadhly et al., 2001a). Consequently, the diffusion of the metal ions into the sorbent and fluid residence time could increase as the bed height increased. Hence, the solute had sufficient time to diffuse into the entirety of the sorbent mass, treating more BVs in the solution (Hasan et al., 2010). By calculating the removal capacity of Cu(II) by BDST modeling, 2.5- and 3.5-cm bed heights showed 0.34 and 0.40 mmol.g^{-1} at 300 BVs, respectively. However, the 4.5-cm bed height exhibited the highest removal capacity (0.60 mmol.g^{-1}) and a longer column lifetime. K_a, N_0, and R^2 values are reported in Table 4.1.

Table 4.1: BDST parameters for sorption of Cu(II), Ni(II), Pb(II) and Zi(II)

Metals	Flowrate ($mL.min^{-1}$)	Concentration		Bed height (cm)	Slope (m_x) ($min.cm^{-1}$)	K_a ($L.mg^{-1}.h^{-1}$)	N_0 ($mg.L^{-1}$)	RT (Sec)	q_0		R^2	BTP (BV)
		$mmol.L^{-1}$	$mg.L^{-1}$						$mg.g^{-1}$	$mmol.g^{-1}$		
Cu(II)	0.5	1.00	65	4.5	-2933	0.31	8640	1080	38.8	0.61	0.99	102
	1.2				-3542	0.30	7914.2	450	35.6	0.60	0.99	97
	2.5				-3355	0.27	4091.0	216	18.4	0.28	0.92	9
Cu(II)	1.2	1.00	65	4.5	-3542	0.30	7914.2	450	35.6	0.60	0.99	97
		0.54	35		-4314	0.42	3531.6	450	15.8	0.24	0.98	100
		0.31	20		-3803	0.79	2202.7	450	9.9	0.15	0.99	110
Cu(II)	1.2	1.00	65	2.5	-1680	0.54	5759.7	250	22.1	0.34	0.96	25
				3.5	-2303	0.40	6315.5	350	26.0	0.40	0.97	52
				4.5	-3542	0.30	7914.2	450	35.6	0.60	0.99	97
Cu(II)	1.2	1.00	65	4.5	-3542	0.30	7914.2	450	35.6	0.60	0.99	97
Ni(II)		1.10			-4706	0.19	5940.5	450	26.7	0.45	0.96	36
Zn(II)		0.99			-2466	0.37	3226.1	450	14.5	0.22	0.80	25
Pb(II)		0.31			-2169	0.42	4397.4	450	19.7	0.09	0.86	66

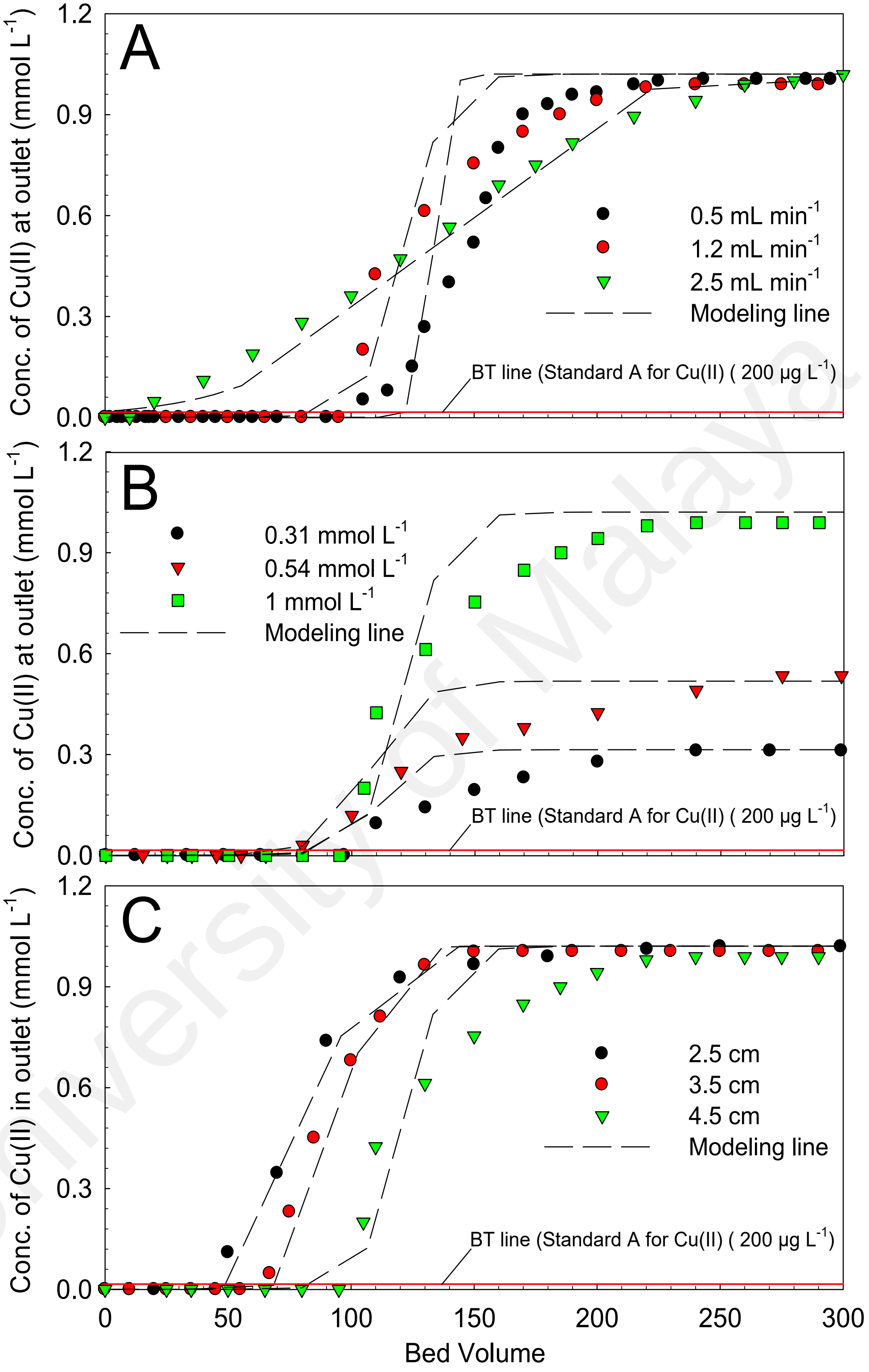

Figure 4-4: Effect of (A) bed height, (B) inlet Cu(II) concentration, and (C) flow-rate on Cu(II) removal

4.1.5 Bed depth service time

Figure 4-5 shows the plot of service time at 0.0157 mmol.L^{-1} BT versus bed height (cm) at a flow rate of 1.2 mL.min^{-1}. The plot was linear, and the correlation coefficient ($R^2 = 0.9734$) indicated the validity of the BDST model for the present system. The value of K_a characterizes the rate of transfer from the fluid phase to the solid phase. Generally, if K_a is large, even a short bed will avoid BTP, but as K_a decreases, a progressively longer bed is required to avoid BTP. The BDST model can be helpful in scaling up the process for other flow rates in the absence of experimental data or analysis (Vinodhini & Das, 2010). As shown in, by increasing the bed depth, the residence time of the fluid inside the fixed-bed column increased, allowing the metal ions to be removed. Thus, the bed capacity changed with bed height.

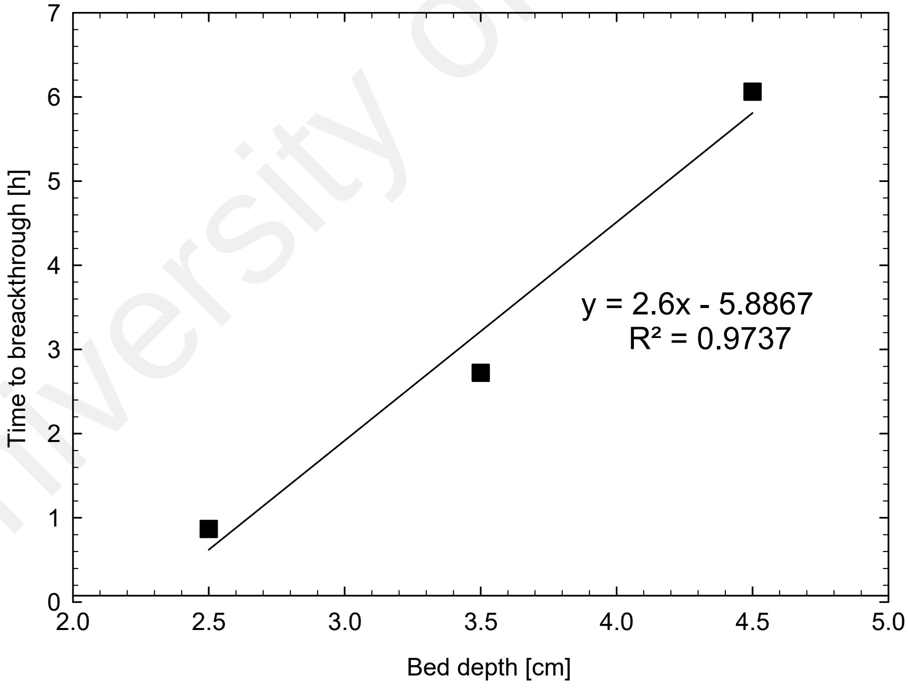

Figure 4-5: A plot of time to breakthrough according to bed depth

4.1.6 Mechanism of metal removal by PU/CaO-25

The BT curves for adsorption of Zn(II), Ni(II), Pb(II), and Cu(II) ions in the column are shown in Figure 4-6. Column tests were conducted at a 1.2 mL.min^{-1} constant flow rate and 65 mg.L^{-1} initial concentration at the column inlet. The sorption data matched well with BDST modeling and showed a normal S-type sorption curve (Mohan & Sreelakshmi, 2008). There are two domain mechanisms of metal removal by CaO: ion exchange and precipitation. At lower concentrations, ion exchange is dominant, while precipitation is the main mechanism at higher concentrations (Al-Degs et al., 2006). Due to the alkaline situation, CaO has positively charged species, such as $CaOH_2^+$ or $CaOHCa^+$. Then, positively charged metals can be exchanged for the metal species. When the pH is low, however, H^+ ions compete with metal ions and are even released from the adsorbed species, resulting in a low removal capacity. Amarasinghe and Williams reported that metal properties such as mobility, ionic radius, and hydration enthalpy could control metal adsorption (Amarasinghe. & Williams., 2007). Metal ions with a lower radius have a higher probability of reacting with cationic surfaces by ion exchange. When the hydration radius of the metal ions is larger than the surface cations, ion exchange can be difficult. The radius of Cu(II) is the smallest of the metal ions tested and even smaller than that of Ca(II). Thus, Cu(II) ions can react with Ca(II) by ion exchange. However, because of their larger radii, Ni(II), Pb(II), and Zn(II) may have weak affinities for the active sorption sites. Based on the column results, adsorption capacities were in the order Cu(II) > Ni(II) > Pb(II) > Zn(II), while BTPs were in the order Cu(II) > Pb(II) > Ni(II) > Zn(II). The maximum adsorption capacities of Cu(II), Ni(II), Pb(II), and Zn(II) are shown in Table 4.1. Metal precipitation occurs mainly with hydrolysis at higher pH values and concentrations (Yu et al., 2001). In this study, selective precipitation was interpreted using the chemical equilibrium-modeling software, 'Medusa.' Table 4.2 shows the soluble and solid species of individual metals, terms of reaction, and equilibrium constants (log K). Using the software, it was found that CuO (cr), $Pb(OH)_2$ (c), $Ni(OH)_2$ (c), and ZnO (cr) existed dominantly as solid species at pH > 6.5, 7, 8, and 9, respectively. Because the outlet pH of all columns was in the range 7–8, metal precipitation would be expected to occur in the sequence Cu(II) > Pb(II) > Ni(II) > Zn(II), which is identical to that for BTPs.

Table 4.2: Chemical equilibrium diagram for individual metal ions complexes

Metals	Soluble and solid pieces	Species	Reactions	Log K
Cu(II)	Soluble species	$Cu(OH)_2$	$Cu^{2+} = 2H^+ + Cu(OH)^2$	-16.2
		$Cu(OH)_3^-$	$Cu^{2+} = 3H^+ + Cu(OH)^{3-}$	-26.7
		$Cu(OH)_4^{2-}$	$Cu^{2+} = 4H^+ + Cu(OH)_4^{2-}$	-39.6
		$Cu(OH)_2^{2+}$	$Cu^{2+} = 2H^+ + Cu_2(OH)_2^{2+}$	-10.3
		$Cu_2(OH)^{3+}$	$Cu^{2+} = H^+ + Cu_2(OH)^{3+}$	-6.70
		$CU_3(OH)_4^{2+}$	$3Cu^{2+} = 4H^+ + Cu_3(OH)_4^{2+}$	-21.1
		$Cu(OH)^+$	$Cu^{2+} = H^+_+ Cu(OH)^+$	-7.90
	Solid species	$Cu(OH)_{2\ (C)}$	$Cu^{2+} = 2H^+ + Cu(OH)_{2\ (c)}$	-8.60
		$CuO_{\ (Cr)}$	$Cu^{2+} = 2H^+ + CuO_{\ (c)}$	-7.60
Pb(II)	Soluble species	$Pb(OH)_2$	$Pb^{2+} = 2H^+ + Pb(OH)^2$	-17.1
		$Pb(OH)^{3-}$	$Pb^{\ 2+} = 3H^+ + Pb(OH)^{3-}$	-28.0
		$Pb(OH)_4^{2-}$	$Pb^{\ 2+} = 4H^+ + Pb(OH)_4^{2-}$	-39.7
		$Pb_2(OH)^{3+}$	$2Pb^{\ 2+} = H^+ + Pb_2(OH)^{3+}$	-6.36
		$Pb_3(OH)_4^{2+}$	$3Pb^{\ 2+} = 4H^+ + Pb_3(OH)_4^{2+}$	-23.8
		$Pb_4(OH)_4^{4+}$	$4Pb^{\ 2+} = 4H^+ + Pb_4(OH)_4^{4+}$	-20.8
		$Pb_6(OH)_8^{4+}$	$6Pb^{\ 2+} = 8H^+_+ Pb(OH)_8^{4+}$	-43.6
		$Pb(OH)^+$	$Pb^{\ 2+} = H^+ + Pb(OH)^+$	-7.70
	Solid species	$Pb(OH)_{2\ (C)}$	$Pb^{2+} = 2H^+ + Pb(OH)^2_{(c)}$	-8.15
		$PbO_{\ (Cr)}$	$Pb^{2+} = 2H^+ + PbO_{\ (Cr)}$	-12.9
		$Pb(OH)_{2\ (C)}$	$2Pb^{2+} = 4H^+ + PbO : Pb(OH)^2_{(C)}$	-26.2
Ni(II)	Soluble species	$Ni(OH)_2$	$Ni^{2+} = 2H^+ + Ni(OH)^2$	-20.0
		$Ni(OH)^{3-}$	$Ni^{2+} = 3H^+ + Ni(OH)^{3-}$	-29.7
		$Ni(OH)_4^{2-}$	$Ni^{2+} = 4H^+ + Ni(OH)_4^{2-}$	-45.0
		$Ni_2(OH)^{3+}$	$2Ni^{2+} = H^+ + Ni_2(OH)^{\ 3+}$	-9.80
		$Ni_4(OH)_4^{4+}$	$4Ni^{2+} = 4H^+ + Ni_4(OH)_4^{4+}$	-27.9
		Ni(OH)+	$Ni^{2+} = H^+ + NiOH^+$	-9.50
	Solid species	$Ni(OH)_{2\ (C)}$	$Ni^{2+} = 2H^+ + Ni(OH)^2{}_{\ (C)}$	-10.5
		$NiO_{\ (C)}$	$Ni^{2+} = 2H^+ + NiO_{(C)}$	-12.4
		$Ni(O)_{(Cr)}$	$Ni^{2+} = 2H^+ + NiO_{(Cr)}$	-12.6
Zn(II)	Soluble species	$Zn(OH)_2$	$Zn^{2+} = 2H^+ + Zn(OH)^2$	-16.4
		$Zn(OH)^{3-}$	$Zn^{2+} = 3H^+ + Zn(OH)^{3-}$	-28.2
		$Zn(OH)_4^{2-}$	$Zn^{2+} = 4H^+ + Zn(OH)_4^{2-}$	-41.3
		$Zn_2(OH)_6^{-2}$	$2Zn^{2+} = 6H^+ + Zn_2(OH)_6^{2-}$	-54.3
		$Zn_2(OH)^{3+}$	$2Zn^{2+} = H^+ + Zn_2(OH)^{3+}$	-9.00
		$Zn_4(OH)_4^{4+}$	$4Zn^{\ 2+} = 4H^+ + Zn_{\ 4}(OH)_4^{4+}$	-27.0
		$Zn(OH)^+$	$Zn^{\ 2+} = H^+_+ Zn\ (OH)^+$	-7.50
	Solid species	$\alpha\text{-}Zn(OH)_{2\ (Cr)}$	$Zn^{\ 2+} = H^+ + \alpha\text{-}Zn(OH)^+$	-12.4
		$\varepsilon\text{-}Zn(OH)_{2\ (Cr)}$	$Zn^{2+} = 2H^+ + \varepsilon\text{-}Zn(OH)^2{}_{\ (Cr)}$	-11.5
		ZnO (Cr)	$Zn^{2+} = 2H^+ + ZnO_{\ (Cr)}$	-11.2

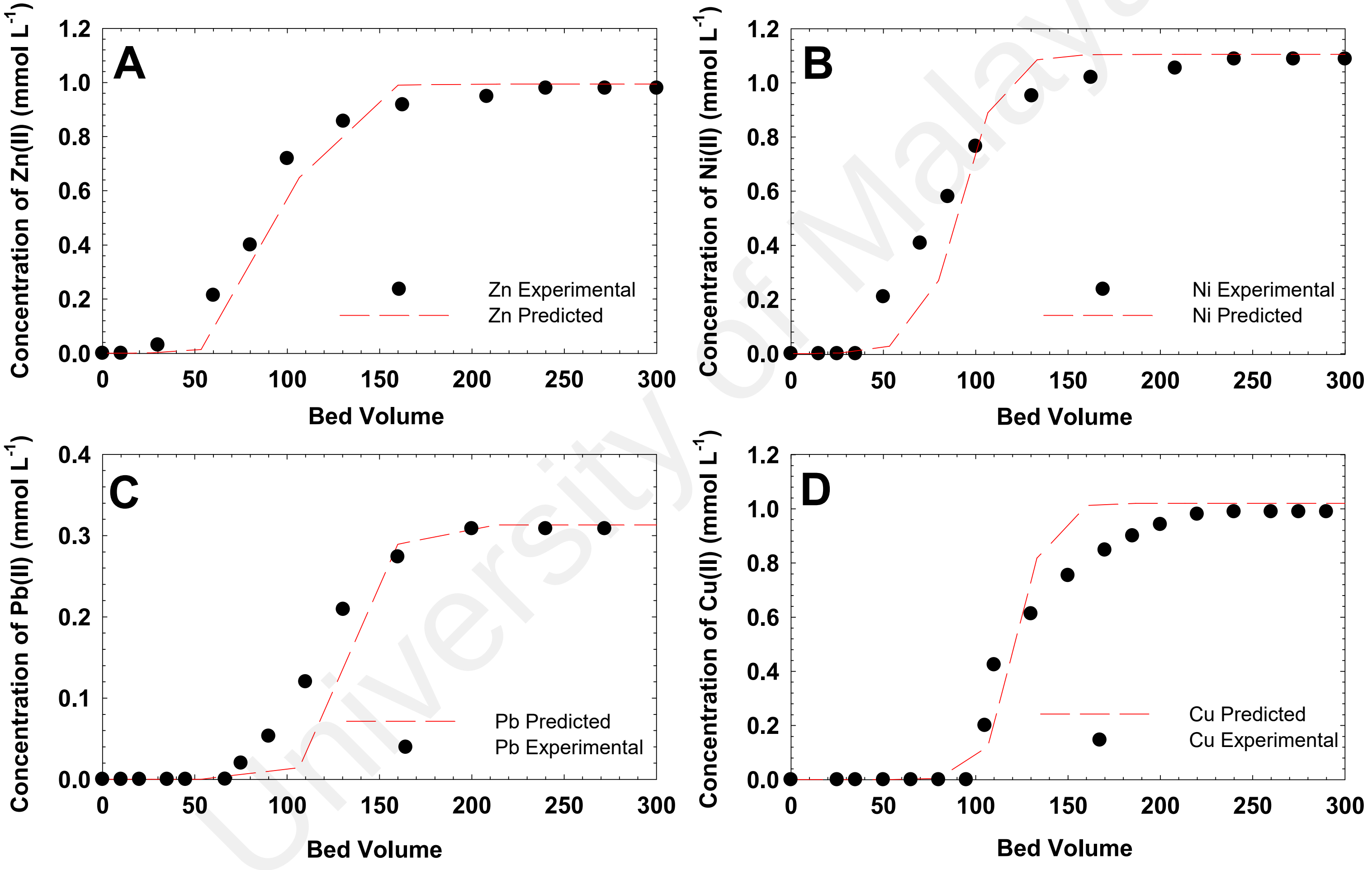

Figure 4-6: Different type of heavy metals removal by PU/CaO-25

4.1.6.1 SEM-EDX

SEM-EDX was used to evaluate the surface morphological changes of pure PU, PU/CaO-25, Pb(II)-retained PU/CaO-25, and Cu(II)-retained PU/CaO-25. Figure 4-7 shows pure PU had a smooth surface without pores (Choi et al., 2014), while the surface was torn at the domain of CaO when 25% CaO was incorporated into the PU framework, shown in Figure 4-8. Figure 4-9 shows the elemental mapping of C, O, and Ca, respectively, for PU/CaO-25, indicating that CaO on the surface of PU. Figure 4-10 shows the EDX analysis of PU/CaO-25 and the existence of CaO on the surface of PU.

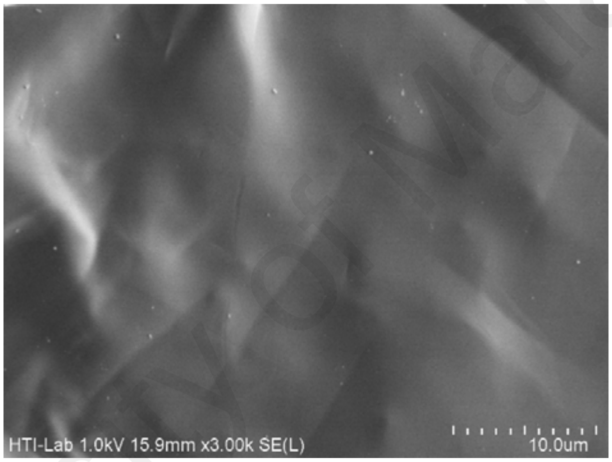

Figure 4-7: Low magnification FESEM image of pure PU

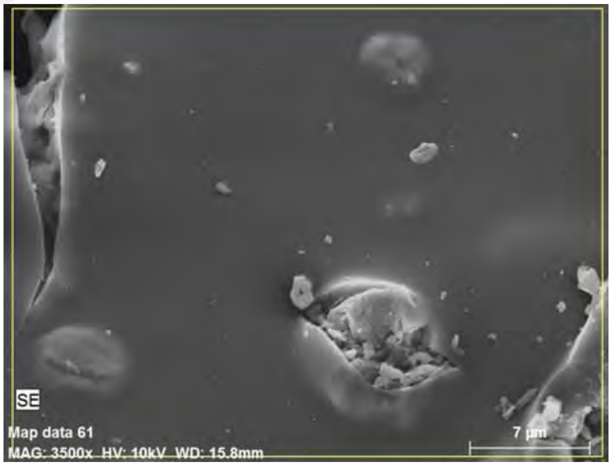

Figure 4-8: Low magnification FESEM image of PU/CaO-25

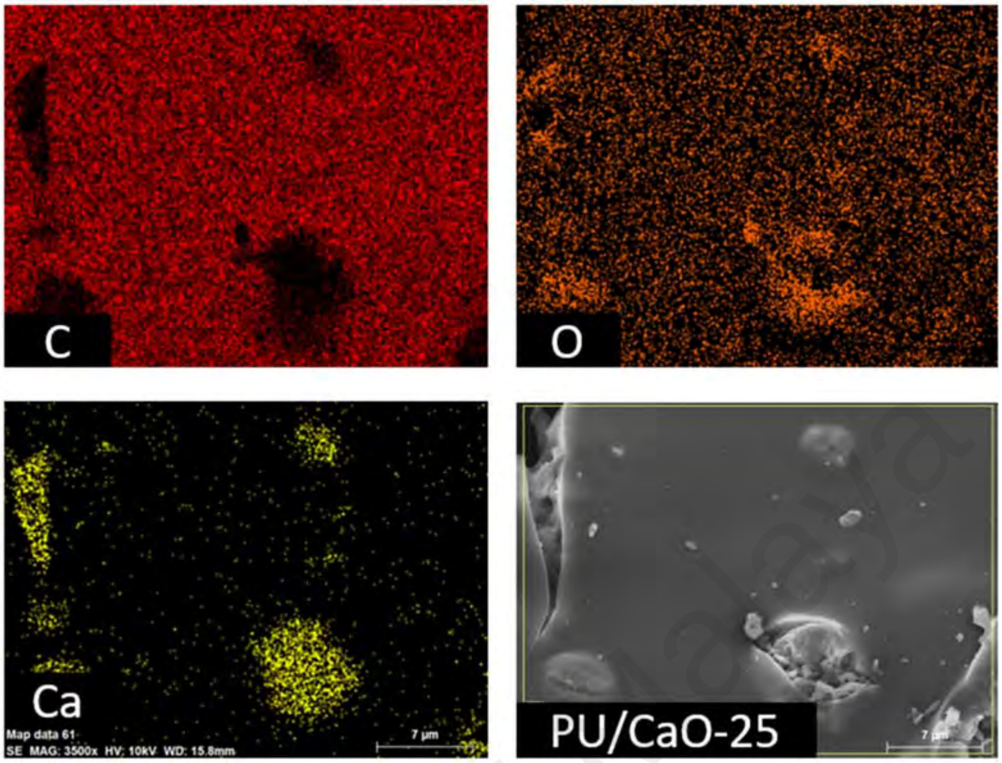

Figure 4-9: Elemental mapping of PU/CaO-25

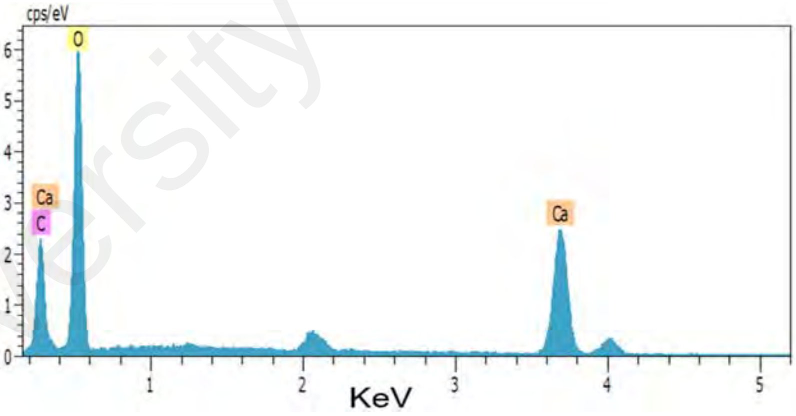

Figure 4-10: EDX analysis of PU/CaO–25

Figure 4-11 shows the morphology and elemental (C, O, Ca, Cu, and Cu) mapping of Cu(II)-retained PU/CaO-25. The major finding was that the locations of Ca(II) and Cu(II) were different. Ca(II) existed mostly under the surface while Cu(II) was on the surface, although not homogeneously distributed. At the stripped parts, Ca(II) was not detected so that the CaO may have dissolved out. Thus, we suggest that PU/CaO-25 provides an environment that facilitates retention of metal precipitates without occupying the surface of the CaO. Besides, similar results of Pb(II) removal were observed for Pb(II)-retained PU/CaO-25. The morphology and elemental (C, O, Ca, Cu, and Pb) mapping of Pb(II)-retained PU/CaO-25 can be seen in Figure 4-12. The EDX analysis Figure 4-13A and B revealed that Cu(II) and Pb(II) was precipitated and present predominantly on the surface of the PU, respectively.

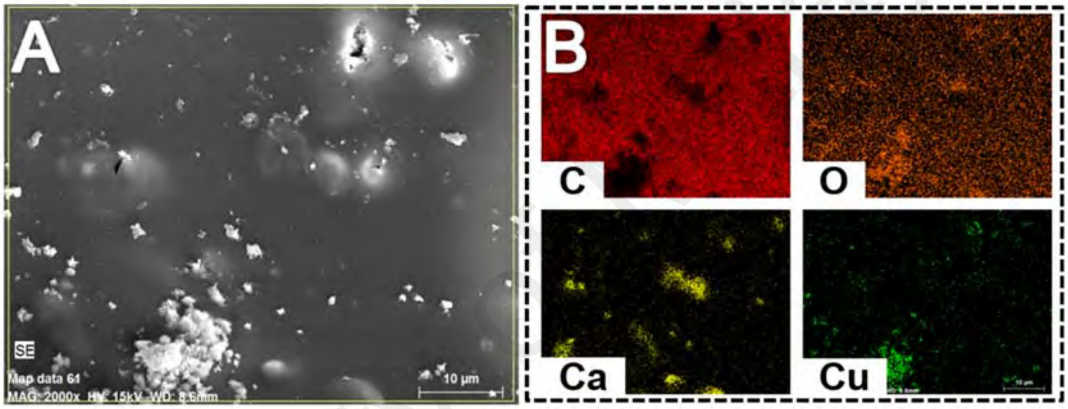

Figure 4-11: (A) FE-SEM image, and (B) Elemental mapping of Cu(II) retained PU/CaO–25

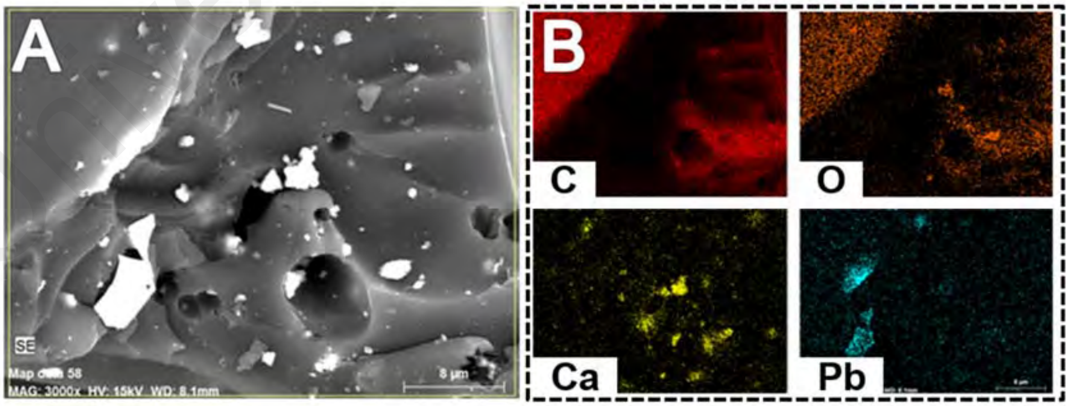

Figure 4-12: (A) FE-SEM image, and (B) Elemental mapping of Pb(II) retained PU/CaO–25

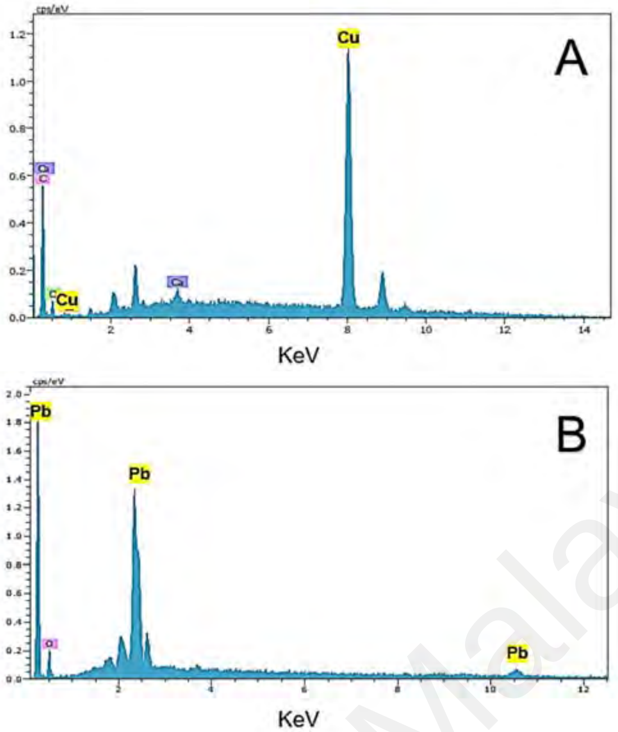

Figure 4-13: EDX for (A) Cu(II), and (B) Pb(II) retained PU/CaO–25

4.1.6.2 XRD Analysis of PU/CaO

XRD was used to investigate the phase structures of the PU/CaO-25, and Cu(II)- and Zn(II)-retained PU/CaO-25 and can be seen in Figure 4-14. Sharp peaks at 64°, 18°, 48°, and 51° were assigned to $Ca(OH)_2$ (JCPDS file 84-1264), indicating that CaO is hydrated during the synthesis of PU/CaO-25 and located mostly on the surface of the PU. Weak peaks at 29°, 34°, 54°, and 63° were assigned to CaO (JCPDS file 77-2376) and were noticeable because CaO was covered by a PU framework. XRD analysis also confirmed that the precipitates of Zn(II) were ZnO (47°, 56°) and $Zn(OH)_2$ (33°), while those of Cu(II) were CuO (32°, 46°, 48°, 56°) and $Cu(OH)_2$ (57°). The intensities of the CaO peaks for PU/CaO-25 were similar to those for metal-retained PU/CaO-25, while the $Ca(OH)_2$ peaks were much reduced. From this result, we suggest that CaO was trapped in the framework of polymer and its hydrated form, $Ca(OH)_2$, mostly located at the surface, was used to remove Cu(II) or Zn(II). Thus, precipitation may be the dominant removal mechanism, as indicated by the modeling.

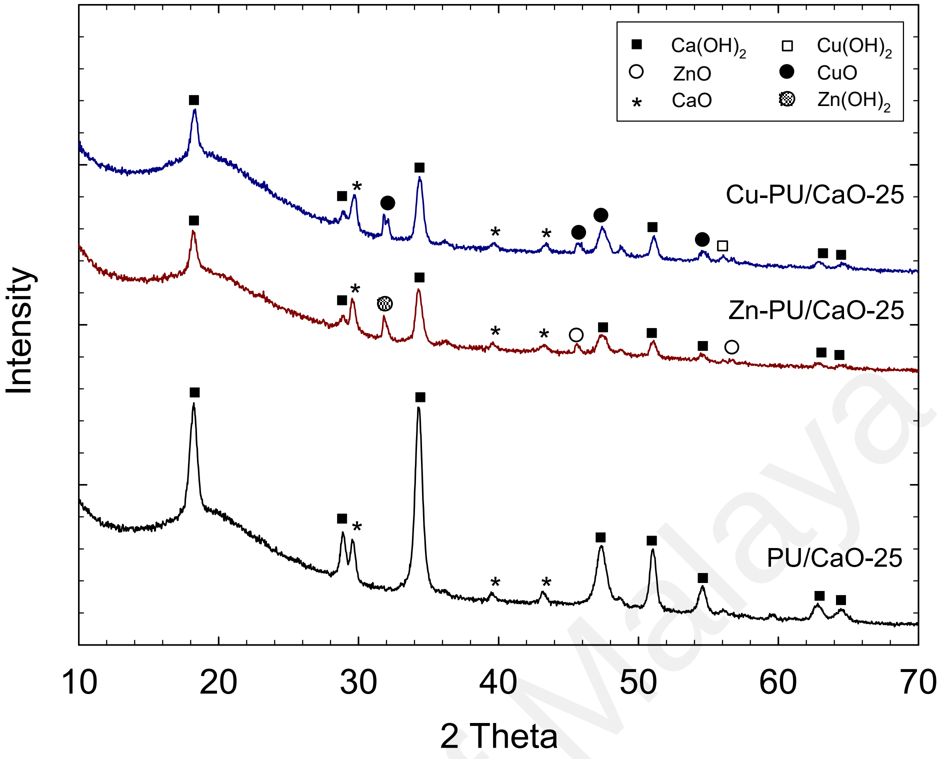

Figure 4-14: XRD of PU/CaO–25, Zn-PU/CaO–25, and Cu-PU/CaO–25

4.1.6.3 BET analysis of PU/CaO

The BET surface areas of pure PU, PU/CaO-25 and Cu-PU/CaO-25 were 0.18, 1.0, and 0.92 $m^2.g^{-1}$, while the pore volumes were 0.1×10^{-3}, 2.0×10^{-3}, and 2.85×10^{-3} $cm^3.g^{-1}$, respectively. Thus, when CaO was incorporated at 25%, the surface area and pore volume increased by ~5.5- and ~19.2-fold, respectively. Thus, the addition of CaO created pore structures. Especially, according to the BJH desorption pore volume in Figure 4-15, meso- (2–50 nm) and macropore structures (>50 nm) developed with the addition of CaO, whereas PU had no pores, as seen in the FESEM. Thus, these pore structures might be created around CaO and become the channel for release of OH^- ions. In the case of Cu(II)-retained PU/CaO-25, the pore volume increased over a range of pore sizes because of inter-particle spaces of metal precipitates.

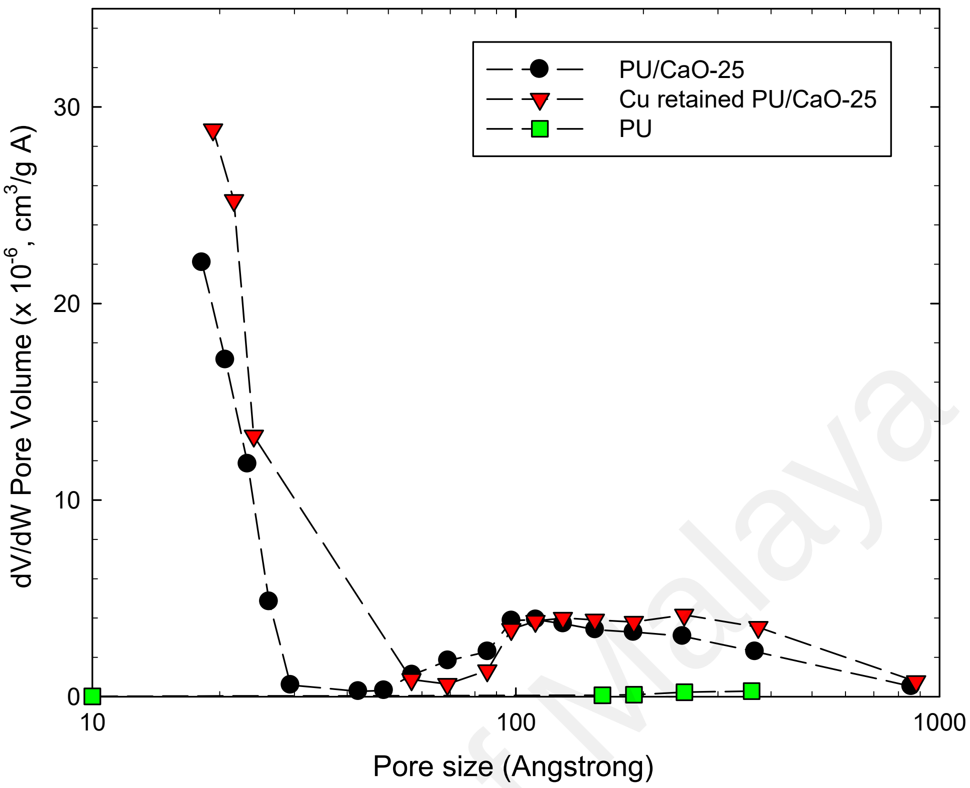

Figure 4-15: BJH desorption pore volume according to pore size

4.1.7 Compression of PU/CaO-25 removal capacities with other materials

Table 4.3 shows the reported sorption capacities of Cu(II), Zn(II), Pb(II), and Ni(II) by various adsorbents in columns (Han et al., 2006; Hasfalina et al., 2012; Li & Champagne, 2009; Nguyen et al., 2015; Unuabonah et al., 2012; Vengris et al., 2001; Yan & Viraraghavan, 2001). As observed, PU/CaO-25 possessed higher removal capacities for all metal species than the other listed adsorbents, although comparison is difficult due to use of different concentrations and HRTs. The higher removal capabilities with PU/CaO-25 may be due to its unique structural features. Based on the results of FESEM/EDX, N_2 gas isotherm, XRD, and chemical equilibrium modeling, we show schematics of PU, PU/CaO-25, and overall removal mechanisms for heavy metals, which can be seen in Figure 4-16. CaO is the major reactive domain in PU/CaO-25, producing OH^- ions and could not be fully used if the surface of the CaO became armored by the hydrolyzed colloids of heavy metals. Thus, the PU pores supply the sites for deposition of metal precipitates so that no covering occurs; instead, OH^- is released through pores created by CaO to precipitate heavy metals in the liquid phase.

Table 4.3: Comparison of adsorption capacities of PU/CaO–25 and references

Adsorbents	Heavy metals	q_0 (mg.g^{-1})	Concentration (mg.L^{-1})	HRT (Sec)	References
Mucor rouxii	Pb(II)	4.06	10.0	1800	(Yan & Viraraghavan, 2001)
Zeolite		1.67	5.0	440	(Nguyen et al., 2015)
ICZ		2.28	5.0	440	
PVA-MKC		6.30	150.0	990	(Unuabonah et al., 2012)
PVA-MKC (Na^{+} ^{i}mpregnated)		10.40	300.0	1031	
VA-MKC (Ca^{2+} impregnated)		9.98	300.0	1031	
PU/CaO–25		19.70	65.0	450	This study
sodium hydroxide- modified oil palm	Zn(II)	0.016	100.0	1080	(Yan & Viraraghavan, 2001)
Mucor rouxii		3.76	10.0	1800	(Salamatinia et al., 2008)
Zeolite		1.19	5.0	440	(Nguyen et al., 2015)
ICZ		1.66	5.0	440	
PU/CaO–25		14.50	65.0	450	This study
Manganese oxide-coated zeolite	Cu(II)	7.90	62.0	183	(Han et al., 2006)
Zeolite		1.15	5.0	440	(Nguyen et al., 2015)
ICZ		1.70	5.0	440	
sodium hydroxide-modified oil palm		0.019	100.0	1080	(Salamatinia et al., 2008)
PU/CaO–25		35.60	65.0	450	This study
Mucor rouxii	Ni(II)	0.36	10.0	1800	(Yan & Viraraghavan, 2001)
Mollusk shells		0.26	105.0	20790	(Li & Champagne, 2009)
Modified clay		12.90	22.6	100	(Vengris et al., 2001)
PU/CaO–25		26.70	65.0	450	This study

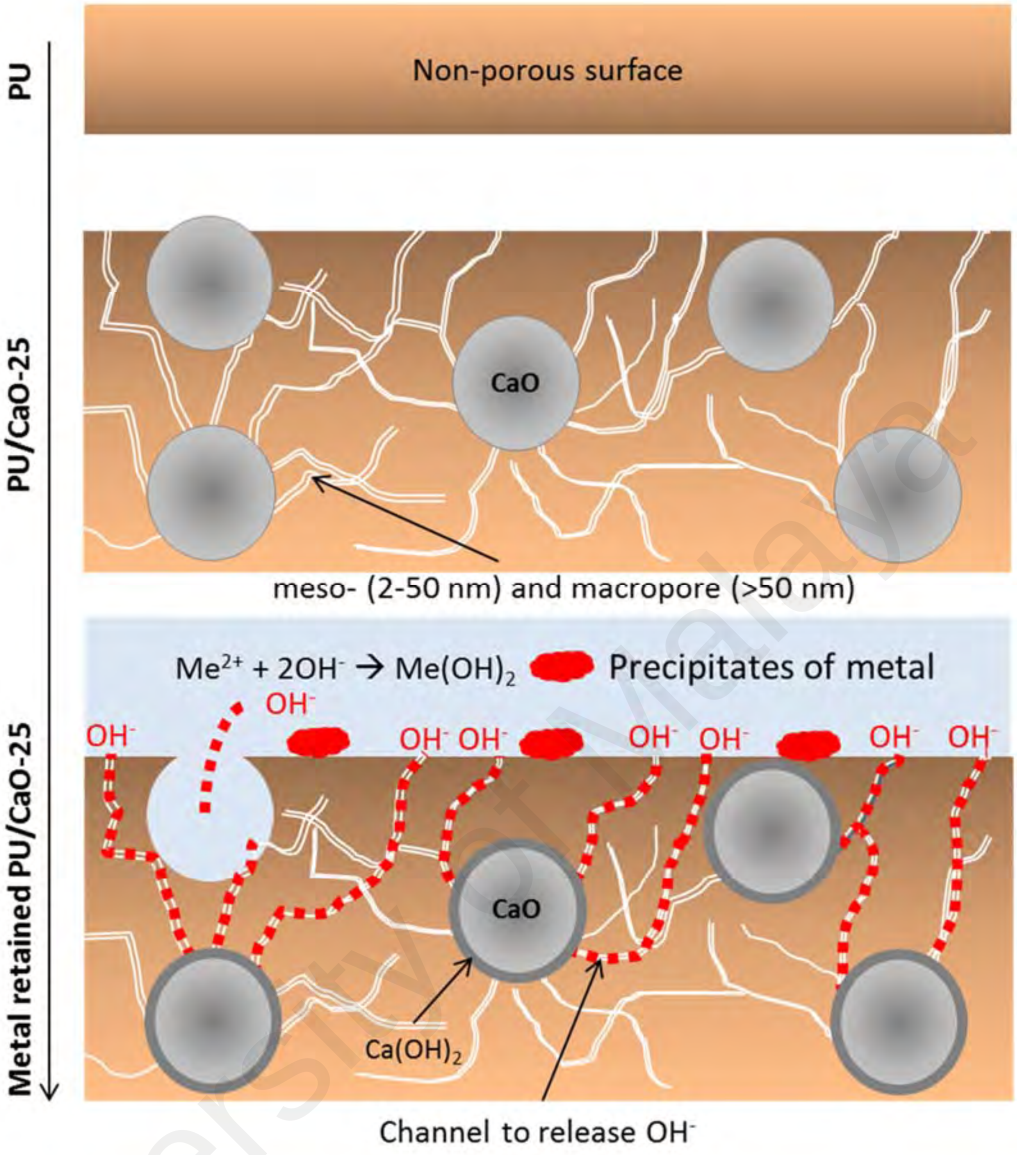

Figure 4-16: Schematics of PU, PU/CaO–25, and metal removal mechanism

4.1.8 Compressive strength and hydraulic conductivity

Compressive stress-strain measurements showed 0.28 and 0.38 MPa for pure PU and PU/CaO-25, respectively, which can be seen in Figure 4-17. The form densities of PU and PU/CaO-25 were 55 and 75 kg.m^{-3}, respectively. Typical rigid PU foams has a compressive strength >0.15 MPa and a form density of 20–50 kg.m^{-3} (Lee & Ramesh, 2004; Oertel & Abele, 1985; Szycher, 1999; Widya & Macosko, 2005). Thus, CaO addition enhanced the rigidity and density of the final PU product.

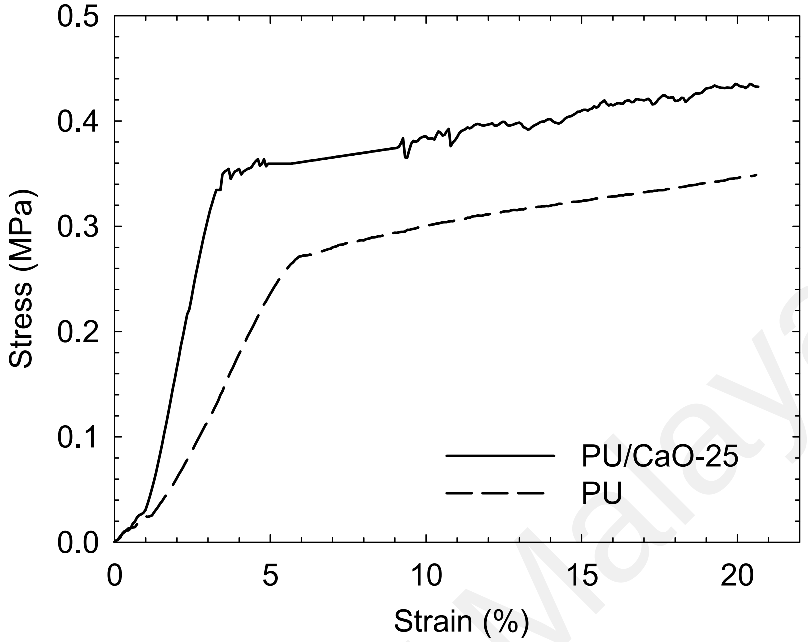

Figure 4-17: Mechanical properties of pure PU and PU/CaO-25%

Table 4.4 shows the HC of PU/CaO-25. There was no significant difference in HC for sampling (A, B, C, and D), and the average HC of PU/CaO-25 was 0.108 cm.s^{-1}. Table 4.5 shows the HC of sands (Hsieh & Davis, 2005; Seifert & Engesgaard, 2012; Smits et al., 2012) with sizes in the range 0.014–0.17 cm s^{-1}. Although PU/CaO-25 has a smaller average size (0.4 mm) than the referenced sands, it had an equivalent or higher HC. The HRT in the permeameter (74-mm ID × 160-mm L) was ~100 s, which was markedly shorter than those in column tests operated at 1.2 mL.min^{-1} for 9-mL columns (450 s). The HC of the medium depends primarily on the pore size. Generally, larger pores conduct water more rapidly (Hillel, 1998). As shown in FESEM images, the smooth surface might be another reason for the high HC.

Table 4.4: Random sampling for hydraulic conductivity measurement

Parameters	Sampling (A)	Sampling (B)	Sampling (C)	Sampling (D)
Q (mL)	216.4	490	1035	2055
T (s)	30.00	70.00	150.0	300.0
K (cm s^{-1})	0.111	0.108	0.107	0.106

Table 4.5: Hydraulic conductivity of PU/CaO-25 and sands

Materials	D (mm)	KC (cm s^{-1})	Ref.
Silica	0.52	0.10	(Smits et al., 2012)
Quartz	0.60	0.17	(Seifert & Engesgaard, 2012)
Mulch/Soil	0.23	0.014	(Hsieh & Davis, 2005)
Soil/Sand	0.57	0.13	

4.1.9 Treatment of simulated USRs by PU/CaO-25

Figure 4-18 shows the column results of PU/CaO-25 with simulated USRs. Columns were operated until the concentration of any heavy metal reached standard A, which is the maximum acceptable concentration for discharge into the environment. The removal trends of most metals were similar at 0.5 and 1.2 mL.min^{-1}. In particular, Cu(II) and Pb(II) concentrations started to increase gradually from 60 BVs, and a reached plateau at ~500 BVs although Cu(II) reached standard A at 1,100 BVs at 1.2 mL.min^{-1}. Outlet concentrations of Zn(II) higher than the inlet level were detected at 1,000 and 1,100 BVs for 1.2 mL.min^{-1} and 0.5 mL.min^{-1}, respectively. Fe(III), Al(III), and Ni(II) showed similar trends, with which all concentrations reaching plateaus within 100 BVs and about 50–70% removal obtained for 1,100 BVs. Thus, this might be controlled by the filtration of precipitate particles rather than ion exchange.

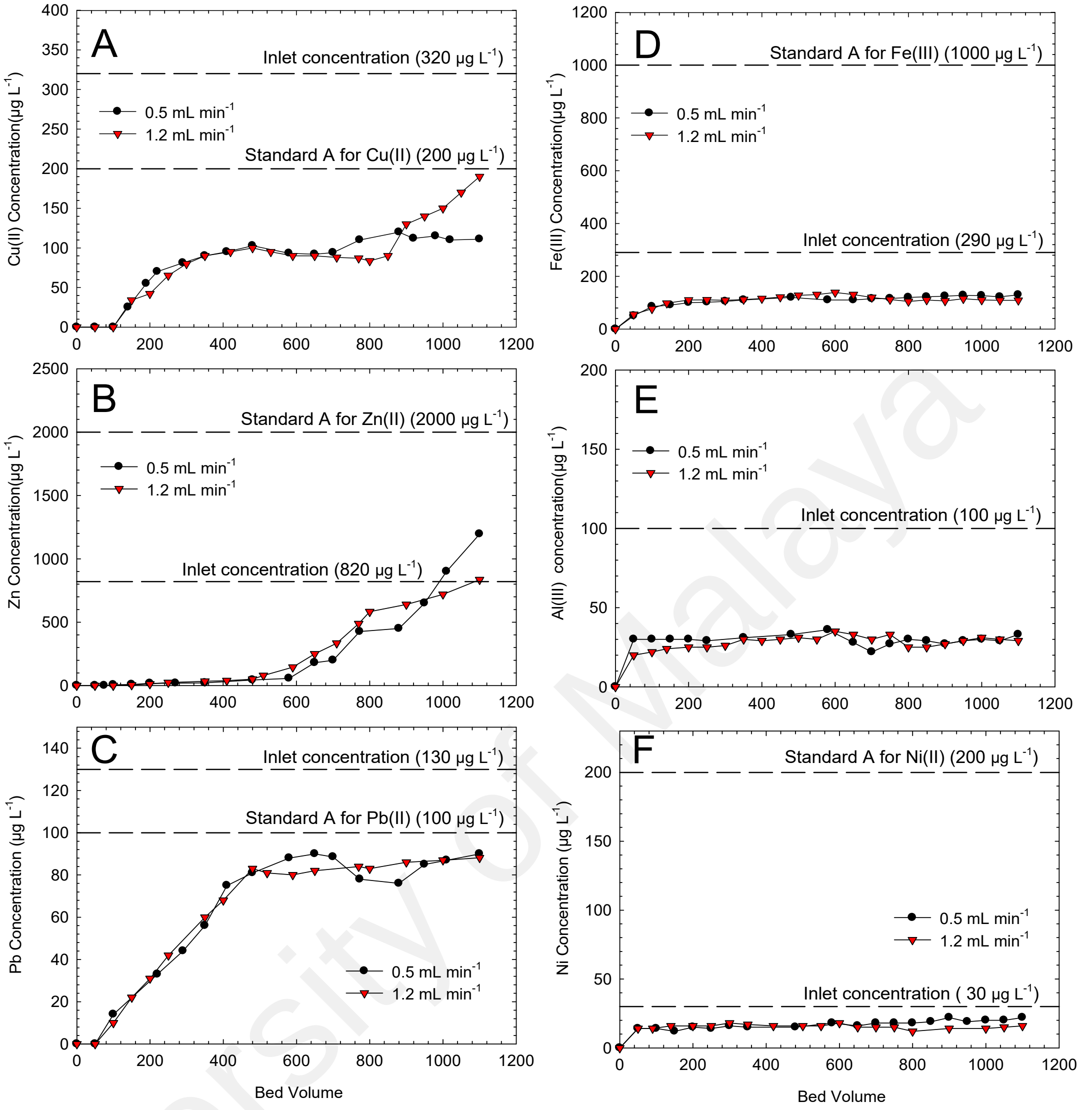

Figure 4-18: Outlet concentrations of heavy metals for simulated USR treatment

Table 4.6 shows the operational conditions of the column, inlet concentrations, and ARCs of heavy metals at 1,100 BVs. Although there were different behaviors in heavy metal removal, the ARCs were strongly correlated with the inlet concentrations of the heavy metals. Figure 4-19 shows that the ARCs of most heavy metals increased linearly with increasing inlet concentrations. In contrast, Zn(II) had a lower ARC than Al(III), although its inlet concentration was higher. Using the Medusa software, selective precipitations were interpreted based on the inlet concentrations of all heavy metals.

Figure 4-20 shows the soluble and solid species of individual metals, terms of reactions, and equilibrium constants (log K) and also the modeling results with the USR conditions. Al(III) and Cu(II) were precipitated as $Al(OH)_3$ (Cr) and $CuFe_2O_4$ (c), respectively, at pH 7–8, which was the pH range during column operation. Fe(III) existed as solids such as Fe_2O_3 (Cr), $CuFe_2O_4$ (c), and $ZnFe_2O_4$ (c). Zn(II)/Pb(II) existed predominantly as ionic species—such as Zn^{2+}/Pb^{2+} and $ZnOH^+$/$PbOH^+$—at pH 7–7.5, and about 40% Zn(II) and 90% Pb(II) were transformed as $ZnFe_2O_4$/$Zn(OH)_2$ (c) and $Pb(OH)_2$ (c) at pH 8. Thus, as pH decreases, Zn(II) and Pb(II) become soluble species that can be removed by ion exchange. As shown in earlier research (Ge et al., 2012), an increase in ionic strength in the water has shown reduction in metal removal efficiency. Although some authors well-explained the decrease in metal removal percentage caused by NaCl increase and the existence of Na^+ ions for metal binding (Fiol et al., 2006), it can be more clarified in terms of the different ionic species existing at different chloride concentrations. An increase in chloride concentration results in a decrease in the free divalent metal ions species and an increase in the corresponding chloro-complexes (Ge et al., 2012). Based on the results above, PU/CaO-25 can be used to treat most heavy metals to below Standard A at 1,100 BVs. If we assume that 2,400-mm precipitation is collected annually in a 1,000- m^2 open space, the theoretical treatment volume and lifetime of a filter [1.5 m (ID) × 2 m (H), 4.4 m^3] containing PU/CaO-25 are 4,800 m^3 and ~2 years, respectively. When PU/CaO-25 is saturated, then we can easily recover it using a vacuum due to a low density.

Table 4.6: Column results by PU/CaO-25 using synthetic USR

Heavy Metals	Flowrate (mL.min^{-1})	EBCT (min)	Bed Depth (mm)	Inlet Conc.		ARCs at 1,100 BVs		Standard A (µg.L^{-1})
				(µg.L^{-1})	(µmol.L^{-1})	(µg.g^{-1})	(µmol.g^{-1})	
Cu(II)	0.5	18.1	45	320	5.00	1180.0	18.50	200
	1.2	7.5	45	320	5.00	1146.0	17.90	
Zn(II)	0.5	18.1	45	820	12.40	2787.0	42.60	2,000
	1.2	7.5	45	820	12.40	2707.0	41.30	
Pb(II)	0.5	18.1	45	130	0.62	217.0	1.05	100
	1.2	7.5	45	130	0.62	367.0	1.77	
Al(III)	0.5	18.1	45	298	11.00	1269.0	47.00	-
	1.2	7.5	45	298	11.00	1348.0	50.00	
Fe(III)	0.5	18.1	45	141	2.52	173.0	3.09	1,000
	1.2	7.5	45	141	2.52	149.1	2.67	

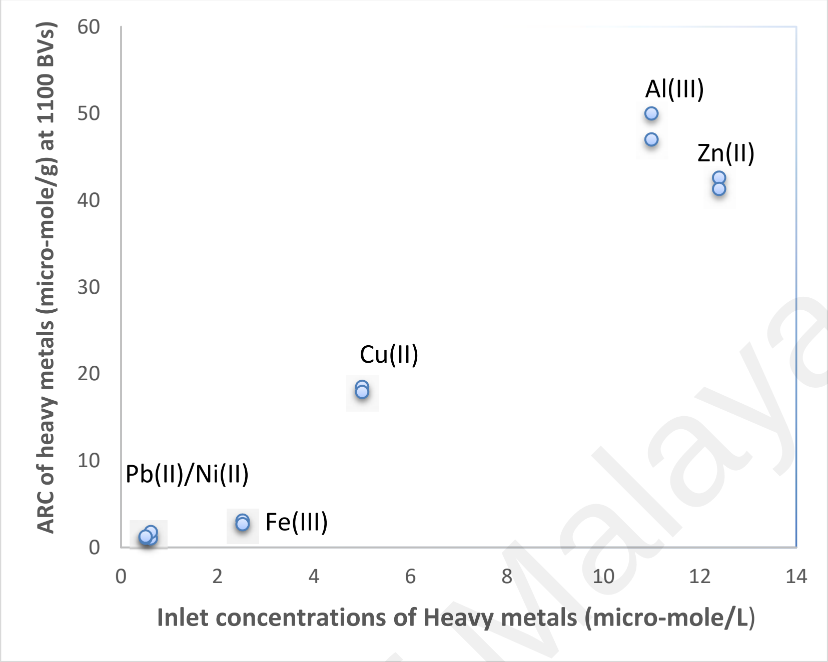

Figure 4-19: ARCs of heavy metals at 1100 BVs versus inlet concentrations

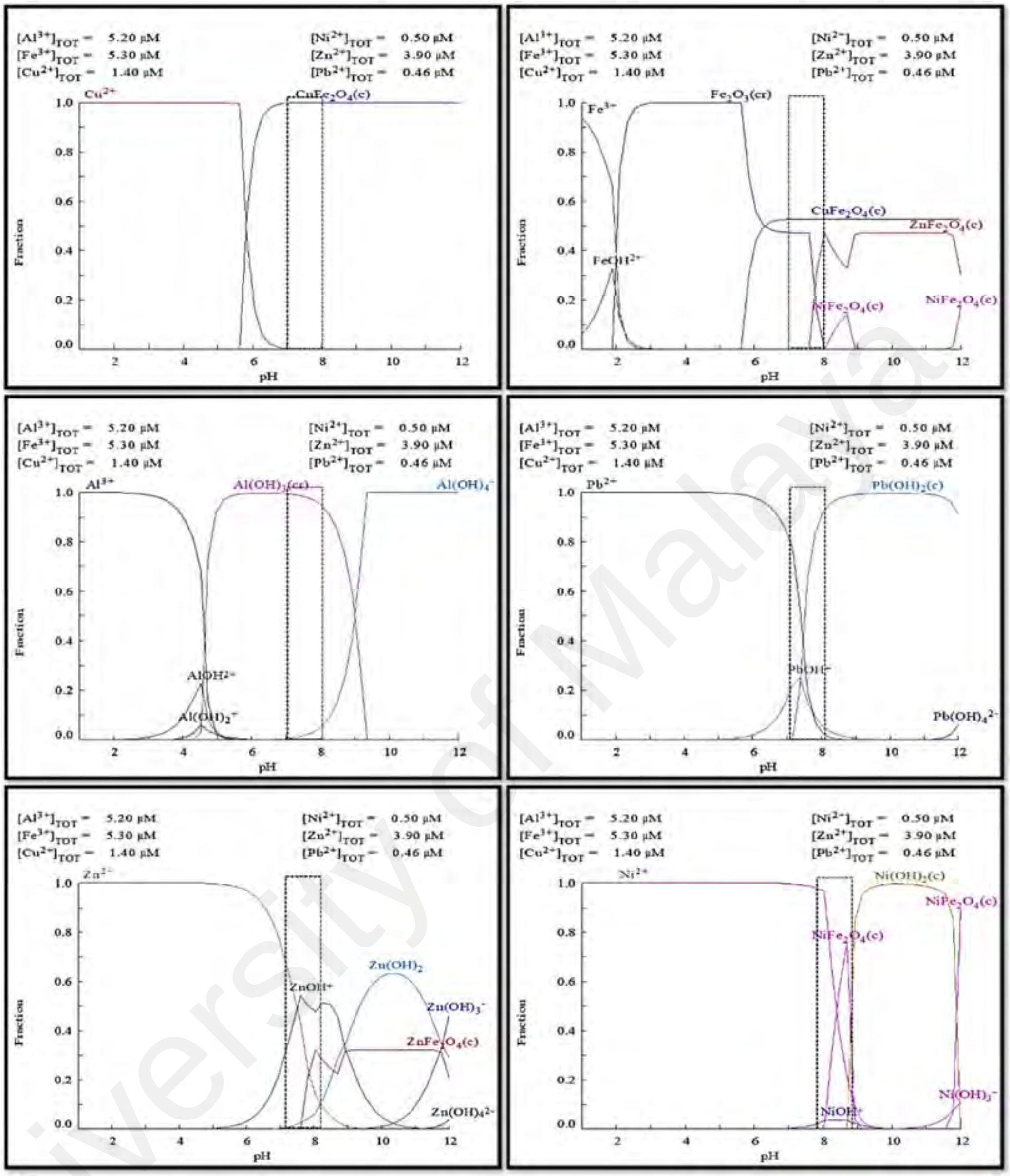

Figure 4-20: Chemical speciation diagrams of metal ions in USR

4.2 Three-dimensional flowerlike magnesium hydroxide -incorporated granular polyurethane (gPU-FMH)

4.2.1 Characterization of self-assembled gPU-FMH

It was described earlier in section 3.4.1 that PU foam was ground to obtain the powder form of PU media with the particle sizes between 210 and 841 μm (70–20 U.S. Mesh). Hence, due to the loss of the CO_2 during the synthesis process, the ground PU structure is concave/hollow, as can be seen in Figure 4-21. In addition, a smooth surface with no pore structures were seen in the observed FESEM micrograph of the ground PU, as can be seen in Figure 4-22(A). Furthermore, the morphology of the commercial MgO that is shown in Figure 4-22(B) is irregular and heterogeneous with a thickness of ~100 nm and a diameter from 80–500 nm, which was also observed by FESEM; therefore, it is much smaller than that of gPU particles.

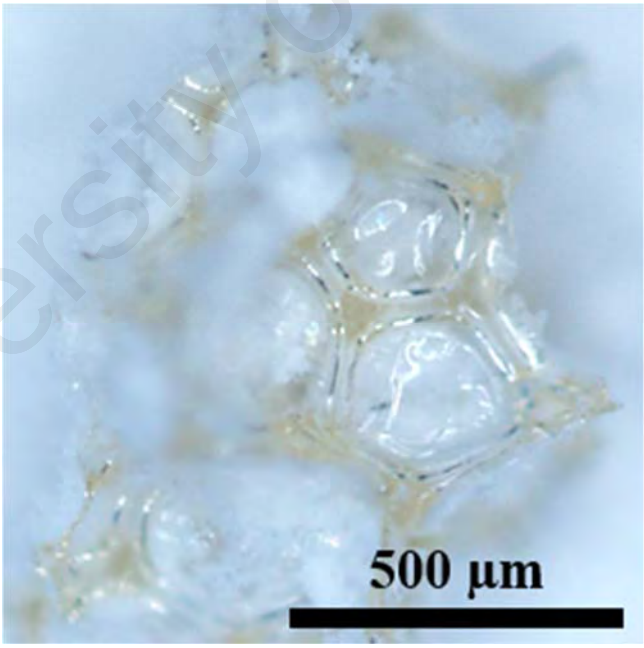

Figure 4-21: Digital image of gPU structure

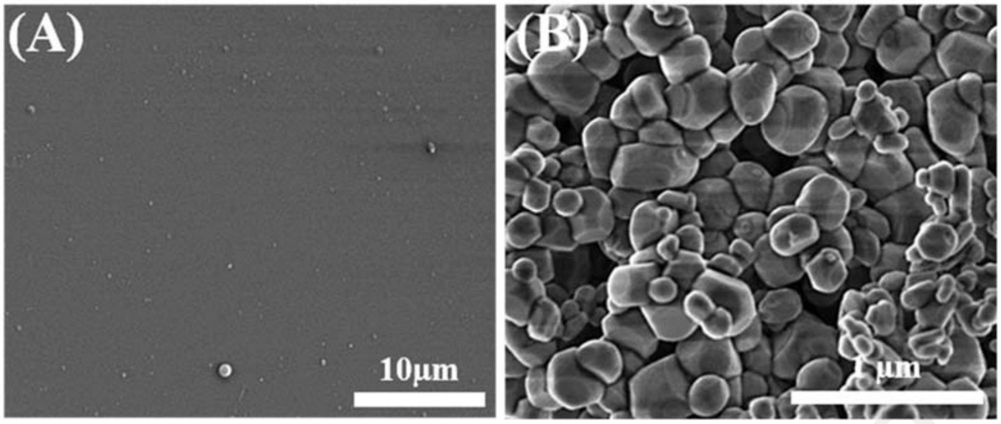

Figure 4-22: FE-SEM image of (A) gPU surface, and (B) commercial MgO

Figure 4-23(A) shows the post-treated gPU that had been aggregated into larger particles (30–16 U.S. Mesh, 600–1180 µm) and contains the white material in the hollow-gPU area, as shown in Figure 4-23(B).

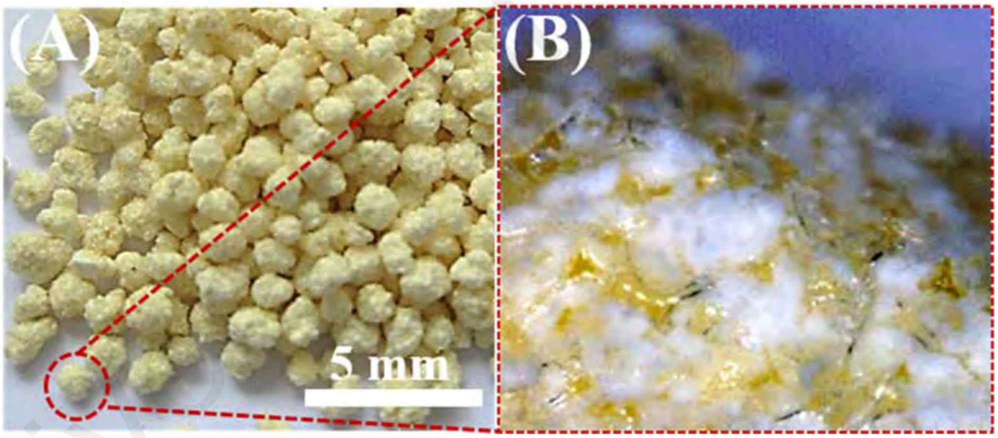

Figure 4-23: (A) Post-treated gPU, and (B) close look at the surface of post-treated gPU

Figure 4-24 (A- I) display the plentiful well-defined flowerlike single or garden structures that formed on the gPU surface, which was observed by FESEM; however, different nanostructural morphologies were observed at the various hydrothermal temperatures (50–120°C). When a temperature higher than 120°C was applied, the PU foam could be burned. So the maximum temperature applied for the hydrothermal process was 120°C. The micrographs of gPU-FMH that can be seen in Figure 4-24

(A)–(I) were prepared at various temperatures, and they show a 3D flowerlike structure with irregular and curved-petal morphologies of a ~10-nm thickness. Interestingly, the garden structures from 50–120°C show different patterns of the 3D flowerlike structure with dissimilar petal morphologies; for example, at 50°C (Figure 4-24 (A)–(C)), coherent flowers were synthesized using curved and incomplete hexagonal petals (gPU-FMH$_{50}$). The petal morphology, however, was developed as a complete hexagonal shape at 80°C (gPU-FMH$_{80}$), which can be seen in Figure 4-24 (D)–(F). Eventually, Figure 4-24 (G)–(I) shows that at the maximum temperature, 120°C, more-compact flowerlike structures with smaller hexagonal petals were prepared (gPU-FMH$_{120}$).

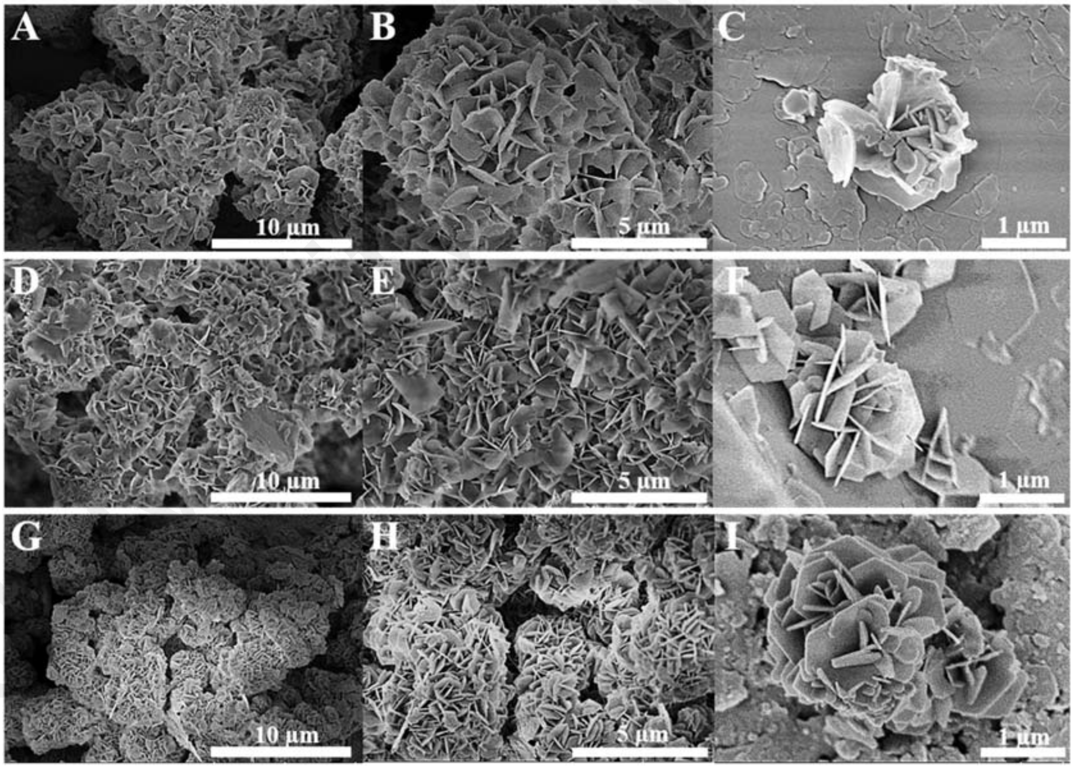

Figure 4-24: FE-SEM micrographs of (A-C) gPU-FMH$_{50}$, (D-F) gPU-FMH$_{80}$, and (G-I) gPU-FMH$_{120}$

The morphology of the two prepared control samples (CS-1 and CS-2) were also observed by FESEM. The gPU/MgO morphology (CS-1) in Figure 4-25 (A) did not reveal flowerlike magnesium hydroxide formation in the absence of the hydrothermal treatment.

Figure 4-25 (B) shows that $Mg(OH)_2$ (CS-2) nanoplates were formed with a thickness from 20–50 nm and a diameter of ~500 nm. Therefore, without forming 3D flowerlike structures, CS-2 had much larger and thicker nanoplates than gPU-FMH. The production of these MgO nanoplates might be due to the epitaxial growth of the $Mg(OH)_2$ nanoplates in the H_2O vapor under the hydrothermal treatment (Fruhwirth et al., 1985).

Since the complete 3D flowerlike morphology was produced and an appropriate range of temperatures was considered, the gPU-FMH_{80} was selected for the heavy-metal adsorption, and it was further characterized by XRD (Figure 4-26), elemental mapping, EDX (Figure 4-27), FTIR (Figure 4-28), and N_2-gas isotherms and Figure 4-29 and Table 4.7).

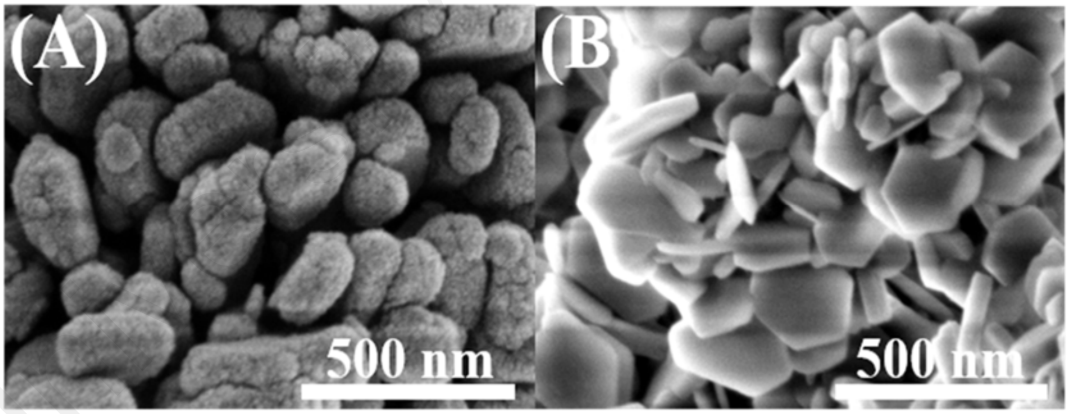

Figure 4-25: High magnification FESEM image of (A) Control sample 1 (CS-1), and (B) control sample 2 (CS-2)

The XRD results show that all of the diffraction peaks can be labeled as $Mg(OH)_2$ crystallites, and this is consistent with the values of the JCPDS 7-239 standard of the International Centre for Diffraction Data (ICDD). MgO peaks were not observed, so the

MgO became fully hydrated to the Mg(OH)$_2$, which can be seen in Figure 4-26. The elemental-mapping and EDX data of the single-flower displays that are presented in Figure 4-27 (a) show that the Mg and oxygen (O) are significantly dispersed on the FMH spots, while carbon (C) is not shown on the FMH. In Figure 4-28, the FTIR peak for the stretching vibration of the O–H of Mg(OH)$_2$ was observed at 3700 cm^{-1} (Cao et al., 2010). The symmetric- and asymmetric stretching vibrations of the N–H correspond to the broad absorption bands in gPU near 3340 cm^{-1} and 3360 cm^{-1}, as shown in Figure 4-28 (a), and gPU-FMH$_{80}$, as shown in Figure 4-28 (b). After the FMH was incorporated, however, the sharp-peak intensity at 1512 cm^{-1} was reduced to support the claim that the N species of gPU might be extracted during the hydrothermal-treatment process (L. Jiao et al., 2013).

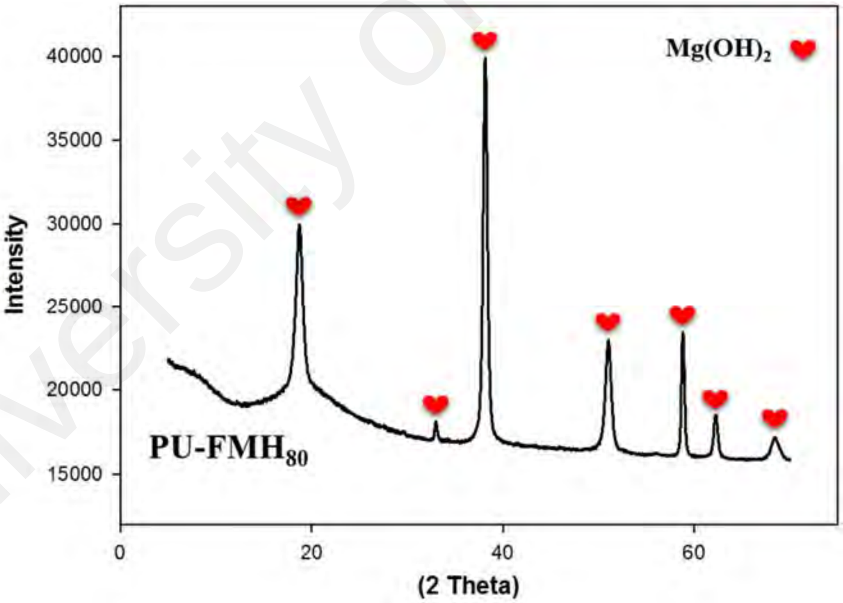

Figure 4-26: XRD pattern of gPU-FMH$_{80}$

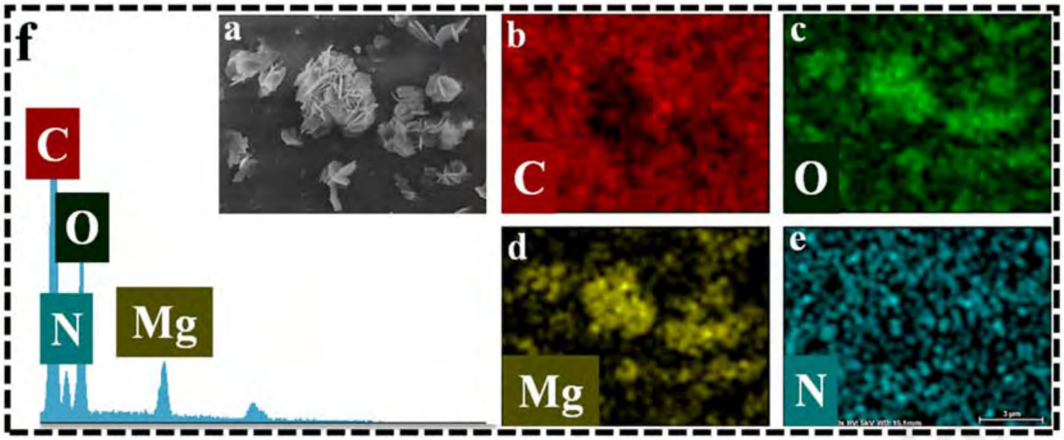

Figure 4-27: (a) FE-SEM image, (b-e) the elemental mapping, and (f) EDX of single gPU-FMH$_{80}$

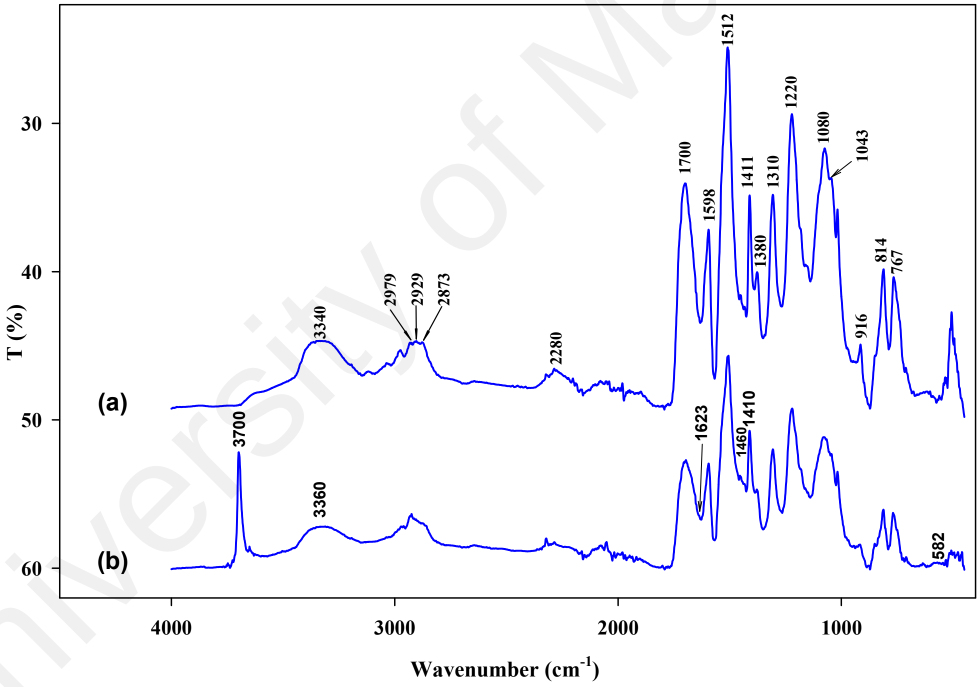

Figure 4-28: FTIR patterns of (a) gPU, and (b) gPU-FMH$_{80}$

The N$_2$-gas-isotherm results were observed base on the following information. The total surface area was observed base on the single-point surface area at p/p° = 0.120223755. BJH surface area and micropore volume was observed by BJH desorption cumulative volume of pores between 17.000 Å and 3,000.000 Å width. BJH pore volume results were observed by Single point adsorption at p/p° = 0.997. The N_2-gas-isotherm (Figure 4-29 and Table 4.7) results indicate that the surface area of gPU-FMH_{80} (20.2 $m^2.g^{-1}$) is two or 117 times higher than that of MgO (9.6 $m^2.g^{-1}$) or gPU (0.18 $m^2.g^{-1}$), and this is because of 3D flowerlike nanostructured $Mg(OH)_2$. Based on the previously described results in Section 4.2.1, the following hypothesis is proposed: MgO nanoparticles can grow as hexagonal $Mg(OH)_2$ nanosheets, and the self-assemblage of flowerlike-structure 3D building blocks can occur in the presence of gPU under hydrothermal treatment. The hydrothermal temperature might play a key role in the controlling of the FMH morphology, which will be explained in the next section.

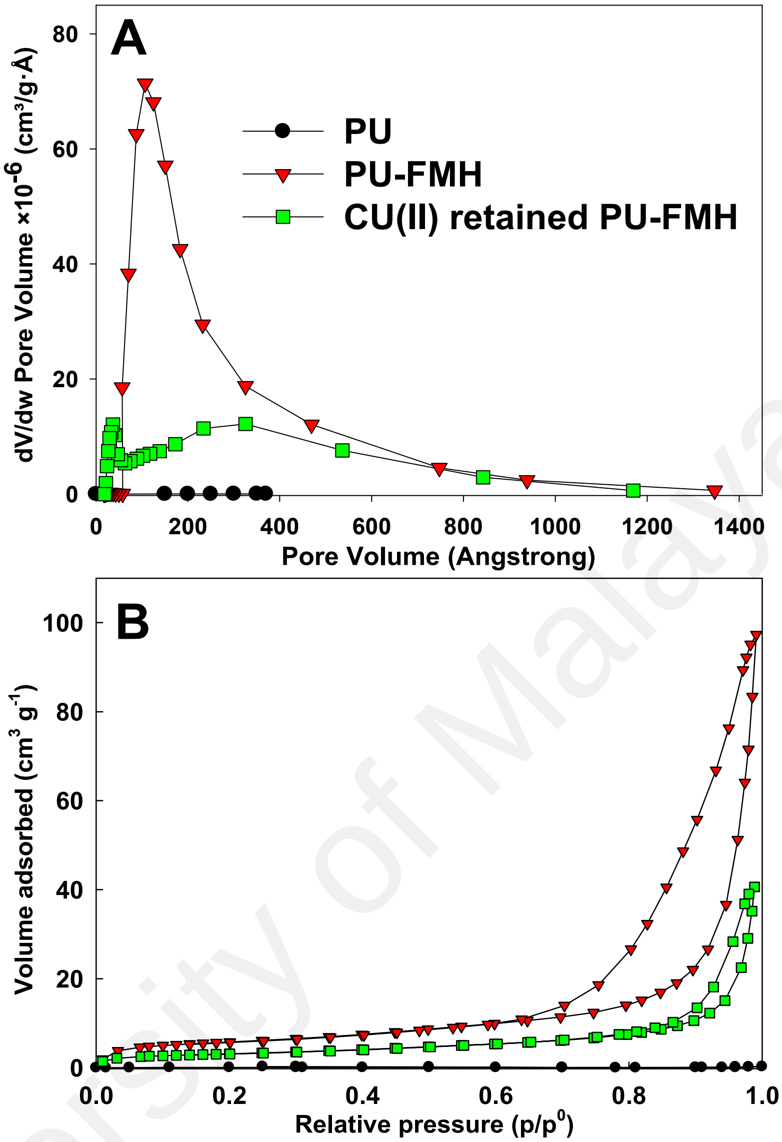

Figure 4-29: (A) and (B) BJH desorption pore volume according to pore size A

Table 4.7: Texture and Surfaces of gPU, commercial MgO, and gPU-FMH$_{80}$

Surface characteristics		gPU	Commercial MgO	gPU-FMH$_{80}$
Total Surface area	(m^2.g^{-1})	0.18000	9.50	20.20
BET Surface area	(m^2.g^{-1})	0.18000	9.60	20.90
Micropore area	(m^2.g^{-1})	0.04500	2.39	2.99
BJH surface area	(m^2.g^{-1})	0.01400	6.53	37.10
Total pore volume	(cm^3.g^{-1})	0.00035	0.01	0.15
Micropore volume	(cm^3.g^{-1})	0.00004	0.00	0.00
BJH pore volume	(cm^3.g^{-1})	0.00010	0.03	0.15

4.2.2 Proposed mechanism for the self-assembled gPU-FMH

Based on the FESEM results, the proposed mechanism for the formation of gPU-FMH consists of the following three stages: nucleation, growth, and self-assembly. Prior to the hydrothermal treatment, the nucleation was started by the hydrolysis of the commercial MgO, which is of an irregular round shape, as can be seen in Figure 4-22(B). Then, the hydrolyzed product, $Mg(OH)_2$, will be further dissolved into Mg^{2+} and OH^-, as follows:

$$\mathrm{MgO} + H_2O \rightarrow \mathrm{Mg(OH)_2} \tag{4.2}$$

$$Mg(OH)_{2\leftrightarrow}Mg^{2+} + 2OH^- \tag{4.3}$$

At the pH of 9.5, however, the OH^- species will rebind to the Mg^{2+}, thereby forming the $Mg(OH)_2$ nuclei that is the primary $Mg(OH)_2$. In the hydrothermal condition, the nanosheet growth will start via the dissolution of the initial $Mg(OH)_2$, as shown in Figure 4-25 (B). As a new structure, which is shown in Figure 4-24 (A)–(I), $Mg(OH)_2$ nanoplate crystallites might be formed by alternating layers of the Mg^{2+} and OH^- ions, in which the Mg^{2+} ion has a coordination of sixfold oxygen ions (Wu et al., 2008). This reaction develops into the Ostwald ripening process, a thermodynamically driven spontaneous process, during the hydrothermal treatment so that the larger primary $Mg(OH)_2$ particles can grow as the small particles are deposited onto the larger particles due to their different solubilities (Voorhees, 1985). Besides, the gPU is hydrolyzed (with the presence of H_2O), and reusable diamines, glycols, and CO_2 are subsequently released during the hydrothermal treatment (Siskin & Katritzky, 1991).

Regarding an important role in the control and growth of the self-assembled $Mg(OH)_2$, diamine, benzene, and glycol might act as special bases in the syntheses of the 3D flowerlike $Mg(OH)_2$ due to the lone pair of electrons on the N atom in the diamine compound (Li et al., 2007). The self-assembly process of the $Mg(OH)_2$ nanosheets that occurs through electrostatic repulsion might lead to the formation of 3D flowerlike structures. Since the pH, at the isoelectric point (pH_{IEP}) of the $Mg(OH)_2$ nanosheet in H_2O is 12, and the measured pH of the MgO suspension is 10.2, the net residual electric charge of the $Mg(OH)_2$ surface will be positive, which might be a result of the weak bonding interactions with the negatively charged O molecule of the gPU-particle surface (Larson & Buswell, 1940). Especially, the two-dimensional (2D) hexagonal $Mg(OH)_2$ nanosheets (approximate thickness of 10 nm and width of 300–400 nm) were stacked on the PU surface due to the following fact: all self-assembling systems are driven by energy minimization (Jiao et al., 2006). Besides the electrostatic repulsion, the hydrogen (H) bonds between the 2D nanosheets are favorable for self-assembling structures that are without chemical reactions, as they align one another perpendicularly to the surface (Cao et al., 2010).

4.2.3 Heavy-metal adsorption mechanism

4.2.3.1 Isotherm and kinetics study of PU-FMH_{80}

The results of the batch experiments revealed that the maximum sorption capacities of gPU-FMH80 regarding Cu(II), Cd(II), and Pb(II) are 472, 1041, and 1321 $mg.g^{-1}$, respectively, which are shown in Figure 4-30 (a). The experiment data fitted well with the nonlinear Langmuir model, which was obtained with the following experimental condition; weight of PU-FMH_{80}= 0.1 g; the volume of metal solution= 100 mL; the shacking rate= 150 rpm at 27±5°C for 24 h; and the initial pH of the solution before adding the PU-FMH_{80} media was adjusted at pH= 4.0 (Table 4.8). Langmuir and Freundlich parameters for the adsorption of Cu(II), Pb(II), and Cd(II) were reported for the comparison in Appendix B. The experimental data indicated a better fit with Langmuir compare to Freundlich model. The molar amounts of the removed metal ions and the released Mg(II) per gPU-FMH_{80} mass in the solution are shown in Table 4.9, Table 4.10, and Table 4.11 with the following experimental condition: weight of gPU-FMH_{80}= 0.1 g; the volume of metal solution: 100 mL; Shacked (150 rpm) at room temperature (27±5°C) for 24 h; initial pH = 4.0. In Figure 4-30 (b), the results show that the quantity of the released Mg(II) is fitted with the line (slope = 1) until ~1.8 mmol.g^{-1} of the Cu(II), ~2.0 mmol.g^{-1} of the Cd(II), and ~0.3 mmol.g^{-1} of the Pb(II) were removed from the solution, as displayed in Figure 4-30 (b). According to the equal molar amount of the adsorbed metal and the released Mg(II) ions, the ion exchange that was expected as the dominant removal mechanism (Cao et al., 2012) and reaction 4.4 occurred, as follows:

$$\mathrm{Mg(OH)_2(s) + Me(II) \rightarrow Mg(II) + Me(OH)_2(s)} \quad (4.4)$$

Where Me(II) denotes the metal species, the possibility of ion-exchange metal sorption was found in the order of Cu(II) > Cd(II) > Pb(II) due to a smaller hydrated ionic radius and an electronic metal-ion structure (Amarasinghe. & Williams., 2007).

Alternatively, when higher amounts of the metal ions [Cu(II) > 1.8 mmol.g^{-1}, Cd(II) > 2.0 mmol.g^{-1}, and Pb(II) > 0.3 mmol.g^{-1}] were removed, the Mg(II) concentrations in the solution were deviated to lower ranges compared with that of the slope with different patterns. Since the Mg(II) can be released in lesser amounts compared to the removed metal ions, another reaction and mechanism is speculated here. According to reaction 4.5, $Mg(OH)_2$ dissociation in the metal solution produces two OH^- ions that subsequently react with the metal ions. Based on the stoichiometry, this reaction can render the production of insoluble precipitates through coupling with the anionic species that exist in the solution (Brauer, 2012). Further, the precipitates will become trapped in the gaps of the FMH particles, and the precipitation might be the dominant removal mechanism at the higher metal-ion concentrations.

$$\mathrm{Mg(OH)_2(s) \rightarrow Mg(II) + 2OH^-} \quad (4.5)$$

Figure 4-30 (c) shows the kinetics of the heavy-metal removal by gPU-FMH$_{80}$.The removal speed of the heavy metals by the gPU-FMH$_{80}$ are fast, and more than 90% of the metal ions (initial concentration of 500 mg.L^{-1}) was removed in the first 60 min. The experimental data were recorded and reported in Table 4.12. The results were observed with the following experimental condition; the weight of gPU-FMH$_{80}$= 0.5 g; the volume of metal solution= 500 mL; Shacked at 150 rpm at room temperature (27±5°C) for 24 h; initial pH of the heavy metal solution= 4.0. According to the pseudo-second-order kinetic model, the K$_2$ values are 23.5 × 10^{-4}, 2.99 × 10^{-4}, and 2.4 × 10^{-4} g.mg^{-1}.min^{-1} for Pb(II), Cu(II), and Cd(II), respectively Table 4.13. The sequence of Pb(II) > Cu(II) > Cd(II) might be strongly related to the hydrolysis condition of the metal ions. Considering the logarithmic values of the hydrolysis constant for the heavy-metal order (log K$_{Pb}$ = 7.71 > log K$_{Cu}$ = 8.00 > log K$_{Cd}$ = 10.80), the adsorption of Pb(II) by the gPU-FMH$_{80}$ is much faster than those of the Cu(II) and the Cd(II).

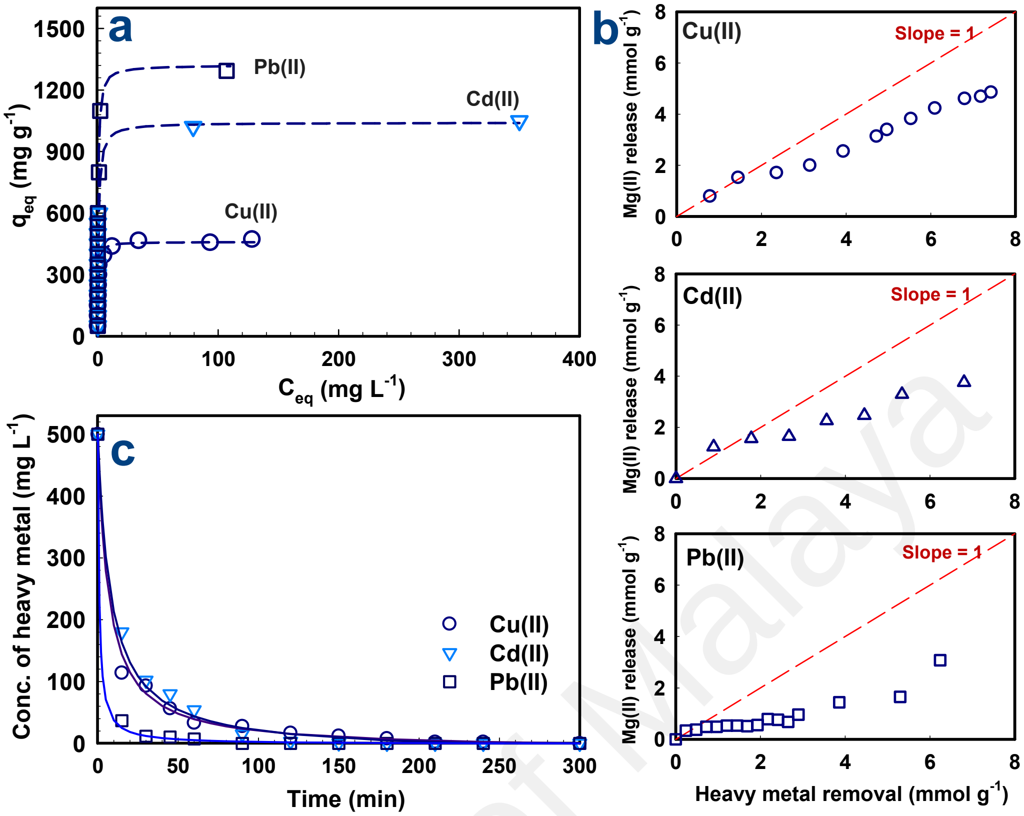

Figure 4-30: (a) Adsorption isotherms, (b) molar of released Mg(II), and (c) kinetics adsorption by gPU-FMH$_{80}$

Table 4.8: Langmuir isotherm parameters for the adsorption of Cu(II), Pb(II), and Cd(II) by gPU-FMH$_{80}$

Heavy metals	Isotherm (Langmuir model)		
	K_L (L.mg^{-1})	q_{eq} (mg.g^{-1})	R^2
Cu(II)	2.54	459.5	0.98
Pb(II)	2.17	1321.0	0.99
Cd(II)	1.35	1041.1	0.99

Table 4.9: The initial Cu(II) concentration, Cu(II) removal, and Mg(II) release in the solution

Initial Cu(II) Concentration (mmol.L^{-1})	Cu(II) removed (mmol.g^{-1})	Mg(II) released (mmol.g^{-1})
0.78	0.78	0.78
1.57	1.45	1.51
2.36	2.36	1.70
3.14	3.14	1.99
3.93	3.93	2.54
4.72	4.72	3.13
5.50	4.96	3.38
6.29	5.53	3.81
7.08	6.09	4.22
7.86	6.80	4.60
8.65	7.18	4.68
9.44	7.42	4.84

Table 4.10: The initial Cd(II) concentration, Cd(II) removal, and Mg(II) release in the solution

Initial Cd(II) Concentration (mmol.L^{-1})	Cd(II) removed (mmol.g^{-1})	Mg(II) released (mmol.g^{-1})
0.88	0.88	1.23
1.77	1.77	1.56
2.66	2.66	1.64
3.55	3.55	2.26
4.44	4.44	2.46
5.33	5.33	3.29
7.11	6.80	3.75
9.78	9.08	5.69
12.4	9.34	6.87

Table 4.11: The initial Pb(II) concentration, Pb(II) removal, and Mg(II) release in the solution

Initial Pb(II) Concentration (mmol.L^{-1})	Pb(II) removed (mmol.g^{-1})	Mg(II) released (mmol.g^{-1})
0.241	0.241	0.337
0.482	0.482	0.374
0.723	0.723	0.488
0.965	0.965	0.488
1.206	1.206	0.534
1.447	1.447	0.534
1.689	1.689	0.513
1.930	1.930	0.557
2.171	2.171	0.785
2.413	2.413	0.761
2.654	2.654	0.678
2.895	2.895	0.962
3.861	3.861	1.439
5.308	5.299	1.651
6.756	6.240	3.076

Table 4.12: The concentration of Cu(II), Cd(II), and Pb(II) in the solution versus time

Time (min)	Concentration of Cu(II) (mg.L^{-1})	Concentration of Cd(II) (mg.L^{-1})	Concentration of Pb(II) (mg.L^{-1})
0	500.0	500.0	500
15	114.0	180.0	36.6
30	93.0	102.0	11.4
45	56.4	80.0	10.2
60	33.0	54.0	7.2
90	27.6	15.0	Not detected
120	16.8	3.0	Not detected
150	12.0	0.6	Not detected
180	7.8	Not detected	Not detected
210	2.4	Not detected	Not detected
240	2.4	Not detected	Not detected
270	Not detected	Not detected	Not detected
300	Not detected	Not detected	Not detected

Table 4.13: Kinetic parameters for Cu(II), Pb(II), and Cd(II) uptake onto PU-FMH$_{80}$

Heavy metals	Pseudo-second order kinetic constant (K$_2$) ($\times10^{-4}$.g.mg^{-1}.min^{-1})	R^2	Experimental q$_m$ (mg.g^{-1})
Cd(II)	2.40	0.99	500
Cu(II)	2.99	0.99	500
Pb(II)	23.50	0.99	500

4.2.3.2 Compression of PU-FMH$_{80}$ removal capacities with other materials

The adsorption capacity results of gPU-FMH$_{80}$ for the Cu(II), Cd(II), and Pb(II), and the comparison with the other flowerlike adsorbents are reported in Table 4.14. The results show that the obtained metal-ion sorption capacity of the gPU-FMH$_{80}$ is much higher than those of the reported materials in the literature that are listed in Table 4.14, with the exception of the flowerlike MgO (Cao et al., 2012). However, it should be noted that 1.0 g of the gPU-FMH$_{80}$ contains 0.44 g of the flowerlike Mg(OH)$_2$, which was determined using the aqua-regia extraction. Therefore, the heavy-metal sorption densities (mg per g of FMH) for the Cu(II), Cd(II), and Pb(II) can be calculated as 1072, 2383, and 2936 mg.g^{-1}, respectively, which are much higher than the reported flowerlike-MgO values. Especially, the maximum-sorption capacities of the gPU-FMH$_{80}$ were obtained at the pH of 4.0, while those of the flowerlike MgO were obtained at the pH of 7.0.

Table 4.14: Adsorption results of gPU-FMH$_{80}$ and comparison with the Other flowerlike adsorbents

Adsorbent	Q$_{max}$ (mg.g^{-1})			pH
	Cu(II)	Cd(II)	Pb(II)	
gPU-FMH$_{80}$ (this study)	472	1050	1293	4.0
Flowerlike MgO (Cao et al., 2012)	-	1500	1980	7.0
Flowerlike ɣ-AlOOH (Zhang et al., 2012)	-	-	124	7.0
Flowerlike TiO$_2$-GO (Lee & Yang, 2012)	-	73	66	5.0
Flowerlike zinc silicate (Qu et al., 2012)	-	-	210	7.0

4.2.4 Heavy-metal removal characterization

The morphologies of the gPU-FMH$_{80}$ were studied after the adsorption of the Cu(II) (Figure 4-31), Cd(II) (Figure 4-32a), and Pb(II) (Figure 4-32b) on gPU-FMH$_{80}$ surface.

The micrograph of the Cu(II)/PU-FMH$_{80}$ displays that the Cu precipitants were found on the space gaps of the 3D FMH (Figure 4-31 (a)). Overall, as described in the removal mechanism section, the $Mg(OH)_2$ could be dissolved, and the metal precipitants are trapped in the FMH spaces. An elemental-mapping analysis of the Cu(II)/gPU-FMH$_{80}$ was also performed; as a result, the Cu(II)-precipitation and Cl^- complexation formed at the position indicated by the green and pink color in Figure 4-31 (f and h), of the remaining Mg(II), which is in the red area of Figure 4-31 (g), is the same and appeared in 3D white-colored products, as shown in Figure 4-31 (b). The higher oxygen density is located at the positions of the Cu(II) precipitants, which is due to the structure of $Cu_2(OH)_3Cl$, as can be seen in Figure 4-31 (e). Meanwhile, as is evident in Figure 4-31 (c and d), C and N are not apparent at the Cu(II) precipitants. Similar morphologies were observed for the Cd(II)/gPU-FMH$_{80}$, and the Pb(II)/gPU-FMH$_{80}$ in FESEM images, which can be seen in Figure 4-32, respectively. Likewise, additional FESEM micrographs of Cd(II)/gPU-FMH$_{80}$ (Figure 4-33(a)) and Cd(II)/gPU-FMH$_{80}$ (Figure 4-34 (a)) were also showed that Cd(II) and Pb(II) exist on the surface of PU-FMH$_{80}$, which then used for the EDX analysis. Moreover, the EDX results confirmed that Cd(II) and Pb(II) was observed at the surface of PU-FMH$_{80}$ and presented in Figure 4-33 (b, c), and Figure 4-34 (b, c), correspondingly.

The specific surface area (BET) of the gPU-FMH$_{80}$ was measured before and after the metal sorption (Table 4.15), revealing that the gPU-FMH$_{80}$ surface area (20.2 $m^2.g^{-1}$) was reduced to 10.9 $m^2.g^{-1}$, 8.7 $m^2.g^{-1}$, and 14 $m^2.g^{-1}$ for the Cu(II)/gPU-FMH$_{80}$, Cd(II)/gPU-FMH$_{80}$, and Pb(II)/gPU-FMH$_{80}$, respectively. The N_2-gas-isotherm results were observed base on the following information. The total surface area was observed base on single point surface area at p/p° = 0.120223755. BJH surface area and micropore volume was observed by BJH desorption cumulative volume of pores between 17.000 Å and 3,000.000 Å width. BJH pore volume results were observed by Single point adsorption at p/p° = 0.997. These results are closely linked to the conclusion that the metal precipitation can effectively occur on the space of the nanostructured $Mg(OH)_2$.

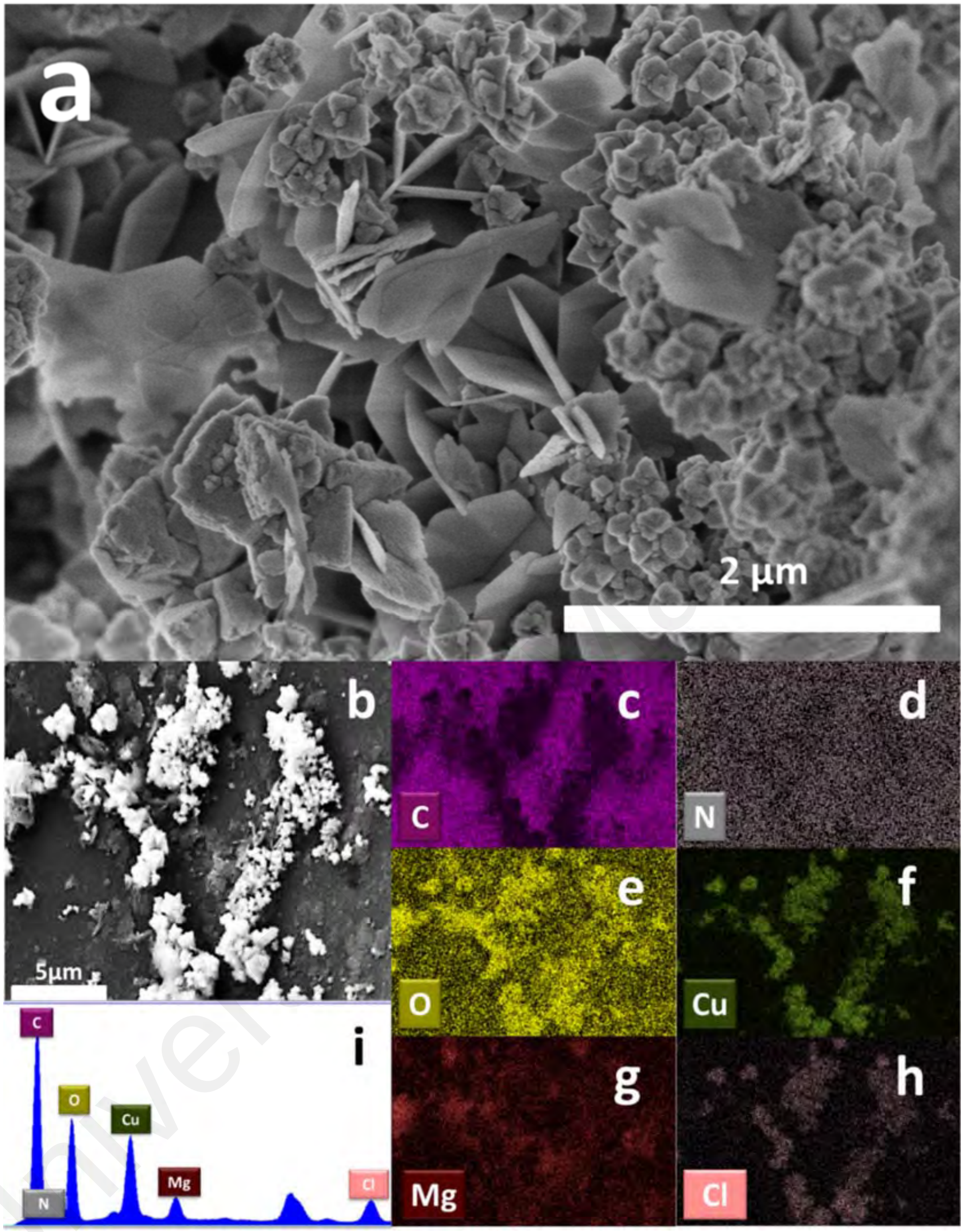

Figure 4-31: (a, b) High and low magnification FESEM image of Cu(II)/PU-FMH$_{80}$, (c-h) elemental mapping, and (i) EDX analysis of Cu(II)/PU-FMH$_{80}$

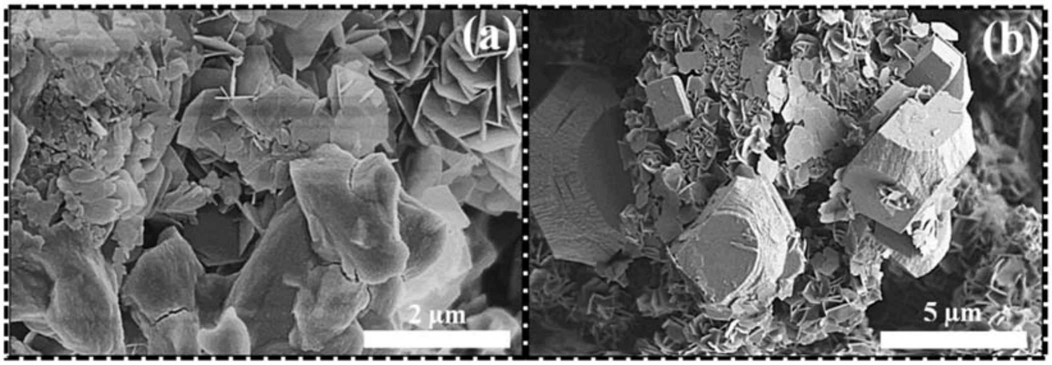

Figure 4-32: FESEM image of (a) Cd(II)/gPU-FMH$_{80}$, and (b) Pb(II)/gPU-FMH$_{80}$

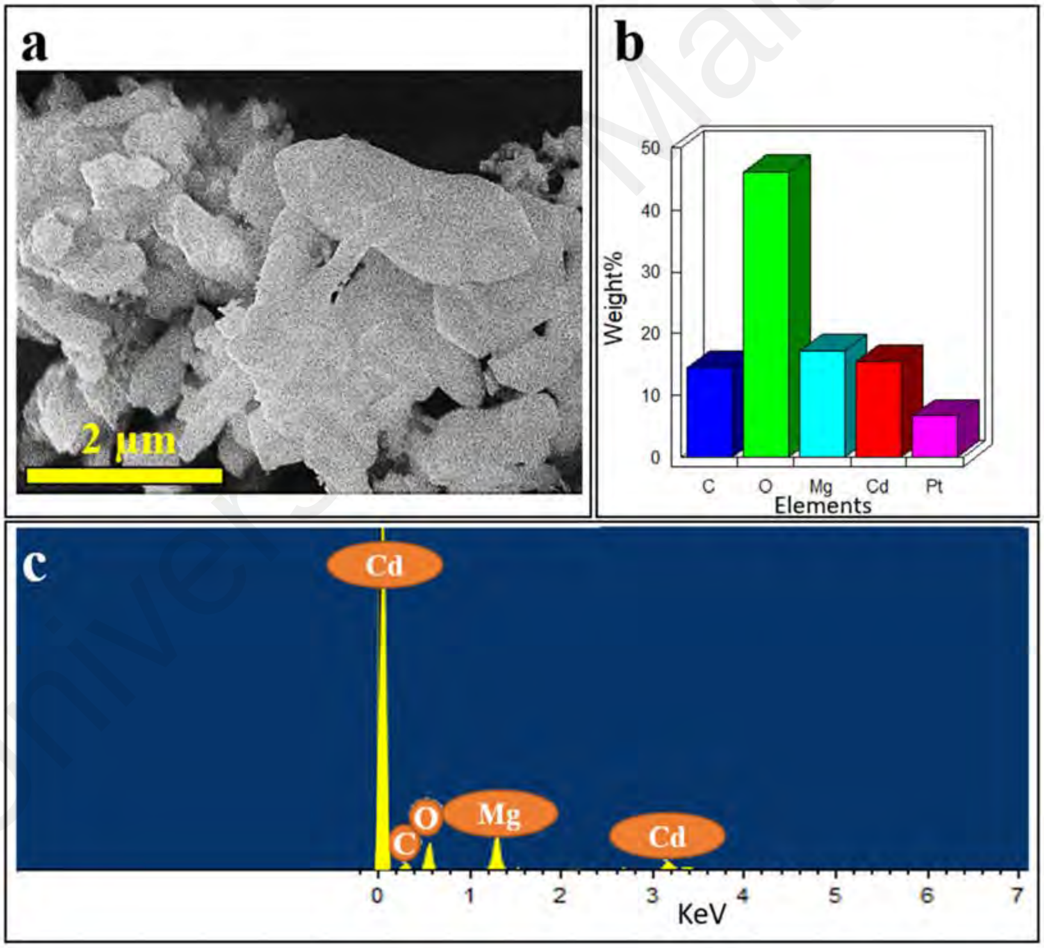

Figure 4-33: (a) FESEM, and (b, c) EDX analysis of Cd(II)/gPU-FMH$_{80}$

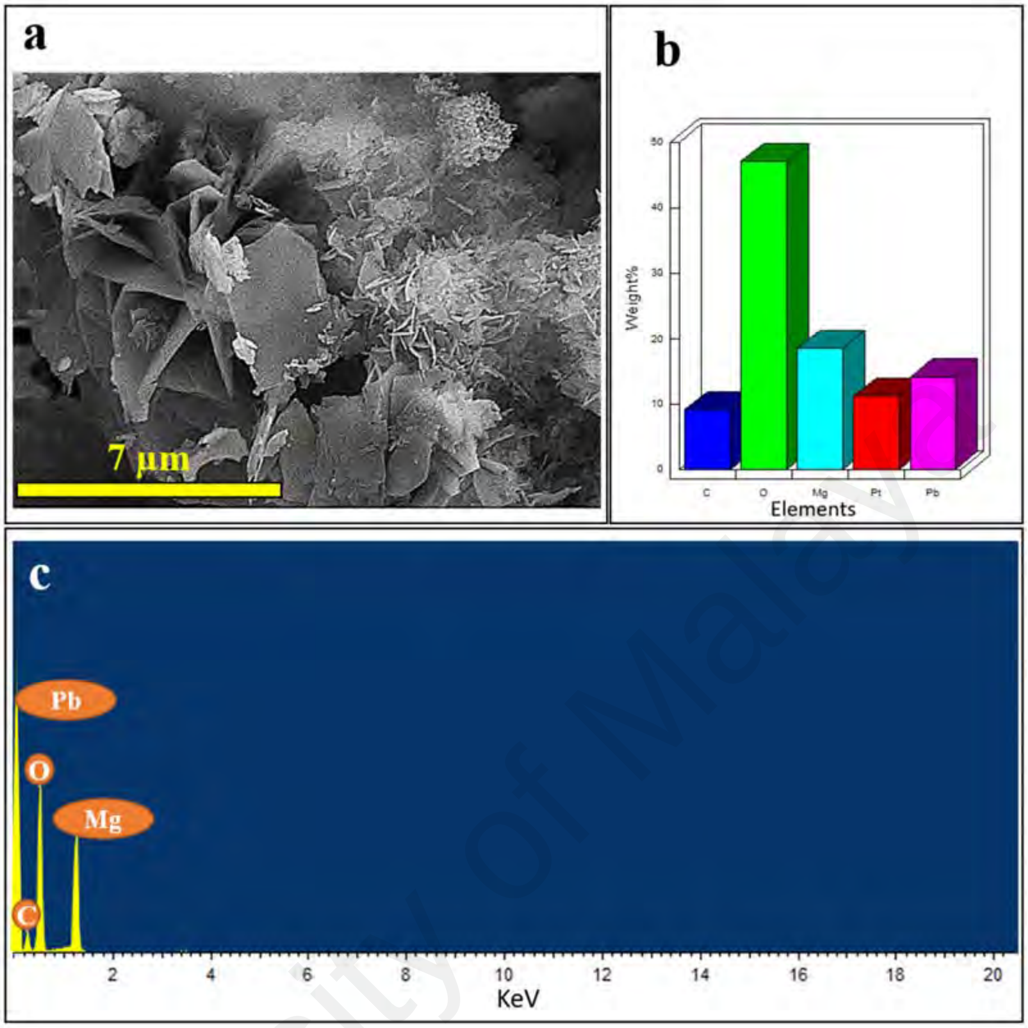

Figure 4-34: (a) FESEM, and (b, c) EDX analysis of Pb(II)/gPU-FMH$_{80}$

Table 4.15: Texture and surfaces of gPU-FMH$_{80}$, Cu(II)/gPU-FMH$_{80}$, Cd(II)/gPU-FMH$_{80}$, and Pb(II)/gPU-FMH$_{80}$

Surface characteristics	gPU-FMH$_{80}$	Cu(II)/gPU-FMH$_{80}$	Cd(II)/gPU-FMH$_{80}$	Pb(II)/gPU-FMH$_{80}$
Total Surface area (m^2.g^{-1})	20.20	10.90	8.70	14.00
BET Surface area (m^2.g^{-1})	20.90	11.30	8.82	14.50
Micropore area (m^2.g^{-1})	2.99	1.04	2.70	1.80
BJH surface area (m^2.g^{-1})	37.10	12.30	6.50	12.50
Total pore volume (cm^3.g^{-1})	0.15	0.06	0.04	0.07
Micropore volume (cm^3.g^{-1})	0.00	0.00	0.00	0.07
BJH pore volume (cm^3.g^{-1})	0.15	0.06	0.04	0.07

4.2.5 Column tests by PU-FMH$_{80}$

The Cu(II)-removal performances of the gPU, commercial MgO, and gPU-FMH$_{80}$ were examined in small-scale columns, as shown in Figure 4-35(a). Figure 4-35(b) shows that the BTP of the Cu(II) limitation in drinking water (0.2 mg.L^{-1}) occurred at column 1 (gPU) after 1 BV of the Cu(II) solution had passed. In column 2 (MgO), the Cu(II) was detected after 5 BVs, and the BTP occurred at 25 BVs. As a result, the pH was raised to 10 for the 12 BVs, and it was instantly dropped by 30 BVs to a pH of 4.0 (Figure 4-35 (c)). The early BTP might occur since MgO has a low reactive surface area and armoring effect (Stumm, 2012), even though its sizes are fine. Along with a low capacity, the commercial MgO is not practical due to its clogging effect. The longest BTP was found in column 3 (gPU-FMH$_{80}$) after ~570 BVs. The gPU-FMH$_{80}$ (184 mg.g^{-1}) showed the highest Cu(II)-sorption capacity, which is much higher than those of all referenced materials (Flowerlike MgO (Cao et al., 2012), flowerlike ɣ-AlOOH (Zhang et al., 2012), flowerlike TiO_2–GO (Lee & Yang, 2012), and flowerlike zinc silicate (Qu et al., 2012)), which are listed in Table 4.16. The pH in column 3 increased from a pH of 4.0 to a pH of approximately 11.0 for 600 BVs, and it dropped slowly to a pH of 8.0 until 700 BVs had passed. Moreover, the yellowish color of the gPU-FMH$_{80}$ in the column, which is apparent in Figure 4-36, was changed to the green-bluish color of Figure 4-37 after the Cu(II) was saturated. As a special feature, the gPU-FMH$_{80}$ has a high potential for the sensing or removal of heavy metals because metals can be saturated at the outermost side of media. In the replacement of the saturated media, the color change of the column can be easily understood via the flow direction and the metal contents PU-FMH$_{80}$ surface.

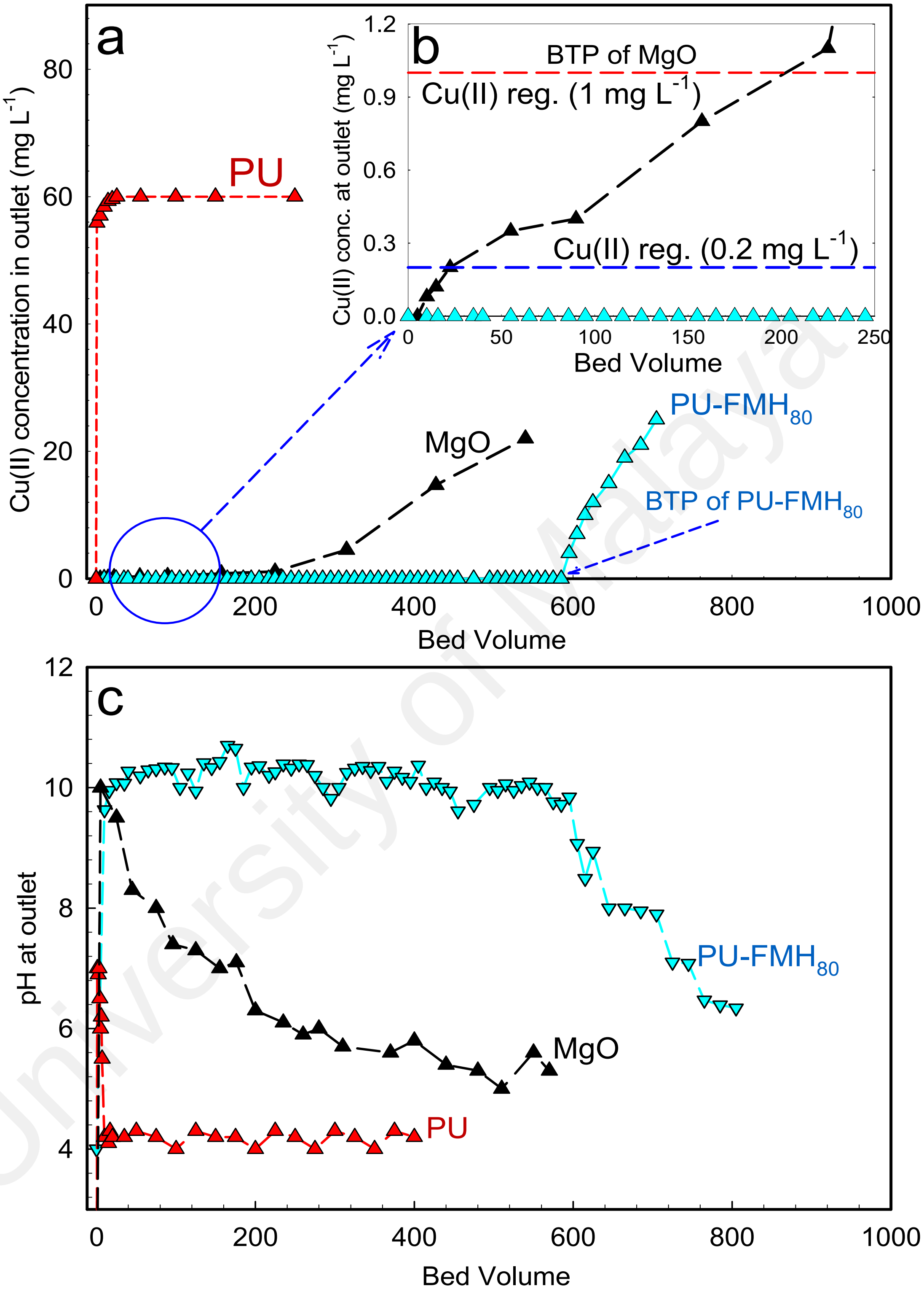

Figure 4-35: (a and b) The concentration of Cu(II) at the outlet of the column, and (c) pH changes

Figure 4-36: Digital image of fresh PU-FMH_{80}

Figure 4-37: Digital image of saturated PU-FMH_{80}

Table 4.16: Comparison of the PU, Commercial Magnesium Oxide, and gPU-FMH$_{80}$ adsorption capacity by various adsorbents in column mode

Adsorbents	Inlet pH	EBCT (min)	Inlet Cu(II) concentration (mg.L^{-1})	Maximum Cu(II) capacity (mg.g^{-1})
MnO-activated carbon (Fan & Anderson, 2005)	6.0	4.0	2	86
Diboron trioxide/titanium dioxide (Al-Rashdi et al., 2012)	5.0	30.0	1000	82
Sargassum sinicola (Patron-Prado et al., 2013)	5.5	5.0	200	64
Marine-green alga ulva reticulata (Vijayaraghavan et al., 2005c)	5.5	16.0	100	57
Calcined colloidal pyrite (Chen et al., 2014)	5.0	90.0	99	84
gPU (this study)	4.0	7.5	65	0
Commercial MgO (this study)	4.0	7.5	65	17
gPU-FMH$_{80}$ (this study)	4.0	7.5	65	184

According to the discussed results, the overall proposed hypothesis for the gPU-FMH synthesis and heavy-metal removal can be shown as Figure 4-38. Hence, to prove the previously described hypothesis, column tests were conducted in addition to the physicochemical analyses such as XRD, that of the N_2-gas isotherm, FE-SEM, and EDX. The XRD peak of the Cu(II) that was retained by the gPU-FMH_{80} [Cu(II)/gPU-FMH_{80}), as shown in Figure 4-39, shows that the Cu(II) was removed from the solution as dicopper-trihydroxide-chloride [$Cu_2(OH)_3Cl$], as per the JCPDS 19-0389 standard of the ICDD. Likewise, the gPU-FMH_{80} was changed to a green-bluish color after the Cu(II) adsorption, which agreed with the color of $Cu_2(OH)_3Cl$ (Figure 4-40a). Furthermore, the XRD peaks of the Cd(II)/gPU-FMH_{80} and the Pb(II)/gPU-FMH_{80} revealed that the cadmium-hydroxide-chloride [Cd(Cl)OH], as per the JCPDS 98-009-1087 standard, and the laurionite [Pb(Cl)OH], as per the JCPDS 98-002-8035 standard, are the gPU-FMH_{80}-surface precipitants of Cd(II) and the Pb(II), respectively (Figure 4-39). Since the colors of the particles match well with the colors of Cd(OH)Cl and Pb(OH)Cl, as can be seen in Figure 4-40 (b, and c), this finding can serve as the premise for the existence of Cd(II) and Pb(II) precipitants on the PU-FMH_{80}.

Figure 4-38: The proposed hypothesis for the synthesis of gPU-FMH and removal mechanism of heavy metals

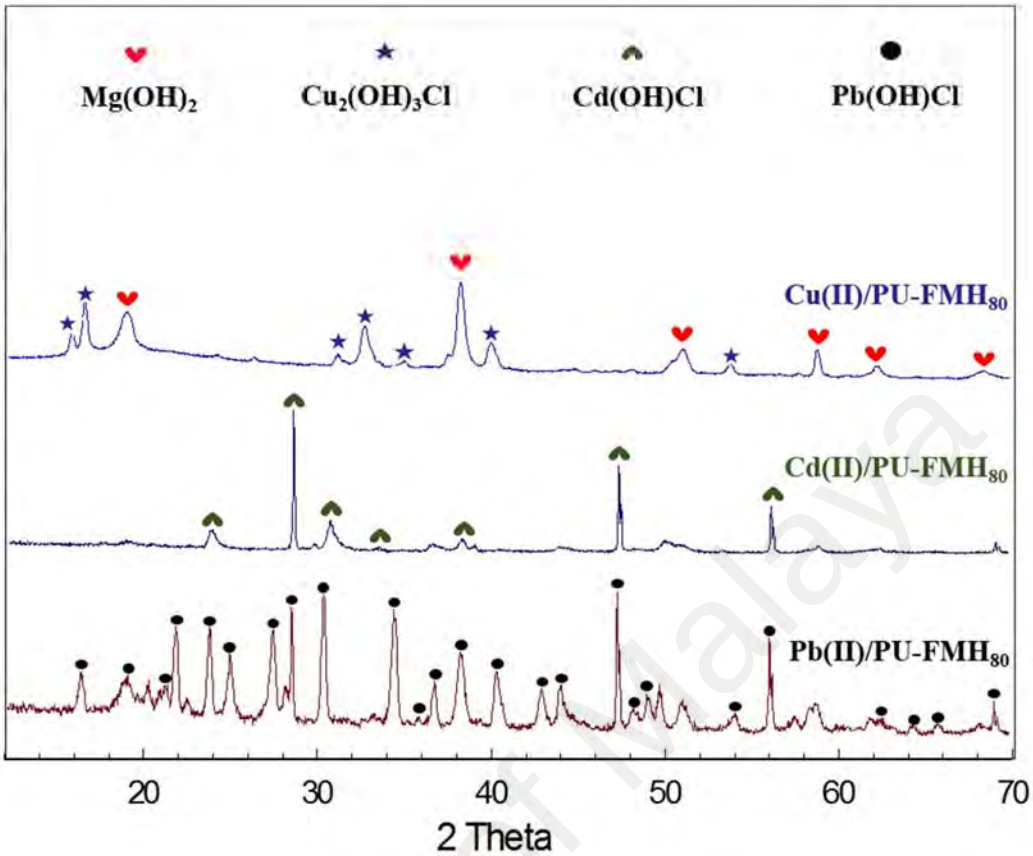

Figure 4-39: XRD patterns of Cu(II)/gPU-FMH$_{80}$, Cd(II)/gPU-FMH$_{80}$, Pb(II)/gPU-FMH$_{80}$

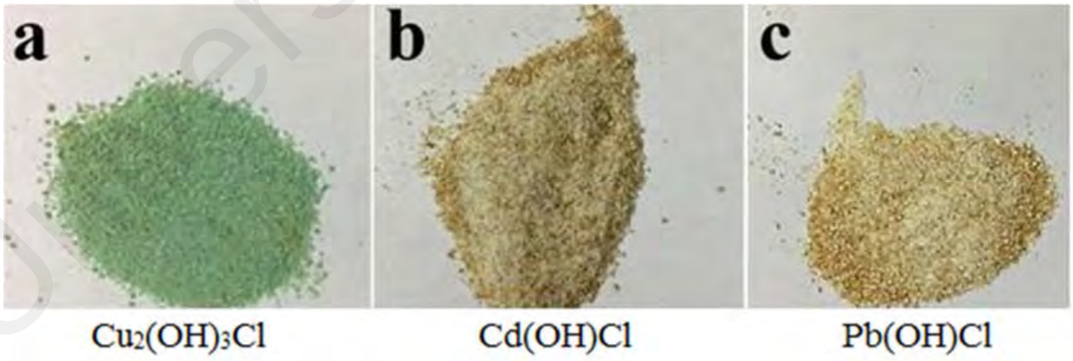

Figure 4-40: Digital image of (a) Cu$_2$(OH)$_3$Cl, (b) Cd(OH)Cl, and (c) Pb(OH)Cl

4.2.6 Cost analysis for gPU-FMH$_{80}$

Table 4.17 indicated the cost of gPU, MgO, distilled water, and power consumption. The estimated cost in Malaysia for the production of gPU-FMH$_{80}$ is 18.83 USD per 1 Kg, which is a reasonable cost according to the removal efficiency, practical and the simple preparation method of gPU-FMH$_{80}$. The transportation cost and manpower was added in the cost gPU and it the total cost to purchase and delivery to the laboratory was 6.56 USD per Kg of gPU. The cost for the commercial MgO was about 11.83 USD per Kg including the transportation and delivery to the laboratory. However, water price in this region is lower than many other countries and is the lowest to contribute to the total cost of PU-FMH$_{80}$ in Malaysia. The power generation could be reduced in industrial-scale production. However, due to the low temperature required for the preparation of gPU-FMH$_{80}$ (Only 80 °C), the power generation cost is not affecting much on the final price. It can be seen that 0.11 USD and 0.33 USD was added to the cost for the distilled water and electricity consumption, respectively. Thus, the overall cost for the synthesis of 1 Kg of gPU-FMH$_{80}$ was calculated at 18.83 USD, which can be seen in Table 4.17.

Table 4.17: Estimated cost of gPU-FMH$_{80}$

Cost descriptions for 1Kg of gPU-FMH$_{80}$	Price (USD)
gPU (including transportation)	6.56
MgO (including transportation)	11.83
Distilled water	0.11
Electricity consumption	0.33
Total	18.83 USD

CHAPTER 5: CONCLUSION AND RECOMMENDATION

5.1 Research summary and conclusion

In this study, the synthesis of rigid polyurethane incorporated by CaO (PU/CaO), and ground polyurethane coated by flowerlike $Mg(OH)_2$ (gPU-FMH) as an adsorbent for remediation of heavy metal ions from water was investigated.

The first stage of this study focused on the removal efficiency of metal ions from water by synthesis of rigid PU foam incorporated by CaO (PU/CaO-25) in an economical and effective manner. Urban stormwater run-off (USR) was used and treated by PU/CaO-25 through a fixed-bed column (Filtration system) to treat and reuse urban stormwater runoff.

The results showed that CaO had a positive effect on the physical properties of the PU/CaO composite. However, the ration between polyol and MDI plays the most important role in the synthesis of PU, and the maximum PU rigidity was achieved at a ratio of 1:2 (polyol/MDI). As special features, PU/CaO-25 had high rigidity (0.38 MPa) and permeability (0.108 cm s^{-1}), as well as relatively high removal capacities for several heavy metals.

The PU/CaO-25 is capable of removing Cu(II), Pb(II), Zn(II), and Ni(II) ions by both adsorption and ion exchange mechanisms. However, precipitation was the dominant mechanism for the removal of metal ions. The results indicated that PU/CaO-25 was the most efficient sorbent with the highest removal capacity of those metal ions. The maximum capacity of PU/CaO-25 media to remove have metal ions (Cu(II), Pb(II), Zn(II), and Ni(II)) were observed. The maximum sorption capacity of metal ions by PU/CaO-25 was observed at 32 mg.g^{-1} for Cu(II). All column data were predicted by use of BDST modeling, and the results showed a good fit of predicted data with experimental data. The N_2 gas isotherm revealed that meso- and macropore structures developed as CaO was incorporated. This feature of PU/CaO helps to avoid armoring effect on CaO and resulted in continuous release of OH^-, which can precipitate heavy metals. Finally, precipitated metal ions were trapped in the available sites, as confirmed by FESEM/EDX, elemental mapping, and XRD analyses.

Furthermore, PU/CaO-25 was used for the simulated urban stormwater run-off (USR) treatment in a fixed- bed column. Column tests using simulated USR revealed that all heavy metals were remediated by PU/CaO-25 to below their regulation levels at ~1,100 BVs. The USR treatment in the column studies with two different flow rates (0.5 and 1.2 mL.min^{-1}) confirmed that PU/CaO-25 had a similar trend of metal removal for ~1100 BVs. However, shorten the EBCT from 18.1 to 7.5 min did not have a significant effect on USR treatment. Based on its physicochemical properties and functionality, PU/CaO-25 can be used as an effective filter material for USR control and treatment with high capacities to remove heavy metals.

After the investigation in PU rigidness, high permeability, and removal of heavy metals by PU-CaO-25, the study was extended to the synthesis of three dimensional (3D) flowerlike nonstructural $Mg(OH)_2$ (gPU-FMH). For the first time, a novel self-assembled gPU-FMH was synthesized for the removal of metal ions from water using a simple method and without the inclusion of toxic and expensive chemicals. PU-FMH was synthesized via a single-step, rapid and economical process using granular PU, commercial MgO, and distilled water. The gPU and the hydrothermal treatment played important roles in the morphology of the $Mg(OH)_2$ and the formation of the regular flowerlike structures (with uniform hexagonal nanosheet petals), which were synthesized under the low range of temperature (80–120°C). Thus, it was speculated that the released organic component (i.e., diamine) of the gPU during the hydrothermal process might be the main key for the synthesis of the gPU-FMH. The Cu(II)-, Cd(II)-, and Pb(II)-removal batch-test results of the gPU-FMH$_{80}$ showed superb adsorption capacities at 472, 1050, and 1293 mg.g^{-1}, respectively, demonstrating its impressive remediation potential for a broad range of heavy metal-containing waters.

Furthermore, in the column tests, a high Cu(II)-adsorption capacity at 184 mg.g^{-1} might occur due to the flowerlike morphology of the $Mg(OH)_2$ assembled on the surface of the gPU. Besides that, PU-FMH$_{80}$ showed a much higher adsorption capability compare to PU/CaO-25 in the column mode for the removal of Cu(II). Due to its facile preparation and high efficiencies in terms of heavy-metal removal, gPU-FMH could be applied as an efficient sorbent in water-treatment systems and water filtration with a simple design and an easy operation.

5.2 Recommendation for future work

The polyurethane incorporated by calcium oxide and magnesium oxide have been successfully synthesized by using a simple method, and their removal capability was investigated for several types of heavy metals. Besides, there are several recommendations which could be considered in the future.

1- It would be interesting to use PU-FMH for USR treatment.
2- It is recommended to backwash the PU-FMH with acid solution after the sorption process. Backwashing attempts could be applied to recycle the heavy metal ions from PU media.
3- It would be interesting to use waste PU for the synthesis of PU-FMH instead of synthesizing fresh PU.
4- It is recommended to examine the adsorption capability of PU-FMH for the removal of cadmium and lead in column mode.

REFERENCES

Abo-Farha, S., Abdel-Aal, A., Ashour, I., & Garamon, S. (2009). Removal of some heavy metal cations by synthetic resin purolite C100. *Journal of hazardous materials, 169*(1-3), 190-194.

Ahmad, T., Ahmad, K., & Alam, M. (2016). Sustainable management of water treatment sludge through 3 ‘R’concept. *Journal of Cleaner Production, 124*, 1-13.

Aksu, Z., & Gonen, F. (2004). Biosorption of phenol by immobilized activated sludge in a continuous packed bed: prediction of breakthrough curves. *Process Biochemistry, 39*(5), 599-613.

Al-Degs, Y. S., El-Barghouthi, M. I., Issa, A. A., Khraisheh, M. A., & Walker, G. M. (2006). Sorption of Zn (II), Pb (II), and Co (II) using natural sorbents: equilibrium and kinetic studies. *Water Research, 40*(14), 2645-2658.

Al-Ghouti, M. A., & Sweleh, A. O. (2019). Optimizing textile dye removal by activated carbon prepared from olive stones. *Environmental Technology & Innovation, 16*, 100488.

Al-Rashdi, B., Tizaoui, C., & Hilal, N. (2012). Copper removal from aqueous solutions using nano-scale diboron trioxide/titanium dioxide (B2O3/TiO2) adsorbent. *Chemical Engineering Journal, 183*(0), 294-302.

Amarasinghe., & Williams. (2007). Tea waste as a low cost adsorbent for the removal of Cu and Pb from wastewater. *Chemical Engineering Journal, 132*(1), 299-309.

Ambashta, R. D., & Sillanpaa, M. (2010). Water purification using magnetic assistance: a review. *Journal of hazardous materials, 180*(1-3), 38-49.

Anastopoulos, I., Bhatnagar, A., Bikiaris, D., & Kyzas, G. (2017). Chitin adsorbents for toxic metals: A review. *International journal of molecular sciences, 18*(1), 114.

Aral, H., Hill, B., & Sparrow. (2004). Salts from saline waters and value added products from the salts. In: CSIRO Minerals Report DMR-2378C.

Azevedo Lemos, V., Novaes Santos, L., Oliveira Alves, A. P., & David, G. T. (2006). Chromotropic acid ‐ functionalized polyurethane foam: A new sorbent for on ‐ line preconcentration and determination of cobalt and nickel in lettuce samples. *Journal of separation science, 29*(9), 1197-1204.

Azimi, A., Azari, A., Rezakazemi, M., & Ansarpour, M. (2017). Removal of heavy metals from industrial wastewaters: a review. *ChemBioEng Reviews, 4*(1), 37-59.

Bashir, A., Malik, L. A., Ahad, S., Manzoor, T., Bhat, M. A., Dar, G., & Pandith, A. H. (2019). Removal of heavy metal ions from aqueous system by ion-exchange and biosorption methods. *Environmental Chemistry Letters, 17*(2), 729-754.

Bilal, M., Shah, J. A., Ashfaq, T., Gardazi, S. M. H., Tahir, A. A., Pervez, A., Haroon, H., & Mahmood, Q. (2013). Waste biomass adsorbents for copper removal from industrial wastewater—a review. *Journal of hazardous materials, 263*, 322-333.

Bojic, A. L, Bojic, D., & Andjelkovic, T. (2009). Removal of Cu2+ and Zn2+ from model wastewaters by spontaneous reduction–coagulation process in flow conditions. *Journal of hazardous materials, 168*(2-3), 813-819.

Bolisetty, S., Peydayesh, M., & Mezzenga, R. (2019). Sustainable technologies for water purification from heavy metals: review and analysis. *Chemical Society Reviews, 48*(2), 463-487.

Bowen, H. (1970). Absorption by polyurethane foams; new method of separation. *Journal of the Chemical Society A: Inorganic, Physical, Theoretical*, 1082-1085.

Boxall, A. B., & Maltby, L. (1995). The characterization and toxicity of sediment contaminated with road runoff. *Water Research, 29*(9), 2043-2050.

Brauer, G. (2012). *Handbook of preparative inorganic chemistry* (Vol. 2): Elsevier.

Braun, T. & Farag. (1972). Foam chromatography solid foams as supports in column chromatography. *Talanta, 19*(6), 828-830.

Cao, C.-Y., Qu, J., Wei, F., Liu, H., & Song, W.-G. (2012). Superb adsorption capacity and mechanism of flowerlike magnesium oxide nanostructures for lead and cadmium ions. *ACS applied materials & interfaces, 4*(8), 4283-4287.

Cao,H., Zheng, H., Yin, J., Lu, Y., Wu, S., Wu, X., & Li, B. (2010). Mg(OH)2 Complex Nanostructures with Superhydrophobicity and Flame Retardant Effects. *The Journal of Physical Chemistry C, 114*(41), 17362-17368.

Chang, Q., Wang, Q., Jia, F., & Song, S. (2019). Adsorption of heavy metals on molybdenum disulfide in water: A critical review. *Journal of Molecular Liquids, 292*, 111390.

Chang, Q, Zhang, M., & Wang, J. J. o. h. m. (2009). Removal of Cu2+ and turbidity from wastewater by mercaptoacetyl chitosan. *Journal of hazardous materials, 169*(1-3), 621-625.

Charumathi, D., & Das, N. (2012). Packed bed column studies for the removal of synthetic dyes from textile wastewater using immobilised dead C. tropicalis. *Desalination, 285*, 22-30.

Chen, Q., Luo, Z., Hills, C., Xue, G., & Tyrer, M. (2009). Precipitation of heavy metals from wastewater using simulated flue gas: sequent additions of fly ash, lime and carbon dioxide. *Water Research, 43*(10), 2605-2614.

Chen, T., Yang, Y., Li, P., Liu, H., Xie, J., Xie, Q., & Zhan, X. (2014). Performance and characterization of calcined colloidal pyrite used for copper removal from aqueous solutions in a fixed bed column. *International Journal of Mineral Processing, 130*, 82-87.

Chitsiga, T. L., Daramola, M. O., Wagner, N., & Ngoy, J. M. (2018). Parametric effect of adsorption variables on CO2 adsorption of amine-grafted polyaspartamide composite adsorbent during post-combustion CO2 capture: a response surface methodology approach. *International Journal of Oil, Gas*

Coal Technology, 17(3), 321-336.

Choi, H., Woo, N. C., Jang, M., Cannon, F. S., & Snyder, S. A. (2014). Magnesium oxide impregnated polyurethane to remove high levels of manganese cations from water. *Separation and Purification Technology, 136*, 184-189.

Crini, G., & Lichtfouse, E. (2019). Advantages and disadvantages of techniques used for wastewater treatment. *Environmental Chemistry Letters, 17*(1), 145-155.

Czikkely, M., Neubauer, E., Fekete, I., Ymeri, P., & Fogarassy, C. (2018). Review of Heavy Metal Adsorption Processes by Several Organic Matters from Wastewaters. *Water Research, 10*(10), 1377.

Danna, Z. (2015). Applications of Chemical Equilibrium Diagram Software HYDRA/MEDUSA in Teaching College Chemistry. *University Chemistry*(4), 4.

Davis, A., & Ashenberg, D. (1989). The aqueous geochemistry of the Berkeley pit, Butte, Montana, USA. *Applied Geochemistry, 4*(1), 23-36.

De Gois, E. H. B., Rios, C. A. S., & Costanzi, R. N. (2015). Evaluation of water conservation and reuse: a case study of a shopping mall in southern Brazil. *Journal of Cleaner Production, 96*(0), 263-271.

Duan, J., Lu, Q., Chen, R., Duan, Y., Wang, L., Gao, L., & Pan, S. (2010). Synthesis of a novel flocculant on the basis of crosslinked Konjac glucomannan-graft-polyacrylamide-co-sodium xanthate and its application in removal of Cu 2+ ion. *Carbohydrate Polymers, 80*(2), 436-441.

El-Samrani, A., Lartiges, B., & Villiéras, F. (2008). Chemical coagulation of combined sewer overflow: Heavy metal removal and treatment optimization. *Water Research, 42*(4-5), 951-960.

Fan, H. J., & Anderson, P. R. (2005). Copper and cadmium removal by Mn oxide-coated granular activated carbon. *Separation and Purification Technology, 45*(1), 61-67.

Feng, W., Hatt, B. E., McCarthy, D. T., Fletcher, T. D., & Deletic, A. (2012). Biofilters for stormwater harvesting: understanding the treatment performance of key metals that pose a risk for water use. *Environmental science & technology, 46*(9), 5100-5108.

Figueiredo, H., & Quintelas, C. (2014). Tailored zeolites for the removal of metal oxyanions: Overcoming intrinsic limitations of zeolites. *Journal of hazardous materials, 274*, 287-299.

Fiol, N., Villaescusa, I., Martínez, M., Miralles, N., Poch, J., & Serarols, J. (2006). Sorption of Pb (II), Ni (II), Cu (II) and Cd (II) from aqueous solution by olive stone waste. *Separation and Purification Technology, 50*(1), 132-140.

Fournier, D., De Geest, B. G., & Du Prez, F. E. (2009). On-demand click functionalization of polyurethane films and foams. *Polymer, 50*(23), 5362-5367.

Fruhwirth, O., Herzog, G., Hollerer, I., & Rachetti, A. (1985). Dissolution and hydration kinetics of MgO. *Surface Technology, 24*(3), 301-317.

Fu, F., & Wang, Q. (2011). Removal of heavy metal ions from wastewaters: a review. *Journal of environmental management, 92*(3), 407-418.

Ge, F., Li, M.-M., Ye, H., & Zhao, B.-X. (2012). Effective removal of heavy metal ions Cd2+, Zn2+, Pb2+, Cu2+ from aqueous solution by polymer-modified magnetic nanoparticles. *Journal of hazardous materials, 211*, 366-372.

Gesser, H. D., Chow, A., Davis, F., Uthe, J. F., & Reinke, J. (1971). The extraction and recovery of polychlorinated biphenyls (PCB) using porous polyurethane foam. *Analytical Letters, 4*(12), 883-886.

Ghaedi, M., & Mosallanejad, N. (2018). Removal of heavy metal ions from polluted waters by using of low cost adsorbents. *Journal of Chemical Health Risks, 3*(1).

Ghernaout, D., Al-Ghonamy, A. I., Boucherit, A., Ghernaout, B., Naceur, M. W., Messaoudene, N. A., Aichouni, M., Mahjoubi, A. A., & Elboughdiri, N. A. (2015). Brownian motion and coagulation process. *Am. J. Environ. Prot, 4*, 1-15.

Global Market Insights, I. (2017). Polyurethanes market.

Gunashekar, S., & Abu-Zahra, N. (2014). Characterization of functionalized polyurethane foam for lead ion removal from water. *International Journal of Polymer Science, 2014*.

Gunashekar, S., & Abu-Zahra, N. (2015). Synthesis of functionalized polyurethane foam using BES chain extender for lead ion removal from aqueous solutions. *Journal of Cellular Plastics, 51*(5-6), 453-470.

Han, R., Zou, W., Li, H., Li, Y., & Shi, J. (2006). Copper (II) and lead (II) removal from aqueous solution in fixed-bed columns by manganese oxide coated zeolite. *Journal of hazardous materials, 137*(2), 934-942.

Hasan, S. H., Ranjan, D., & Talat, M. (2010). Agro-industrial waste 'wheat bran' for the biosorptive remediation of selenium through continuous up-flow fixed-bed column. *Journal of hazardous materials, 181*(1–3), 1134-1142.

Hasfalina, C., Maryam, R., Luqman, C., & Rashid, M. (2012). Adsorption of copper (II) from aqueous medium in fixed-bed column by kenaf fibres. *Apcbee Procedia 3*, 255-263.

Hassan, M. M., & Carr, C. M. (2018). A critical review on recent advancements of the removal of reactive dyes from dyehouse effluent by ion-exchange adsorbents. *Chemosphere, 209*, 201-219.

Hayes, M. (1970). Adsorption of triazine herbicides on soil organic matter, including a short review on soil organic matter chemistry. In *Single Pesticide Volume: The Triazine Herbicides* (pp. 131-174): Springer.

Hillel, D. (1998). *Environmental soil physics: Fundamentals, applications, and environmental considerations*: Academic press.

Hong, Lim, J. S., Hwang, J. Y., Kim, M., Jeong, H. S., & Park, M. S. (2018). Carboxymethlyated cellulose nanofibrils (CMCNFs) embedded in polyurethane foam as a modular adsorbent of heavy metal ions. *Carbohydrate Polymers, 195*, 136-142.

Hong, Yu, L., Wang, Y., Zhang, J., Chen, Z., Dong, L., Zan, Q., & Li, R. (2019). Heavy metal adsorption with zeolites: The role of hierarchical pore architecture. *Chemical Engineering Journal, 359*, 363-372.

Hsieh, C.-h., & Davis, A. P. (2005). Evaluation and optimization of bioretention media for treatment of urban storm water runoff. *Environ Eng-ASCE, 131*(11), 1521-1531.

Hu, J., & Shipley, H. J. (2013). Regeneration of spent TiO 2 nanoparticles for Pb (II), Cu (II), and Zn (II) removal. *Environmental Science*

Pollution Research, 20(8), 5125-5137.

Hua, G., & Odelius, K. (2016). From Food Additive to High-Performance Heavy Metal Adsorbent: A Versatile and Well-Tuned Design. *ACS Sustainable Chemistry & Engineering, 4*(9), 4831-4841.

Huang, Wu, D., Wang, X., Huang, W., Lawless, D., & Feng, X. (2016). Removal of heavy metals from water using polyvinylamine by polymer-enhanced ultrafiltration and flocculation. *Separation Purification Technology, 158*, 124-136.

Huang, J., Zeng, G.-M., Zhou, C.-F., Li, X., Shi, L.-J., & He, S.-B. (2010). Adsorption of surfactant micelles and Cd 2+/Zn 2+ in micellar-enhanced ultrafiltration. *Journal of hazardous materials, 183*(1), 287-293.

Huber, M., Welker, A., & Helmreich, B. (2016). Critical review of heavy metal pollution of traffic area runoff: Occurrence, influencing factors, and partitioning. *Science of the Total Environment, 541*, 895-919.

Hutchins, R. A. (1973). New method simplifies design of activated system. *Chem Eng-New York, 80*, 138.

Hwang, H.-M., Fiala, M. J., Park, D., & Wade, T. L. (2016). Review of pollutants in urban road dust and stormwater runoff: Part 1. Heavy metals released from vehicles. *International Journal of Urban Sciences, 20*(3), 334-360.

Iakovleva, E., Makila, E., Salonen, J., Sitarz, M., Wang, S., & Sillanpaa, M. (2015). Acid mine drainage (AMD) treatment: Neutralization and toxic elements removal with unmodified and modified limestone. *Ecological Engineering, 81*, 30-40.

Ibrahim, Y., Abdulkarem, E., Naddeo, V., Banat, F., & Hasan, S. W. (2019). Synthesis of super hydrophilic cellulose-alpha zirconium phosphate ion exchange membrane via surface coating for the removal of heavy metals from wastewater. *Science of the Total Environment, 690*, 167-180.

Ibrahim, B. M., & Fakhre, N. A., (2019). Crown ether modification of starch for adsorption of heavy metals from synthetic wastewater. *International journal of biological macromolecules, 123*, 70-80.

Inyang, M. I., Gao, B., Yao, Y., Xue, Y., Zimmerman, A., Mosa, A., Pullammanappallil, P., Ok, Y. S., & Cao, X. (2016). A review of biochar as a low-cost adsorbent for aqueous heavy metal removal. *Critical Reviews in Environmental Science and Technology, 46*(4), 406-433.

Jamil, T. S., Ibrahim, H. S., El-Maksoud, I. A., & El-Wakeel, S. (2010). Application of zeolite prepared from Egyptian kaolin for removal of heavy metals: I. Optimum conditions. *Desalination, 258*(1-3), 34-40.

Jang, S. H., Min, B. G., Jeong, Y. G., Lyoo, W. S., & Lee, S. C. (2008). Removal of lead ions in aqueous solution by hydroxyapatite/polyurethane composite foams. *Journal of hazardous materials, 152*(3), 1285-1292.

Jiao, C. M., Wang, Z. Z., Ye, Z., Hu, Y., & Fan, W. C. (2006). Flame Retardation of Ethylene-Vinyl Acetate Copolymer Using Nano Magnesium Hydroxide and Nano Hydrotalcite. *Journal of Fire Sciences, 24*(1), 47-64.

Jiao, L., Xiao, H., Wang, Q., & Sun, J. (2013). Thermal degradation characteristics of rigid polyurethane foam and the volatile products analysis with TG-FTIR-MS. *Polymer Degradation and Stability, 98*(12), 2687-2696.

Joshi, U. M., & Balasubramanian, R. (2010). Characteristics and environmental mobility of trace elements in urban runoff. *Chemosphere, 80*(3), 310-318.

Kalaivani, S., Muthukrishnaraj, A., Sivanesan, S., & Ravikumar, L. (2016a). Novel hyperbranched polyurethane resins for the removal of heavy metal ions from aqueous solution. *Process Safety and Environmental Protection, 104*, 11-23.

Kalaivani, S., Muthukrishnaraj, A., Sivanesan, S., & Ravikumar, L. (2016b). Novel hyperbranched polyurethane resins for the removal of heavy metal ions from aqueous solution. *Process Safety*

Environmental Protection, 104, 11-23.

Khan, A., Szulejko, J. E., Samaddar, P., Kim, K.-H., Liu, B., Maitlo, H. A., Yang, X., & Ok, Y. S. (2019). The potential of biochar as sorptive media for removal of hazardous benzene in air. *Chemical Engineering Journal, 361*, 1576-1585.

Ko, D. C., Porter, J. F., & McKay, G. (2000). Optimised correlations for the fixed-bed adsorption of metal ions on bone char. *Chem Eng Sci, 55*(23), 5819-5829.

Kononova, O., Bryuzgina, G., Apchitaeva, O., & Kononov, Y. (2015). Ion exchange recovery of chromium (VI) and manganese (II) from aqueous solutions. *Arabian Journal of Chemistry*.

Krupadam, R., Khan, M., & Das, S. (2010). Adsorption of fluoride from water by surface-functionalized polyurethane foam. *Water Science and Technology, 62*(4), 759-765.

Kutluay, S., Baytar, O., & Sahin, O. (2019). Equilibrium, kinetic and thermodynamic studies for dynamic adsorption of benzene in gas phase onto activated carbon produced from elaeagnus angustifolia seeds. *Journal of Environmental Chemical Engineering, 7*(2), 102947.

Lalezary, S., Pirbazari, M., & McGuire, M. J. (1986). Evaluating Activated Carbons for Removing Low Concentrations of Taste‐and Odor‐Producing Organics. *Journal‐American Water Works Association, 78*(11), 76-82.

Larson, T., & Buswell, A. (1940). Water softening. *Industrial & Engineering Chemistry, 32*(1), 132-134.

Lee, J. G., & Flumerfelt, R. W. (1996). A refined approach to bubble nucleation and polymer foaming process: dissolved gas and cluster size effects. *Journal of colloid and Interface Science, 184*(2), 335-348.

Lee, S. T., Park, C. B., & Ramesh, N. S. (2006). *Polymeric foams: science and technology*: CRC Press.

Lee, S. T., & Ramesh, N. S. (2004). *Polymeric foams: mechanisms and materials*: CRC press.

Lee Y. C., & Yang, J. W. (2012). Self-assembled flower-like TiO 2 on exfoliated graphite oxide for heavy metal removal. *Journal of Industrial and Engineering Chemistry, 18*(3), 1178-1185.

Lee, D. W., & Halmann, M. (1976). Selective separation of nickel (II) by dimethylglyoxime-treated polyurethane foam. *Analytical chemistry, 48*(14), 2214-2217.

Lemos, V., Santos, M., Santos, E., Santos, M., Dos Santos, W., Souza, A., De Jesus, D., Das Virgens, C., Carvalho, M., & Oleszczuk, N. (2007). Application of polyurethane foam as a sorbent for trace metal pre-concentration—a review. *Spectrochimica acta part B: Atomic spectroscopy, 62*(1), 4-12.

Li, C., & Champagne, P. (2009). Fixed-bed column study for the removal of cadmium (II) and nickel (II) ions from aqueous solutions using peat and mollusk shells. *Journal of hazardous materials, 171*(1–3), 872-878.

Li, Y., Liu, J., Huang, X., & Li, G. (2007). Hydrothermal synthesis of Bi2WO6 uniform hierarchical microspheres. *Crystal Growth and Design, 7*(7), 1350-1355.

Li, W., Tekell, M. C., Huang, Y., Bertelsmann, K., Lau, M., & Fan, D. (2018). Synergistic High‐Rate Solar Steaming and Mercury Removal with MoS2/C@ Polyurethane Composite Sponges. *Advanced Energy Materials, 8*(32), 1802108.

Liu, M., Xu, J., Cheng, B., Ho, W., & Yu, J. (2015). Synthesis and adsorption performance of Mg (OH) 2 hexagonal nanosheet–graphene oxide composites. *Applied Surface Science, 332*, 121-129.

Lyu, S., Chen, W., Zhang, W., Fan, Y., & Jiao, W. (2016). Wastewater reclamation and reuse in China: opportunities and challenges. *Journal of Environmental Sciences, 39*, 86-96.

Ma, X., Ma, H., Jiang, X., & Jiang, Z. (2014). Preparation of magnesium hydroxide nanoflowers from boron mud via anti-drop precipitation method. *Materials Research Bulletin, 56*, 113-118.

Mangaleshwaran, L., Thirulogachandar, A., Rajasekar, V., Muthukumaran, C., & Rasappan, K. (2015). Batch and fixed bed column studies on nickel (II) adsorption from aqueous solution by treated polyurethane foam. *Journal of the Taiwan Institute of Chemical Engineers, 55*, 112-118.

MDC Sdn Bhd. (1974). Laws of Malaysia-Environmental Quality Act 1974 and Regulations. *(fourth ed.) (1997)*(Kuala Lumpur, Malaysia).

Meligi, G. A. (2007). Removal of some heavy metal ions using grafted polyurethane foam. *Polymer-Plastics Technology and Engineering, 47*(1), 106-113.

Moawed, E., Zaid, M. A., & El-Shahat, M. (2006). Analytical application of polyurethane foam functionalized with quinolin-8-ol for preconcentration and determination of trace metal ions in wastewater. *Journal of Analytical Chemistry, 61*(5), 458-464.

Mohan, S., & Sreelakshmi, G. (2008). Fixed bed column study for heavy metal removal using phosphate treated rice husk. *Journal of hazardous materials, 153*(1), 75-82.

Musico, Y. L. F., Santos, C. M., Dalida, M. L. P., & Rodrigues, D. F. (2013). Improved removal of lead(ii) from water using a polymer-based graphene oxide nanocomposite. *Journal of Materials Chemistry A, 1*(11), 3789-3796.

Mutamim, N. S. A., Noor, Z. Z., Hassan, M. A. A., & Olsson, G. (2012). Application of membrane bioreactor technology in treating high strength industrial wastewater: a performance review. *Desalination, 305*, 1-11.

Nanseu-Njiki, C. P., Tchamango, S. R., Ngom, P. C., Darchen, A., & Ngameni, E. (2009). Mercury (II) removal from water by electrocoagulation using aluminium and iron electrodes. *Journal of hazardous materials, 168*(2), 1430-1436.

Nasiri, R., Arsalani, N., & Panahian, Y. (2018). One-pot synthesis of novel magnetic three-dimensional graphene/chitosan/nickel ferrite nanocomposite for lead ions removal from aqueous solution: RSM modelling design. *Journal of Cleaner Production, 201*, 507-515.

Netpradit, S., Thiravetyan, P., & Towprayoon, S. (2004). Evaluation of metal hydroxide sludge for reactive dye adsorption in a fixed-bed column system. *Water Research, 38*(1), 71-78.

Nguyen, T. C., Loganathan, P., Nguyen, T. V., Vigneswaran, S., Kandasamy, J., & Naidu, R. (2015). Simultaneous adsorption of Cd, Cr, Cu, Pb, and Zn by an iron-coated Australian zeolite in batch and fixed-bed column studies. *Chemical Engineering Journal, 270*(0), 393-404.

Ni, B. J., Huang, Q. S., Wang, C., Ni, T. Y., Sun, J., & Wei, W. (2019). Competitive adsorption of heavy metals in aqueous solution onto biochar derived from anaerobically digested sludge. *Chemosphere, 219*, 351-357.

Nikkhah, A. A., Zilouei, H., Asadinezhad, A., & Keshavarz, A. (2015). Removal of oil from water using polyurethane foam modified with nanoclay. *Chemical Engineering Journal, 262*, 278-285.

Oertel, G., & Abele, L. (1985). *Polyurethane handbook: chemistry, raw materials, processing, application, properties*: Hanser Publishers. Distributed in USA by Scientific and Technical Books, Macmillan.

Ong, C., Ibrahim, S., & Sen Gupta, B. (2007). A survey of tap water quality in Kuala Lumpur. *Urban Water Journal, 4* (1), 29-41.

Park, J. H., Ok, Y. S., Kim, S. H., Cho, J. S., Heo, J. S., Delaune, R. D., & Seo, D. C. J. C. (2016). Competitive adsorption of heavy metals onto sesame straw biochar in aqueous solutions. *Chemosphere, 142*, 77-83.

Patron-Prado, M., Lodeiro, P., Lluch-Cota, D. B., Serviere-Zaragoza, E., Casas-Valdez, M., Zenteno-Savín, T., & Mendez-Rodriguez, L. (2013). Efficiency of copper removal by Sargassum sinicola in batch and continuous systems. *Journal of Applied Phycology, 25*(6), 1933-1937.

Pepe, F., de Gennaro, B., Aprea, P., & Caputo, D. (2013). Natural zeolites for heavy metals removal from aqueous solutions: modeling of the fixed bed Ba2+/Na+ ion-exchange process using a mixed phillipsite/chabazite-rich tuff. *Chemical Engineering Journal, 219*, 37-42.

Proc. Conf., N. (1996). *Cellular plastics.* Paper presented at the Cellular plastics, Massachutesetts, Washington, D.C. 1967.

Qing, X., Yutong, Z., & Shenggao, L. (2015). Assessment of heavy metal pollution and human health risk in urban soils of steel industrial city (Anshan), Liaoning, Northeast China. *Ecotoxicology and environmental safety, 120*, 377-385.

Qu, J., Cao, C.-Y., Hong, Y.-L., Chen, C.-Q., Zhu, P.-P., Song, W.-G., & Wu, Z.-Y. (2012). New hierarchical zinc silicate nanostructures and their application in lead ion adsorption. *Journal of Materials Chemistry, 22*(8), 3562-3567.

Ramesh, A., Mohan, K. R., Seshaiah, K., & Jeyakumar, N. (2001). Determination of trace elements by inductively coupled plasma-atomic emission spectrometry (ICP-

AES) after preconcentration on a support impregnated with piperidine dithiocarbamate. *Analytical Letters, 34*(2), 219-229.

Rao, S., Lekshmi, R., Mani, A., & Sinha, P. (2009). Treatment of low level radioactive liquid wastes using composite ion-exchange resins based on polyurethane foam. *Journal of radioanalytical and nuclear chemistry, 283*(2), 379-384.

Razzaghmanesh, M., Beecham, S., & Kazemi, F. (2014). The growth and survival of plants in urban green roofs in a dry climate. *Sci Total Environ, 476–477*(0), 288-297.

Riaz, T., Ahmad, A., Saleemi, S., Adrees, M., Jamshed, F., Hai, A. M., & Jamil, T. (2016). Synthesis and characterization of polyurethane-cellulose acetate blend membrane for chromium (VI) removal. *Carbohydrate Polymers, 153*, 582-591.

Ruthven, D. M. (1984). *Principles of adsorption and adsorption processes*: John Wiley & Sons.

Saeedi, A., Jafari, A. J., Kalantary, R. R., & Esrafili, A. (2020). A novel synthetic thin-film nanocomposite forward osmosis membrane modified by graphene oxide and polyethylene glycol for heavy metals removal from aqueous solutions. *Reactive and Functional Polymers, 146*, 104397.

Sahmoune, M, Nasser. (2019). Evaluation of thermodynamic parameters for adsorption of heavy metals by green adsorbents. *Environmental Chemistry Letters, 17*(2), 697-704.

Salamatinia, B., Kamaruddin, A. H., & Abdullah, A. Z. (2008). Modeling of the continuous copper and zinc removal by sorption onto sodium hydroxide-modified oil palm frond in a fixed-bed column. *Chemical Engineering Journal, 145*(2), 259-266.

Sample, D. J., Grizzard, T. J., Sansalone, J., Davis, A. P., Roseen, R. M., & Walker, J. (2012). Assessing performance of manufactured treatment devices for the removal of phosphorus from urban stormwater. *Journal of environmental management, 113*, 279-291.

Sanger, D., Holland, A., & Scott, G. (1999). Tidal creek and salt marsh sediments in South Carolina coastal estuaries: II. Distribution of organic contaminants. *Archives of Environmental Contamination and Toxicology, 37*(4), 458-471.

Sarvestani, R. A., & Aghasi, M. (2019). Health risk assessment of heavy metals exposure (lead, cadmium, and copper) through drinking water consumption in Kerman city, Iran. *Environmental Earth Sciences, 78*(24), 714.

Saucedo-Rivalcoba, V., Martínez-Hernandez, A., Martínez-Barrera, G., Velasco-Santos, C., Rivera-Armenta, J., & Castano, V. (2011). Removal of hexavalent chromium from water by polyurethane–keratin hybrid membranes. *Water, Air, Soil Pollution, 218*(1-4), 557-571.

Seifert, D., & Engesgaard, P. (2012). Sand box experiments with bioclogging of porous media: Hydraulic conductivity reductions. *Contam Hydrol, 136–137*(0), 1-9.

Siskin, M., & Katritzky, A. R. (1991). Reactivity of organic compounds in hot water: Geochemical and technological implications. *Science, 254*(5029), 231-237.

Siyal, A. A., Shamsuddin, M. R., Khan, M. I., Rabat, N. E., Zulfiqar, M., Man, Z., Siame, J., & Azizli, K. A. (2018). A review on geopolymers as emerging materials for the adsorption of heavy metals and dyes. *Journal of environmental management*.

Smits, K. M., Ngo, V. V., Cihan, A., Sakaki, T., & Illangasekare, T. H. (2012). An evaluation of models of bare soil evaporation formulated with different land surface boundary conditions and assumptions. *Water Resour Research 48*(12).

Sone, H., Fugetsu, B., & Tanaka, S. (2009). Selective elimination of lead (II) ions by alginate/polyurethane composite foams. *Journal of hazardous materials, 162*(1), 423-429.

Standard, A. (2007). D5856-95 *Standard test method for measurement of hydraulic conductivity of porous material using a rigid-wall, compaction-mold permeameter*.

Standard, A. (2010). D1621-10. *Standard test method for compressive properties of rigid cellular plastics. west conshohocken, pa: american society of testing materials*.

Stumm, W., Morgan, James. (2012). *Aquatic chemistry: chemical equilibria and rates in natural waters* (Vol. 126): John Wiley & Sons.

Sundarram, S. S., Jiang, W., & Li, W. (2014). Fabrication of small pore-size nickel foams using electroless plating of solid-state foamed immiscible polymer blends. *Journal of Manufacturing Science and Engineering, 136*(2), 021002.

Szycher, M. (1999). *Szycher's handbook of polyurethanes*: CRC press.

Tang, X., Guo, L., Liu, Q., Li, Y., Li, T., Zhu, Y., & Technology. (2015). Morphology analysis of magnesium hydroxide prepared by magnesium oxide hydration within seawater. *Crystal Research, 50*(3), 203-209.

Tao, W., Chen, G., Zeng, G., Yan, M., Chen, A., Guo, Z., Huang, Z., He, K., Hu, L., & Wang, L. (2016). Influence of silver nanoparticles on heavy metals of pore water in contaminated river sediments. *Chemosphere, 162*, 117-124.

Tokuyama, H., Hisaeda, J., Nii, S., & Sakohara, S. (2010). Removal of heavy metal ions and humic acid from aqueous solutions by co-adsorption onto thermosensitive polymers. *Separation and Purification Technology, 71*(1), 83-88.

Tran, N. H., Ngo, H. H., Urase, T., & Gin, K. Y.-H. (2015). A critical review on characterization strategies of organic matter for wastewater and water treatment processes. *Bioresource technology, 193*, 523-533.

Uddin, M. T., Rukanuzzaman, M., Khan, M. M. R., & Islam, M. A. (2009). Adsorption of methylene blue from aqueous solution by jackfruit (Artocarpus heteropyllus) leaf powder: a fixed-bed column study. *Environ Manage, 90*(11), 3443-3450.

Unuabonah, E. I., Khaiary, M. I., Olu-Owolabi, B. I., & Adebowale, K. O. (2012). Predicting the dynamics and performance of a polymer–clay based composite in a fixed bed system for the removal of lead (II) ion. *Chemical Engineering Research and Design, 90*(8), 1105-1115.

Venerus, D. C., & Yala, N. (1997). Transport analysis of diffusion ‐ induced bubble growth and collapse in viscous liquids. *AIChE journal, 43*(11), 2948-2959.

Vengris, T., Binkiene, R., & Sveikauskaite, A. (2001). Nickel, copper and zinc removal from waste water by a modified clay sorbent. *Applied Clay Science 18*(3–4), 183-190.

Vijayaraghavan, K., Jegan, J., Palanivelu, K., & Velan, M. (2005a). Batch and column removal of copper from aqueous solution using a brown marine alga Turbinaria ornata. *Chemical Engineering Journal, 106*(2), 177-184.

Vijayaraghavan, K., Jegan, J., Palanivelu, K., & Velan, M. (2005b). Biosorption of cobalt (II) and nickel (II) by seaweeds: batch and column studies. *Separation and Purification Technology, 44*(1), 53-59.

Vijayaraghavan, K., Jegan, J., Palanivelu, K., & Velan, M. (2005c). Biosorption of copper, cobalt and nickel by marine green alga Ulva reticulata in a packed column. *Chemosphere, 60*(3), 419-426.

Vijayaraghavan, K., & Prabu, D. (2006). Potential of Sargassum wightii biomass for copper (II) removal from aqueous solutions: Application of different mathematical models to batch and continuous biosorption data. *Journal of hazardous materials, 137*(1), 558-564.

Vinodhini, V., & Das, N. (2010). Packed bed column studies on Cr (VI) removal from tannery wastewater by neem sawdust. *Desalination, 264*(1), 9-14.

Visa, M, J. P. T. (2016). Synthesis and characterization of new zeolite materials obtained from fly ash for heavy metals removal in advanced wastewater treatment. *Powder Technology, 294*, 338-347.

Voorhees, P. W. (1985). The theory of Ostwald ripening. *Journal of Statistical Physics, 38*(1-2), 231-252.

Wan, S., Qu, N., He, F., Wang, M., Liu, G., & He, H. (2015). Tea waste-supported hydrated manganese dioxide (HMO) for enhanced removal of typical toxic metal ions from water. *RSC Advances, 5*(108), 88900-88907.

Widya, T., & Macosko, C. W. (2005). Nanoclay ‐ modified rigid polyurethane foam. *Macromol Sci B, 44*(6), 897-908.

Woods, G. (1982). *Flexible polyurethane foams*: Springer.

Wu, J., Yan, H., Zhang, X., Wei, L., Liu, X., & Xu, B. (2008). Magnesium hydroxide nanoparticles synthesized in water-in-oil microemulsions. *Journal of colloid and Interface Science, 324*(1–2), 167-171.

Xu, J., Cao, Z., Zhang, Y., Yuan, Z., Lou, Z., Xu, X., & Wang, X. (2018). A review of functionalized carbon nanotubes and graphene for heavy metal adsorption from water: Preparation, application, and mechanism. *Chemosphere, 195*, 351-364.

Yan, G., & Viraraghavan. (2001). Heavy metal removal in a biosorption column by immobilized M. rouxii biomass. *Bioresource Technol, 78*(3), 243-249.

Yan, L., Yin, H., Zhang, S., Leng, F., Nan, W., & Li, H. (2010). Biosorption of inorganic and organic arsenic from aqueous solution by Acidithiobacillus ferrooxidans BY-3. *Journal of hazardous materials, 178*(1-3), 209-217.

Yang, X., Wan, Y., Zheng, Y., He, F., Yu, Z., Huang, J., Wang, H., Ok, Y. S., Jiang, Y., & Gao, B. (2019). Surface functional groups of carbon-based adsorbents and their roles in the removal of heavy metals from aqueous solutions: a critical review. *Chemical Engineering Journal, 366*, 608-621.

Yeon, K. H., Lee, J. W., Lee, J. S., & Moon, S. H. (2002). Preparation and characterization of cation‐exchange media based on flexible polyurethane foams. *Journal of applied polymer science, 86*(7), 1773-1781.

Yu, B., Zhang, Y., Shukla, A., Shukla, S. S., & Dorris, K. L. (2001). The removal of heavy metals from aqueous solutions by sawdust adsorption — removal of lead and comparison of its adsorption with copper. *Journal of hazardous materials, 84*(1), 83-94.

Yu, L., Han, M., & He, F. (2017). A review of treating oily wastewater. *Arabian Journal of Chemistry, 10*, S1913-S1922.

Yuan, X., Meng, Y., Zeng, G., Fang, Y., & Shi, J. (2008). Evaluation of tea-derived biosurfactant on removing heavy metal ions from dilute wastewater by ion flotation. *Colloids and Surfaces A: Physicochemical and Engineering Aspects, 317*(1), 256-261.

Yun, C. H., Prasad, R., Guha, A. K., & Sirkar, K. K. (1993). Hollow fiber solvent extraction removal of toxic heavy metals from aqueous waste streams. *Industrial & engineering chemistry research, 32*(6), 1186-1195.

Zewail, T., & Yousef, N. (2015). Kinetic study of heavy metal ions removal by ion exchange in batch conical air spouted bed. *Alexandria Engineering Journal, 54*(1), 83-90.

Zhang, Y. X., Jia, Y., Jin, Z., Yu, X., & Xu, W. (2012). Self-assembled, monodispersed, flower-like [gamma]-AlOOH hierarchical superstructures for efficient and fast removal of heavy metal ions from water. *CrystEngComm, 14*(9), 3005-3007.

Zhong, L. S., Hu, J. S., Liang, H. P., Cao, A. M., Song, W. G., & Wan, L. J. (2006). Self‐Assembled 3D flowerlike iron oxide nanostructures and their application in water treatment. *Advanced Materials, 18*(18), 2426-2431.

Zhuang, Y. T., Gao, W., Yu, Y.-L., & Wang, J.-H. (2016). A three-dimensional magnetic carbon framework derived from Prussian blue and amylopectin impregnated polyurethane sponge for lead removal. *Carbon, 108*, 190-198.

Zia, Q., Tabassum, M., Gong, H., & Li, J. (2019). A Review on Chitosan for the Removal of Heavy Metals Ions. *Journal of Fiber Bioengineering and Informatics, 12*(3), 103-128.

Zulfadhly, Z., Mashitah, M., & Bhatia, S. (2001a). Heavy metals removal in fixed-bed column by the macro fungus Pycnoporus sanguineus. *Environmental Pollution, 112*(3), 463-470.

Zulfadhly, Z., Mashitah, M. D., & Bhatia, S. (2001b). Heavy metals removal in fixed-bed column by the macro fungus Pycnoporus sanguineus. *Environ Pollut, 112*(3), 463-470.

LIST OF PUBLICATIONS AND PAPERS PRESENTED

1. Vafaeifard, M., Lee, G., Akib, S., Ibrahim, S., Yoon, Y., Jang, M., 2016. “Facile and economic one-pot synthesis of rigid functional-polyurethane for the effective treatment of heavy metal-contaminated urban storm water run-off.” Desalination Water Treatment 57(54), 26114-26129.

2. Vafaeifard, M., Ibrahim, S., Wong, K. T., Pasbakhsh, P., Pichiah, S., Choi, J., Jang, M. J. J. o. c. p. (2019). “Novel self-assembled 3D flower-like magnesium hydroxide coated granular polyurethane: Implication of its potential application for the removal of heavy metals”. Journal of Cleaner Production, 216, 495-503.